UNIVERSIDADE FEDERAL DE MINAS GERAIS
Programa de Pós-Graduação em Engenharia Elétrica
Research group MACRO - Mechatronics, Control and Robotics

Jean Carlos Pereira

NONLINEAR MODEL PREDICTIVE CONTROL ON SE(3) FOR AGGRESSIVE MANEUVERS

Belo Horizonte
2022

Jean Carlos Pereira

NONLINEAR MODEL PREDICTIVE CONTROL ON SE(3) FOR AGGRESSIVE MANEUVERS

Final version

Thesis submitted to the Graduate Program in Electrical Engineering of Escola de Engenharia at the Universidade Federal de Minas Gerais, in partial fulfillment of the requirements for the degree of Doctor in Electrical Engineering.

Advisor: Guilherme Vianna Raffo
Co-advisor: Valter Júnior de Souza Leite

Belo Horizonte
2022

Pereira, Jean Carlos.
P436n Nonlinear model predictive control on SE(3) for aggressive maneuvers [recurso eletrônico] / Jean Carlos Pereira.- 2022.
1 recurso online (135 f. : il., color.) : pdf.

Orientador: Guilherme Vianna Raffo.
Coorientador: Valter Júnior de Souza Leite.

Tese (doutorado) - Universidade Federal de Minas Gerais, Escola de Engenharia.

Apêndices: f. 130-135.
Bibliografia: f. 110-129.
Exigências do sistema: Adobe Acrobat Reader.

1. Engenharia elétrica - Teses. 2. Veículos – Teses. 3. Sistemas não lineares – Teses. 4. Controle preditivo – Teses. I. Raffo, Guilherme Vianna. II. Leite, Valter Júnior de Souza. III. Universidade Federal de Minas Gerais. Escola de Engenharia. IV. Título.

CDU: 621.3(043)

Ficha catalográfica elaborada pela Bibliotecária Letícia Alves Vieira - CRB-6/2337
Biblioteca Prof. Mário Werneck - Escola de Engenharia da UFMG

UNIVERSIDADE FEDERAL DE MINAS GERAIS
ESCOLA DE ENGENHARIA
PROGRAMA DE PÓS-GRADUAÇÃO EM ENGENHARIA ELÉTRICA

FOLHA DE APROVAÇÃO

"NONLINEAR MODEL PREDICTIVE CONTROL ON SE(3) FOR AGGRESSIVE MANEUVERS"

JEAN CARLOS PEREIRA

Tese de Doutorado submetida à Banca Examinadora designada pelo Colegiado do Programa de Pós-Graduação em Engenharia Elétrica da Escola de Engenharia da Universidade Federal de Minas Gerais, como requisito para obtenção do grau de Doutor em Engenharia Elétrica. Aprovada em 26 de agosto de 2022. Por:

Prof. Dr. Guilherme Vianna Raffo
DELT (UFMG) - Orientador

Prof. Dr. Valter Júnior de Souza Leite
DEMDV (CEFET-MG) - Coorientador

Prof. Dr. Luciano Cunha de Araújo Pimenta
DELT (UFMG)

Prof. Dr. Antonio Ferramosca
DMIPE (University of Bergamo)

Prof. Dr. Tito Luis Maia Santos
DEE (UFBA)

Prof. Dr. Rubens Junqueira Magalhães Afonso
IEE (ITA)

Documento assinado eletronicamente por **Guilherme Vianna Raffo**, **Professor do Magistério Superior**, em 06/09/2022, às 10:46, conforme horário oficial de Brasília, com fundamento no art. 5º do Decreto nº 10.543, de 13 de novembro de 2020.

A autenticidade deste documento pode ser conferida no site https://sei.ufmg.br/sei/controlador_externo.php?acao=documento_conferir&id_orgao_acesso_externo=0, informando o código verificador **1706953** e o código CRC **00C0ED03**.

To Otávio, Júlia
and my dedicated parents

Acknowledgements

To my son Otávio, who was born near the end of this journey and provided me the motivation to keep working. To my wife, Júlia, who has supported me since the beginning of this project, giving me resilience when necessary. To my parents, Jorge and Marília, who have always inspired me to become a better person and taught me to pursue my dreams. Also to my whole family, especially my sister Michelly and my brother Diego, for their friendship and partnership.

To Prof. Guilherme Raffo and Prof. Valter Leite, who have guided me along this path and contributed to the development of this work. To all my professors of Mechatronics Engineering at CEFET-MG, and to all my professors of graduate programs in Mechanical Engineering and Electrical Engineering at UFMG, who have contributed a lot to my academic career.

To my colleagues from the MACRO Group and from the Mechatronics Engineering Department at CEFET-MG (Divinópolis Campus).

To the UFMG for providing the necessary infrastructure for the preparation of this manuscript. And to the CEFET-MG for allowing me to participate in the Ph.D program and encouraging me to obtain a higher education.

Resumo

Esta tese investiga o controle de movimento agressivo de uma classe de veículos subatuados, com controle total de orientação e apenas uma entrada de força translacional, que possui direção fixa com relação ao corpo do veículo. Este modelo de atuação abrange vários tipos de veículos como helicópteros, drones multi-hélice, drone de ventilador canalizado, satélites e veículos submarinos. Existem vários desafios de controle para este tipo de sistemas, especialmente quando eles navegam em ambientes desordenados com obstáculos desconhecidos. O problema se intensifica quando manobras agressivas são consideradas pelo controlador, exigindo movimentos rápidos e precisos para reduzir o tempo de missão e melhorar a eficiência de desvio de obstáculos. Devido às condições extremas de voo, esses controladores devem ser formulados usando um espaço de configuração adequado. O uso do grupo Euclidiano Especial, abreviado como $\mathsf{SE}(3)$, é apropriado porque a representação é única e independente de quaisquer coordenadas locais, além de descrever efetivamente o acoplamento dos movimentos rotacionais e translacionais. Portanto, esta tese propõe esquemas de controle preditivo não linear baseado em modelo (NMPC), formulados no espaço $\mathsf{SE}(3)$, para regulação, rastreamento de trajetória e movimento rápido em ambientes desordenados com obstáculos desconhecidos. Quando os obstáculos são tratados no problema, os controladores propostos consideram a orientação do veículo durante o desvio do obstáculo. Além disso, como algumas aplicações, por exemplo, missões de busca e resgate, exigem que se chegue ao ponto de destino o mais rápido possível, este trabalho também propõe esquemas de NMPC que consideram a redução do tempo de missão como critério econômico.

Palavras-chave: Estabilidade baseada em dissipatividade. Evitamento de obstáculos. Manobras agressivas. NMPC. Veículos subatuados.

Abstract

This thesis investigates aggressive motion control of a class of underactuated vehicles, with full attitude control and only one translational force input in a body-fixed direction. This actuation model covers a wide range of vehicles such as helicopters, multi-propeller helicopters, ducted fans, satellites, and underwater vehicles. There are several control challenges for this kind of vehicle, especially when they navigate in cluttered environments with unknown obstacles. The problem is intensified when aggressive maneuvers are faced by the controller, requiring fast and accurate movements to reduce mission time and improve the obstacle avoidance efficiency. Due to extreme flight conditions, these controllers must be formulated using an accordingly configuration space. The use of the Special Euclidean group, abbreviated as $\mathsf{SE}(3)$, is appropriated because the representation is both unique and independent of any local coordinates, and it effectively describes the coupling of rotational and translational motions. Therefore, this thesis proposes Nonlinear Model Predictive Control (NMPC) schemes formulated on $\mathsf{SE}(3)$ manifold for regulation, trajectory tracking, and fast motion in cluttered environments with unknown obstacles. When obstacles are considered in the problem, the vehicle's attitude is regarded during the obstacle deviation by the proposed controllers. In addition, since some applications, such as search-and-rescue missions, require to reach the destination point as soon as possible, this work also proposes NMPC schemes that consider the mission time reduction as an economic criterion.

Keywords: Dissipativity-based stability. Obstacle avoidance. Aggressive Maneuvers. NMPC. Underactuated vehicles.

List of Figures

1.1 Caption for LOF 19

3.1 Tangent space and tangent bundle on the unit sphere S^2 manifold. 41
3.2 Rotation of a rigid body about a point. 44
3.3 Coordinate frames for rigid motion specification. 45

4.1 Experiment illustration. The NMPC steers the quadrotor UAV to a desired set point x^e from an initial configuration x_0. 63
4.2 Position and attitude trajectories obtained from the experiments considering the NMPC scheme (4.1). 66
4.3 Position and attitude trajectories obtained from the experiments considering the NMPC scheme (4.2). 66
4.4 UAV position, ξ. 67
4.5 UAV velocity, v. 68
4.6 UAV Euler angles. 68
4.7 UAV Angular Velocities. 69
4.8 UAV propeller forces. The input bounds are correctly respected by the controller. 70
4.9 Variation of $\|\bar{x}\|^2_{Q_{\bar{x}}}$ for each initial condition and for each proposed NMPC scheme. 71
4.10 Variation of $\|\xi^{\mathcal{I}}\|$ for each initial condition and for each proposed NMPC scheme. 71

5.1 Examples of aggressive maneuvers as a result of obstacle avoidance and fast flights. 72
5.2 NMPC structure. 73
5.3 Proposed test circuit illustration. 78
5.4 UAV Position, ξ, during the numerical experiments. The reference is defined by (5.12). 81
5.5 UAV Velocity, $\dot{\xi}$, during the numerical experiments. The sharpest oscillations are due to the aggressive reaction to obstacles with fast deviation movements. 81

5.6 UAV acceleration behavior, $\ddot{\xi}$, during the numerical experiments. Highlighted areas show the rejection of disturbances applied to the system, which are presented in Table 5.2. In addition, high accelerations required in some situations indicate aggressive flight execution. 82
5.7 Ellipsoidal set $\bar{\mathcal{V}}(t)$ during the numerical experiment. The UAV attitude parameterization, considered in the set modeling, allows the aggressive maneuver execution by the NMPC controller. 82
5.8 Minimum distance between the UAV and obstacles along all the numerical experiments, i.e. nominal parameters and with uncertainty of $\pm 10\,\%$ in the parameters of mass and inertia tensor. The term σ_ℓ is always greater than 0 for all cases, which validates the collision avoidance capability of the proposed NMPC. 83
5.9 UAV Euler angles computed from the rotation matrix after the numerical experiments. Large angular excursions corroborate the aggressive maneuver capability. 84
5.10 UAV Angular Velocities during the numerical experiments. Fast motion control has demanded large angular acceleration. 85
5.11 The input bounds are correctly satisfied by the controller, which applied extreme force values when aggressive maneuvers are required. 88
5.12 Performance and aggressiveness evaluation from variation of parameter K_R. As far as K_R increases, the aggressiveness and the performance decrease. . 89

6.1 (a) The UAV performing the proposed maneuver: throwing a narrow and tilted gap. (b)-(d) Ellipsoidal set $\mathcal{V}(t)$ during the numerical experiment. . 96
6.2 Number of iterations required by the NLP solver to find the optimal solution for both the ellipsoidal approach and ellipsoidal-polytopic approach. The latter is less computationally costly. 97
6.3 Illustration of the proposed experiment. 97
6.4 Data obtained in the second round of experiments: motion control with obstacle-avoidance capability using ellipsoidal-polytopic based NMPC. . . 100
6.5 UAV propeller forces. The input bounds are correctly respected by the controller. 101
6.6 Ellipsoidal set $\mathcal{V}(t)$ during the numerical experiment. 102
6.7 Minimum distance between the UAV and obstacles. 102
6.8 The UAV performing the proposed maneuver: throwing a narrow and perpendicular gap. 102
6.9 Comparison between the proposed schemes performing the same maneuver shown in Figure 6.8. 104

6.10 Ellipsoidal set $\mathcal{V}(t)$ during the numerical experiments. The blue ellipsoids represent the UAV controlled by the NMPC scheme given by (6.12) and the magenta ones represent the UAV controlled by fast motion scheme. . . 105
6.11 Minimum distance between the UAV and obstacles along all the numerical experiments. The term σ_ℓ is always greater than 0 for all cases, which shows that the obstacle avoidance capability is maintained by fast motion formulation. 105

List of Tables

4.1 Quadrotor UAV parameters. 64

5.1 Obstacles parameters at each test circuit zone shown in Figure 5.3. 78
5.2 Disturbance parameters considered in the simulation. 79
5.3 Input/State Constraints. 80
5.4 Normalized ISE performance indexes for K_R and v combinations. 86

Acronyms

MPC	Model Predictive Control
NMPC	Nonlinear Model Predictive Control
TONMPC	Time-Optimal Nonlinear Model Predictive Control
EMPC	Economic Model Predictive Control
AGV	Autonomous Ground Vehicle
AUV	Autonomous Underwater Vehicle
UAV	Unmanned Aerial Vehicle
H-rep	Half-space Representation
V-rep	Vertex Representation
LQR	Linear Quadratic Regulator
NLP	Nonlinear Programming
LP	Linear Programming
OCP	Optimal Control Problem
VTOL	Vertical Take-Off and Landing
IPOPT	Interior Point Optimizer

Notation

General symbols and operators

$\mathbb{N}$	Set of natural numbers
$\mathbb{R}$	Set of real numbers
$\mathbb{I}_{0:i}$	The integers set going from 0 to i.
$\mathbf{0}_{n\times m}$	Matrix of zeros with n rows and m columns
$\mathbf{1}_{n\times m}$	Matrix of ones with n rows and m columns
I_n	Identity matrix with dimension n
$\dot{A}$	Time derivative of A
$A^\top$	Transpose of A
A^{-1}	Inverse of A
$\mathtt{diag}(a)$	Diagonal matrix whose diagonal is defined by a
$[\Upsilon]_+$	Operator that denotes $\max\{\Upsilon, 0\}$
$\mathtt{vec}(G)$	Operator that concatenates the columns of matrix G vertically in a vector, i.e, $v = \mathtt{vec}(G) = \begin{bmatrix}\mathtt{e}_1 G^\top & \mathtt{e}_2 G^\top & \cdots & \mathtt{e}_m G^\top\end{bmatrix}^\top$ where m represents the number of columns of G, and $\mathtt{e}_i \in \mathbb{R}^{1\times m}$, $i = 1, \ldots, m$, have the i-th entry equals to 1 with the remaining ones null.
$\mathsf{SO}(\cdot)$	Special Orthogonal Group
$\mathsf{SE}(\cdot)$	Special Euclidean Group
$\mathfrak{so}(\cdot)$	Vector space of skew matrices
$\mathsf{TSE}(3)$	Tangent bundle of $\mathsf{SE}(3)$
$d_{\mathcal{B}}^{\mathcal{A}}$	Displacement vector from $\mathcal{A}$ to $\mathcal{B}$, expressed in $\mathcal{A}$

$R_{\mathcal{B}}^{\mathcal{A}}$	Rotation matrix from $\mathcal{A}$ to $\mathcal{B}$
$\omega_{\mathcal{BC}}^{\mathcal{A}}$	Angular velocity of frame $\mathcal{C}$ with respect to $\mathcal{B}$, expressed in $\mathcal{A}$
$\mathcal{S}(\cdot)$	Skew-symmetric matrix operator

Contents

1 Introduction **18**

1.1 Motivation . . . 18
1.2 Justification . . . 21
1.3 Objectives . . . 22
1.3.1 Specific objectives . . . 22
1.4 Structure of the text . . . 23

2 Literature Review **24**

2.1 Aggressive Maneuvers . . . 24
2.1.1 Agile fixed-wing UAV . . . 24
2.1.2 Rotary-wing UAV . . . 25
2.2 Obstacle Avoidance Methods . . . 27
2.2.1 Artificial Potential Field . . . 27
2.2.2 Vector Field Histogram . . . 28
2.2.3 Dynamic window approach . . . 28
2.2.4 Geometric approaches . . . 29
2.3 MPC for Motion Systems . . . 29
2.3.1 NMPC . . . 31
2.3.2 Time-Optimal NMPC . . . 32
2.3.3 MPC for obstacle avoidance . . . 34
2.3.4 MPC for underactuated systems . . . 37
2.3.5 MPC for UAV . . . 38
2.4 Final Remarks . . . 38

3 Mathematical Preliminaries **39**

3.1 Rigid Body Systems . . . 39
3.1.1 Manifold concepts . . . 39
3.1.1.1 Manifolds . . . 40
3.1.1.2 Tangent vectors, tangent spaces and tangent bundles . . . 40
3.1.1.3 Lie Groups and Lie Algebras . . . 41

3.1.2 Rigid transformation . . . 42
3.1.3 Rotation motion in $\mathbb{R}^3$ . . . 43
3.1.3.1 Representational singularities . . . 43
3.1.3.2 Attitude error function on SO(3) . . . 44
3.1.4 Rigid motion in $\mathbb{R}^3$ . . . 45
3.2 Dynamics of Underactuated Motion System on SE(3) . . . 46
3.2.1 System discretization . . . 47
3.3 Model Predictive Control without Terminal Conditions . . . 48
3.4 Optimal Control Problem Solution . . . 48
3.4.1 Convex versus nonconvex MPC . . . 49
3.4.2 Simultaneous versus sequential approach . . . 50
3.4.3 Direct optimal control parameterizations . . . 50
3.4.4 Nonlinear optimization . . . 51
3.4.4.1 Nonlinear interior point methods . . . 53
3.4.5 CasADi for optimization . . . 54
3.5 MPC stability based on strict dissipativity . . . 54
3.6 Final Remarks . . . 55

4 Point-to-point Motion Control Problem **56**
4.1 Problem Statement . . . 57
4.2 Control Strategies . . . 57
4.2.1 NMPC for motion control of underactuated vehicles on SE(3) . . . 57
4.2.2 NMPC for fast motion control of underactuated vehicles on SE(3) . . . 58
4.3 Feasibility and Stability Analysis . . . 58
4.3.1 NMPC for motion control of underactuated vehicles on SE(3) . . . 58
4.3.2 NMPC for fast motion control of underactuated vehicles on SE(3) . . . 62
4.4 Numerical Example: a Quadrotor UAV . . . 63
4.4.1 Experiment setting . . . 63
4.4.2 Results . . . 65
4.5 Final Remarks . . . 69

5 Trajectory Tracking with Obstacle Avoidance **72**
5.1 Problem Statement . . . 73
5.2 Control Strategy . . . 73
5.2.1 Ellipsoidal collision check approach . . . 74
5.2.2 Nonlinear model predictive control formulation . . . 75
5.2.2.1 Integral action for disturbance rejection . . . 75
5.2.2.2 Relaxed collision constraint for obstacle avoidance . . . 76
5.2.2.3 Optimal control problem . . . 76
5.3 Numerical Example: a Quadrotor UAV . . . 77

5.3.1 Experiment setting . . . 77
5.3.2 Results . . . 80
5.3.2.1 Aggressiveness versus tracking performance . . . 85
5.4 Final Remarks . . . 87

6 Point-to-point Motion with Obstacle Avoidance 90
6.1 Problem Statement . . . 90
6.2 Control Strategies . . . 91
6.2.1 Ellipsoidal-polytopic collision check approach . . . 91
6.2.1.1 Relaxed collision constraint for obstacle avoidance . . . 93
6.2.2 NMPC with obstacle-avoidance capability for motion control of underactuated vehicles on SE(3) . . . 94
6.2.3 NMPC with obstacle-avoidance capability for fast motion control of underactuated vehicles on SE(3) . . . 95
6.3 Numerical Example: a Quadrotor UAV . . . 95
6.3.1 Ellipsoidal versus ellipsoidal-polytopic approach . . . 95
6.3.2 Motion control with obstacle-avoidance capability using ellipsoidal-polytopic based NMPC . . . 97
6.3.3 Fast motion control with obstacle-avoidance capability using ellipsoidal-polytopic based NMPC . . . 101
6.4 Final Remarks . . . 106

7 Conclusions 107
7.1 Overview and contributions . . . 107
7.2 List of Publications . . . 109
7.3 Future Works . . . 109

Bibliography 110

A Rotation Matrices 130
A.1 Properties of rotation matrices . . . 130
A.2 Exponential map for rotation . . . 131
A.3 Derivative of rotation matrices . . . 132

B Newton-Euler Dynamic Equations 134

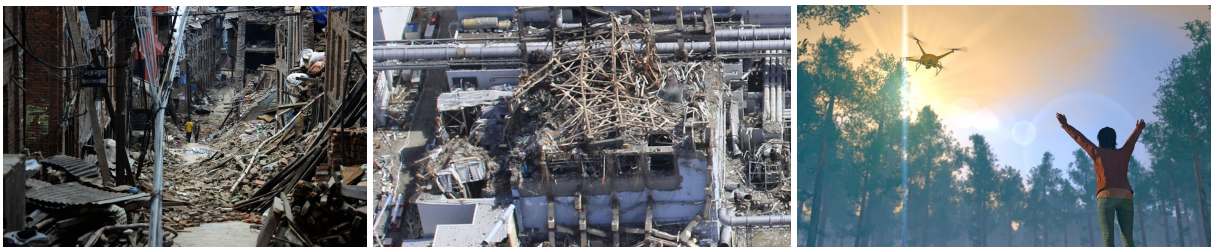
1 Introduction

1.1 Motivation

Unmanned vehicles have attracted considerable research interest in recent decades (He et al., 2022; Viswanathan et al., 2018; Penicka & Scaramuzza, 2022). Security, agriculture, civilian infrastructure inspection, space and underwater exploration, wildlife tracking and conservation, package delivery, and remote sensing are examples of typical applications (Hamrah et al., 2018). There are different kinds of unmanned vehicles, depending on the navigation environment, such as Autonomous Ground Vehicles (AGVs) (Liu et al., 2017), Autonomous Underwater Vehicles (AUVs) (Heshmati-Alamdari et al., 2021), and Unmanned Aerial Vehicles (UAVs)(Hua et al., 2013). These vehicles are usually designed with fewer actuators than degrees of freedom (DOF) in order to reduce weight and cost, resulting in underactuated systems (He et al., 2022).

When compared to other types of underactuated vehicles, the enthusiasm for UAVs has grown significantly in recent years (Castillo et al., 2019; Murilo & Lopes, 2019; Small et al., 2019; Yu et al., 2019; Penicka & Scaramuzza, 2022). They have been originally developed for military purposes, which correspond to most of their applications such as remote monitoring, supply transport, search-and-rescue missions, and war armaments. However, due to technological advances and cost reductions in computational processing, sensing and energy storage, they are also becoming increasingly popular as a commercial product in civil applications. Usually, these vehicles must fly in complex and cluttered environments (Sathya et al., 2018; Small et al., 2019), as illustrated in Figure 1.1. In

these scenarios, the aircraft frequently has to deal with obstacles in constrained spaces, such as search-and-rescue missions through forests or wreckage areas, as well as mapping, exploration, and inspection missions through urban buildings (Morrell et al., 2018; Penicka & Scaramuzza, 2022).



(a) (b) (c)

Figura 1.1: Complex search-and-rescue environments the UAV may deal with: (a) earthquake scenarios[1], (b) nuclear disasters[2], and (c) forest areas[3].

Consequently, the development of UAVs that can execute aggressive maneuvers has been an active research area in the last years (Loianno et al., 2017; Penicka & Scaramuzza, 2022). In Yu et al. (2019), the characterization of aggressive maneuvers depends on the ability of the UAV performs fast changes of direction and attitude with relative ease. Also, high-speed navigation while reacting to obstacles dynamically, demanding an ability to generate and control large linear and angular accelerations, compose other features of aggressive maneuver (Mellinger et al., 2012a). Therefore, in comparison to smooth maneuvers, the aggressive ones require high-performance controllers. Such controllers must mitigate modeling mismatches, such as parametric uncertainties and unmodeled dynamics, as well as the consequences of exogenous disturbances, saturating actuators, and coupling dynamics (Lu, 2015; Sun et al., 2022). Moreover, the challenge of performing aggressive maneuvers includes the UAV attitude being regarded in the obstacle collision check, which is uncommonly found in the literature.

Due to these extreme flight conditions, these controllers for aggressive motion must be formulated using accordingly configuration spaces. A translating and rotating rigid body in three dimensions is globally represented by the Special Euclidean group $\mathsf{SE}(3)$, defined by an ordered pair $(R, \xi) \in \mathsf{SE}(3) \triangleq \mathsf{SO}(3) \ltimes \mathbb{R}^3$, where $R \in \mathsf{SO}(3)$[4] is a rotation matrix describing the rigid body's attitude, and $\xi \in \mathbb{R}^3$ is a vector describing the position of a

[1] https://www.scientificamerican.com/article/killer-landslides-the-lasting-legacy-of-nepal-s-qua

[2] https://www.npr.org/sections/pictureshow/2011/03/31/135008956/utter-destruction-japans-nuclear-plant-seen-from-the-air

[3] http://www.telemedmag.com/article/drone-use-soon-soar-search-rescue-operations/

[4] The notation SO abbreviates *special orthogonal*. Generally, the space of rotation matrices in $\mathbb{R}^{n\times n}$ is given by (Murray et al., 1994)

$$\mathsf{SO}(n) \triangleq \{R \in \mathbb{R}^{n\times n} : RR^\top = I, \det R = +1\}.$$

point in the body, typically the origin of the body-fixed frame, in the inertial frame (Lee et al., 2018). Minimal representations, such as Euler-angles and angle-axis parametrization, suffer from singularities and are only locally effective (Lee, 2015). The unit quaternions, which are singularity-free (Casau et al., 2015), provide a double cover of the attitude space, meaning that every orientation can be represented by two unit quaternions. This ambiguity might lead to inconsistent behavior namely the unwinding phenomenon (Mayhew et al., 2012). Thus, the use of rotation matrix, and consequently the configuration manifold $\mathsf{SE}(3)$, is appropriate for controlling underactuated vehicles, specially for aggressive motion, since the representation is both unique and independent of any local coordinates (Chaturvedi et al., 2011; He et al., 2022). Therefore, it effectively describes the coupling between rotational and translational motions (Nikhilraj et al., 2019).

Within this context, this thesis investigates aggressive motion control of a class of underactuated vehicles globally represented in the $\mathsf{SE}(3)$ manifold, with full attitude control and only one translational force input, that is, with four independent control inputs for the six DOF of translational and rotational motion in the three dimensional Euclidean space. Usually, in these underactuated systems, the control force vector is in a body-fixed direction. This actuation model covers a wide range of UAVs such as helicopters (Frazzoli et al., 2000), multi-propeller helicopters (Hua et al., 2013; Kamel et al., 2015), ducted fans (Pflimlin et al., 2007), and satellites (Yoshimura et al., 2016). Although underwater vehicles (Leonard, 1995; Egeland et al., 1996a; Li et al., 2017a) can be also covered by this class of vehicles, this thesis focuses on UAVs.

The first research topic investigated here is the stabilization of underactuated vehicles modeled on $\mathsf{SE}(3)$, which is a nontrivial problem since underactuated vehicles having rotational degrees of freedom, according to Brockett (1983) and Bhat & Bernstein (2000), cannot be globally asymptotically stabilized to a constant equilibrium via continuous feedback. In order to solve this problem, discontinuous control laws formulated on $\mathsf{SE}(3)$ (Fjellstad & Fossen, 1994; Egeland et al., 1996b), time-varying quaternion continuous feedback control (Pettersen & Egeland, 1999), and hybrid quaternion feedback strategies (Casau et al., 2013, 2015) have been proposed. However, none of these works considers control input constraints (Li & Yan, 2017), which is an important requirement in practical implementation.

The second research topic addressed in this thesis is the fast motion control of underactuated vehicles within cluttered environments with unknown obstacles, in which the aggressive maneuver makes the obstacle-avoidance process more efficient with faster deviation movements. Some approaches in the literature consider the controller design to achieve a given aggressive trajectory, while others concern the motion planner design of collision-free trajectories, decoupled from motion control. In the former, the problem without obstacle-avoidance consideration is handled based on strategies like the adaptive geometric control (Goodarzi et al., 2015), optimal control (Foehn & Scaramuzza, 2018),

backstepping (Yu et al., 2019), and disturbance observer-based control (Castillo et al., 2019). The main contributions of these works concern the robustness and local stability of the closed-loop system. Conversely, works on the second approach group usually propose two-layered frameworks which consider the motion planner in the upper-layer, while dynamic controllers address the motion control problem. In most cases, they use differential flatness property and generate minimum snap (fourth derivative) trajectories (Liu et al., 2018; Loianno et al., 2017).

Recently, Model Predictive Control (MPC) has been applied to autonomous navigation problems, providing efficient collision-avoidance capability (Hoy et al., 2015; Nascimento et al., 2019; Pereira et al., 2021a; Sanchez et al., 2021; Santos et al., 2021a,b). In these cases, a trajectory planner is not necessary, and the vehicle is able of performing online obstacle avoidance while navigating autonomously within cluttered environments with unknown obstacles. Typically autonomous navigation is handled through a hierarchical architecture of planning and control layers (Castillo-Lopez et al., 2018b), since this type of strategy presents good performance and low computational cost. However, when we are pursuing high performance with fast time response, e.g. aggressive maneuvers, these approaches can lead to inappropriate coordination between the layers. In addition, as MPC is able to consider constraints such as obstacles to generate feasible trajectories, the unified navigation framework is safer and less prone to local minima than hierarchical approaches (Shim et al., 2003).

Therefore, the main contribution of this work is to develop Nonlinear Model Predictive Control (NMPC) schemes formulated on Special Euclidean group $\mathsf{SE}(3)$ for a class of underactuated vehicles. The cost functional is unique in terms of position and attitude requirements, considering the entire dynamics of the vehicle without linearization or system decoupling. When obstacles are considered in the control problem, the collision check takes the vehicle's attitude into account, allowing aggressive maneuvers in order to improve the obstacle avoidance performance. In addition, since some applications, such as search-and-rescue missions, require not only safe navigation, but also to reach the destination point as soon as possible, this work also proposes NMPC schemes that consider the mission time reduction as an economic criterion.

1.2 Justification

As mentioned above, there are several control challenges for motion control of underactuated vehicles, specially when they navigate in cluttered environments with unknown obstacles. The problem is intensified when aggressive maneuvers are faced by the controller, requiring fast and accurate movements to reduce mission time and improve the obstacle avoidance efficiency. These vehicles require high-performance controllers to restrict serious dynamic disturbances such as nonlinearities, unmodelled behaviors, couplings effects, external

disturbances, parametric uncertainties, and actuator saturation.

Few works in the literature deal with the problem of aggressive navigation from a unified control perspective. Most of the works addresses only issues of motion planning decoupled from the controller, which can lead to inefficient and undesirable situation due to the lack of proper coordination between layers. In addition, works that propose simultaneous motion planning and control in a single optimization problem usually rely on model simplification, such as model decoupling, local attitude parametrization, and model linearization. More recent works incorporate collision-avoidance requirements as constraints in NMPC frameworks, considering the fully dynamic model. However, they do not explore the change in orientation of the mechanical system during the navigation and, consequently, the vehicle's attitude is not regarded during the obstacle deviation. Therefore, a unified NMPC framework fully exploring the vehicle nonlinear model globally represented in the $\mathsf{SE}(3)$ manifold, which allows execution of aggressive maneuvers during obstacle deviation, is still an open research field. In addition, since the control design is formulated on $\mathsf{SE}(3)$, which is a non euclidean space, the closed-loop stability analysis is nontrivial, and, consequently, for the best knowledge of the author, it is also an open research field.

1.3 Objectives

The main objective of this work is to develop NMPC schemes formulated on Special Euclidean group $\mathsf{SE}(3)$ for motion control problems involving a class of underactuated vehicles. In addition to the standard motion control problems of regulation and trajectory tracking, fast motion with aggressive maneuver capability is also investigated, in which obstacle avoidance and mission time reduction are regarded by the optimal control problem.

1.3.1 Specific objectives

Specifically, it is investigated the following issues:

1. Propose a stabilizing NMPC scheme for motion control of underactuated vehicles modeled on $\mathsf{SE}(3)$.

2. Propose a stabilizing NMPC scheme for motion control of underactuated vehicles modeled on $\mathsf{SE}(3)$, in which the mission time is regarded as an economic criterion.

3. Propose NMPC schemes for fast motion control of underactuated vehicles modeled on $\mathsf{SE}(3)$ with obstacle-avoidance capability. The proposed methods must consider the vehicle's attitude in the collision avoidance, allowing aggressive maneuvers to improve the performance during obstacle deviation.

1.4 Structure of the text

This manuscript is organized as follows:

- **Chapter 2** presents a detailed literature review in aggressive maneuvers, obstacle avoidance methods, and model predictive control for motion systems.
- **Chapter 3** provides the mathematical background used in this thesis.
- **Chapter 4** presents two NMPC schemes without terminal conditions for the stabilization problem of underactuated vehicles globally represented in the $\mathsf{SE}(3)$ manifold.
- **Chapter 5** presents an ellipsoidal based NMPC scheme on $\mathsf{SE}(3)$ without terminal conditions able to perform trajectory tracking while avoiding obstacles with aggressive maneuver capability.
- **Chapter 6** presents two ellipsoidal-polytopic based NMPC schemes on $\mathsf{SE}(3)$ without terminal conditions able to perform point-to-point motion while avoiding obstacles with aggressive maneuver capability.
- **Chapter 7** summarizes the main contributions obtained during this doctoral thesis, depicts the submitted/accepted papers, and concludes the manuscript.

2 Literature Review

This chapter presents a literature review about aggressive maneuvers, the main obstacle avoidance methods applied in autonomous navigation, and MPC for motion systems.

2.1 Aggressive Maneuvers

In the literature, the problem of aggressive maneuver is mostly investigated by UAV applications, and the problem can be divided according to the aircraft. Most of the works focus on rotary-wing (helicopter, quadrotor) UAVs due to their high maneuverability (Penicka & Scaramuzza, 2022). Conversely, a new class of UAVs, called agile fixed-wing aircraft, distinguished by high thrust-to-weight ratios (2-3) and large control surfaces capable of large deflections, has emerged pursuing the maneuvering feature with increased endurance flight capability (Bulka & Nahon, 2019a). Therefore, this section provides a historical perspective on the prior research undertaken in the area of aggressive flight for each UAV configuration, besides a review of the related control strategies.

2.1.1 Agile fixed-wing UAV

For many years, the potential of small radio-controlled aircraft to conduct extreme aerobatic maneuvers has been limited to non-autonomous piloted systems. This has begun with researchers working on the concept of designing fixed-wing aircraft with hovering capabilities, where the aircraft is suspended nose-up by its propeller. The first positive

result was performed in 1954 with the Convair XFY-1 Pogo (Chana & Coleman, 1996), which was manually operated. In addition, a radio-controlled aircraft has been developed at Drexel University (Green & Oh, 2005) and has also had the ability to hover.

Over the last decades, however, researchers have attempted to automate these extreme flight modes from the UAV control design (Bulka & Nahon, 2019a). Although some works focus on flight aggressiveness in general, it can be helpful to evaluate particular agile maneuvers that accomplish a desired objective. Examples of these maneuvers include the aforementioned hovering (Green & Oh, 2006; Frank et al., 2007; Johnson et al., 2008) and perching (Crowther, 2000; Cory & Tedrake, 2008; Moore et al., 2014), where the aircraft moves to a hover position while it lands on a vertical surface. The knife-edge (Park, 2012; Barry et al., 2014) is another useful maneuver that has attracted attention. This technique consists of rolling the aircraft by 90 degrees and, preferably, retaining the angle of roll over a desirable time interval. In addition of being a basic aerobatic technique, the knife-edge allows it to pass through gaps that are narrower than the wingspan of the aircraft. Other movements such as tailslides, inverted spins (Selig, 2014), and turn-around maneuver (Matsumoto et al., 2010; Paranjape et al., 2013) complete the package of the most important aggressive maneuvers of fixed-wing UAVs. More recent works have proposed frameworks for fast flight in unknown (Bulka & Nahon, 2019b) and known (Levin et al., 2019) environments, where aerobatic maneuvers are the result of the ability to avoid obstacles.

Little research has been done on the design of control strategies for aggressive maneuvering of agile fixed-wing UAVs in comparison to rotary-wing UAVs (Bulka & Nahon, 2019a). Most of the works have been established controllers for level flight and hovering conditions, and to switch between these conditions. Control techniques vary from classical methods (Hall & McLain, 2008; Green & Oh, 2009) to more sophisticated ones based on optimal control (Frank et al., 2007; Moore et al., 2014; Bulka & Nahon, 2019a), backstepping control (Sobolic, 2009), and sliding mode control (Ure & Inalhan, 2012). From the best knowledge of the author, there are no works in the literature based on NMPC for aggressive maneuvering of agile fixed-wing UAVs.

2.1.2 Rotary-wing UAV

Most of the rotary-wing UAV works deal with quadrotors which, thanks to technological development in the last decades, have been used to perform aggressive maneuvers. In this regard, Mellinger et al. (2012b) have been pioneers in this research. They have presented a solution for trajectory planning and control of aggressive quadrotor flight. The same authors have also provided in Mellinger & Kumar (2011) a method to compute the trajectories for quadrotors from the solution of a quadratic program, which minimizes the snap (i.e., the fourth derivative of position). In their experiments, agile maneuvers, such as

going through static circular hoops, have been demonstrated using state estimation from a motion-capture system.

From these works, other authors have pursued the problem, proposing solutions for specific maneuvers such as flip (Cutler & How, 2015; Goodarzi et al., 2013; Yu et al., 2019; Castillo et al., 2019), passing through a narrow gap (Neunert et al., 2016; Liu et al., 2018; Falanga et al., 2017), i.e when the diameter of the quadrotor is larger than some part of the width of the path, performing faster trajectories with slalom movements (Loianno et al., 2017), and perching on inverted surface (Mellinger et al., 2012a). Although these works have relevant results, most of them have developed strategies for specific situations with hand-picked beforehand constraints and assumptions. In addition, they are not related to any navigation or mission purpose and focus, exclusively, on the execution of a specific set of maneuvers. Even when different types of aggressive maneuvers are possible, they are divided into parts, and the switch between them may impair the performance of the flight. There is, therefore, a lack of works that deal with aggressive maneuvers as a result of obstacle avoidance and faster flights, in which the aggressiveness improves the achievement of task requirements, such as minimizing the mission time and improving the obstacle deviation performance.

The motion planning proposed by Li et al. (2017b) has been developed to address this research gap. They have utilized the quadrotor maneuverability to produce motion primitive sequences in cluttered environments. They have introduced a way to consider the UAV attitude during the trajectory planning, approximating the UAV as an ellipsoid. Their strategy is able to obtain a safe and optimal trajectory that guides the aircraft to its target as quickly as possible. However, the map has to be completely known for the success of their algorithm. In addition, as most of works dealing with autonomous navigation, the problem has been addressed by a hierarchical combination of planning and control layers. The lack of proper coordination between these layers often leads to inefficient and undesirable situations, and this kind of approach is more prone to local minima than the integrated ones (Shim et al., 2003).

Due to the high angular excursions required by aggressive maneuvers, this thesis is concerned with representational singularities. Also known as mathematical singularities, they are related to the multiple solution regions at the inverse transformation problem, not associated with physical limitations of the rigid body (Lee, 2015). They are undesirable because there are some orientations in space where infinite rotational rates are required to produce a finite angular velocity and acceleration of the rigid body (Paul, 1981). In this context, to avoid this kind of singularity, recent controllers have been formulated on quaternion-based representation using intelligent control (Molenkamp et al., 2017), optimal control (Foehn & Scaramuzza, 2018), disturbance observer-based control (Castillo et al., 2019), and attractive ellipsoid method (Oliva-Palomo et al., 2018).

With the same goal, to avoid singularities, most of controllers found in literature are

formulated on SE(3), where the rigid body attitude is represented by the rotation matrix. Most of them are based on the geometric method proposed by Lee et al. (2010). Goodarzi et al. (2015); Yu et al. (2019) have combined it with the backstepping technique, while Ramp & Papadopoulos (2018) have combined it with surface-based error concept. Also, Mellinger & Kumar (2011); Loianno et al. (2017); Tang et al. (2018); Faessler et al. (2018) have combined it with differential flatness property. The differential flatness principle proposes a set of variables called flat outputs, which are used to demonstrate that the states of the system and the control inputs can be written in terms of this subset of variables and their derivatives. Although the works have relevant results, they have used cascade control structures, and the attitude error function used by them has incorrect critical points (error equal to zero), i.e. the function is equal to zero in situations when the current attitude is not equal to the desired one.

2.2 Obstacle Avoidance Methods

Autonomous navigation of unmanned vehicles is a classic field of research in robotics, giving rise to a wide range of approaches well documented in the literature (Hoy et al., 2015). Mobile robot navigation is classified into two main categories: global navigation and local navigation (Patle et al., 2019). The main difference between them is the amount of available information about the environment. If prior information on the obstacle set is required and, as a result, a full map of the environment is available, global path planning methods may be used to find the optimal path (Hoy et al., 2015). However, when only local information is available, that is, when environmental conditions are obtained as the robot moves, local methods, also known as sensor-based methods, are used.

The knowledge of a global, invariant, and accurate map is a strong hypothesis in practice. In this context, the concept of obstacle avoidance emerges. How a robot can navigate towards a goal in a cluttered environment when obstacles to avoid have just been discovered in real time is the main issue to be addressed (Minguez et al., 2008). Although the problem is directly applicable to local methods, some global ones can be adapted to unknown environments, sometimes with relatively small change (Hoy et al., 2015). Since this thesis proposes an obstacle avoidance solution for UAVs, the following subsections will present the most relevant obstacle avoidance techniques found in the literature.

2.2.1 Artificial Potential Field

The Artificial Potential Field concept has been presented as a collision avoidance technique by Khatib (1985). The algorithm uses an analogy wherein the robot is a particle that moves under the influence of a force field in the configuration space. While a force attracting the particle is exerted by the target location, the obstacles exert a repulsive force. The motion

is computed at each time instant to follow the direction of the artificial force induced by the sum of both potentials (the most promising direction of motion). This is the classic version, where the potentials depend only on the current configuration of the vehicle. There are some variations as potentials also depending on the instantaneous velocity and acceleration of the robot (Minguez et al., 2008). This type of approach is common since it is easy to understand. However, when symmetrical situations occur and when concave obstacles appear, the method is very sensitive to local minima and can cause oscillatory behavior (Oroko & Nyakoe, 2012). Although there are improved versions of the method that address the local minimum problem (Borenstein & Koren, 1989; Kim & Khosla, 1992; Valavanis et al., 2000; Goncalves et al., 2010; Rezende et al., 2020), the robot attitude is rarely taken into account in the problem.

2.2.2 Vector Field Histogram

The Vector Field Histogram (VFH) (Borenstein & Koren, 1991) solves the problem in two steps by computing a set of candidate motion directions and then choosing the best of them. The approach uses a Cartesian two-dimensional histogram grid as a representation of the environment. This world model is continuously modified using on-board range sensors. In the first stage, a constant size subset of the 2D histogram grid is reduced to an one-dimensional polar histogram considered around the current position of the robot. In the polar histogram, each component contains a value representing the obstacle polar density in the corresponding sector. In the second stage, the algorithm selects the most appropriate sector with low obstacle polar density and close to the target direction. The VFH method is formulated to work with probability obstacle distributions and is, therefore, well suited to work with uncertain sensors (Minguez et al., 2008). In addition, the problems related with local minima and oscillatory behavior when navigating through a corridor are eliminated (Oroko & Nyakoe, 2012). The method, however, can cause the robot to move away from the destination and to navigate long and unnecessary distances. Also, the attitude of the robot is not taken into account in the problem.

2.2.3 Dynamic window approach

The dynamic window approach has been proposed by Fox et al. (1997). In contrast to other methods, the dynamic window approach is derived directly from the dynamics of the robot and specifically designed to address the constraints imposed by the velocity and acceleration limitations. The main idea is first to generate a valid search space, defining the admissible sets and, secondly, to select an optimal solution. This is achieved by raising the search space to the dynamic range, which consists of velocities that can be reached within a limited period of time. Within the dynamic window, the approach considers only admissible velocities that yield a trajectory on which the robot can safely stop. The

combination of translational and rotational velocities is chosen by optimizing an objective function among these velocities. The objective function involves a measure of progress towards a target location, the robot forward velocity and the distance on the trajectory to the next obstacle.

2.2.4 Geometric approaches

Geometric approaches are related to the use of constraints based on geometric concepts to generate an appropriate avoidance trajectory. One term based on the collision cone (CC) theory is the velocity obstacle (VO) method, which has gained attention in the multi-agent and intelligent robotics community due to its performance and intuitive design (Douthwaite, 2020). Originally proposed in Fiorini & Shiller (1998), the velocity constraints have been formulated using known obstacle geometries as the robot travels through its field of view. Through this set of constraints, a region containing all collision trajectories is computed from the characteristic radius of the obstacle and transformed into the velocity space. The resulting area limits the admissible velocities in the next time step. The VO concept has been extended in van den Berg et al. (2008), where the Reciprocal Velocity Obstacle (RVO) method has been developed to overcome the oscillatory behavior when used in navigation among autonomous entities with a symmetric collision-avoidance strategy. Instead of selecting only the admissible velocity, the principle considers the average of the admissible velocity and the current velocity.

The Optimal Reciprocal Collision Avoidance (ORCA) presented in van den Berg et al. (2011a) is one of the latest VO concepts. Based on linear programming, the response is smoother when compared to previous VO versions (Douthwaite et al., 2018). There are other optimized VO methods, based on RVO and derived VO methods, such as acceleration velocity space (AVO) (van den Berg et al., 2011b), optimal velocity selection using velocity obstacle (OVVO) (Kim & Oh, 2016), velocity changing space (VCS) (Zhong et al., 2016). Since the positions of both robots and obstacles in real applications are measurable by sensors that are usually not accurate, as well as the rise of modeling mismatches, some recent works have proposed solutions to address uncertainty issues (Gopalakrishnan et al., 2017; Zhu et al., 2020; Verginis & Dimarogonas, 2021).

2.3 MPC for Motion Systems

There are a number of basic tasks for a robotic application, including but not limited to mapping, localization, planning and control (Morin & Samson, 2008). In addition, the motion control problem related to a single robot can be classified as (Kanjanawanishkul, 2010; Aguiar & Hespanha, 2007)

1. **point stabilization** (regulation), known also as point-to-point motion, where the

goal is to steer a motion system to a desired position and orientation, i.e. a desired posture;

2. **trajectory tracking**, where the vehicle is forced to reach and follow a time parameterized reference, i.e., a time varying reference;

3. **path following**, where the vehicle is required to approach and follow a desired path-parameterized reference that is specified without a temporal law.

Model Predictive Control (MPC) is an optimal control method originated in the late seventies and has been developed considerably since then (Camacho & Bordons, 2007). MPC formulations are solved by a finite horizon optimal control problem at each sampling time right after the prediction horizon gets receded, and the optimization problem initial conditions get updated (Camacho & Bordons, 2007). Since MPC has ability to control constrained multiple-input multiple-output nonlinear systems regarding optimal criteria, the method has been used in a considerable number of robotic applications, solving all those types of motion control problems.

For regulation problem of motion systems, studies utilizing MPC have been presented in Kuhne et al. (2005); Worthmann et al. (2015, 2016). In Dongbing Gu & Huosheng Hu (2005), a stabilizing MPC using terminal region constraints and terminal cost has been explored, while in Xie & Fierro (2008), a contraction constraint on the first state in the prediction horizon has been implemented. In addition, in Fontes (2001); Fontes & Magni (2003), the desired set point has been located at the boundary of the closed terminal region, and a non-quadratic terminal cost has been proposed in the terminal region for car-like non-holonomic robots. Grimm et al. (2005) was a pioneer work which has developed an MPC without stabilizing constraints but with terminal costs for non-holonomic systems. MPC without stabilizing constraints is especially desirable for motion systems, as computing (possibly time varying) terminal regions for large and feasible sets can be a challenging task (Grüne & Pannek, 2017).

For trajectory tracking problem, Hess & Jung (1989) was the first related paper where an MPC tracking controller has been designed (Bai et al., 2019). In a similar way, Ollero & Amidi (1991) have proposed a controller for mobile robots using a linearized and discrete model for prediction. Following the same direction, the term linearized MPC appears in Lages & Alves (2006) and, extending for Linear Time-Varying (LTV) model, Falcone et al. (2007) have proposed an LTV-MPC solution for the problem. Since then, many works have been developed using linearized models for prediction (Raffo et al., 2010; Alexis et al., 2011; Eskandarpour & Sharf, 2020; Santos et al., 2021a). Conversely, since the MPC framework is dependent on the model accuracy, and linearized models may not represent the entire dynamics of the system, after 2000s, researchers have proposed Nonlinear MPC (NMPC) trajectory tracking controllers (Dongbing Gu & Huosheng Hu, 2006; Lim et al., 2008; Kamel et al., 2015; Wang et al., 2017; Murilo & Lopes, 2019; Berntorp et al., 2020; Pereira

et al., 2021a; Santos et al., 2021b). The results of (Kamel et al., 2017), where a linear and nonlinear model predictive controllers for trajectory tracking of Micro Aerial Vehicle (MAV) have been compared, have showed that NMPC has a slightly better disturbance rejection capability, step response, tracking performance, and computational effort.

Several effective MPC strategies for path-following problems can be found in the literature. A primary numerical investigation for non-holonomic robots has been presented in Faulwasser et al. (2009). Generalizations and extensions have been explored in the follow-up works (Alessandretti et al., 2013; Yu et al., 2015; Faulwasser & Findeisen, 2016). Stability and path convergence have been considered with additional stabilizing terminal constraints and terminal costs in all those path-following MPC frameworks. Other recent schemes have been proposed in Liu et al. (2017); Yu et al. (2018); Sanchez et al. (2021); Wohner et al. (2021).

2.3.1 NMPC

Nonlinear Model Predictive Control has become an attractive control research in recent years (Chuong La et al., 2017). The term NMPC is used for an advanced optimal control method, where an optimal control problem with a nonlinear objective function is repeatedly optimized online over a given time horizon subject to a nonlinear process model and nonlinear constraints (Wolf & Marquard, 2016). However, linear model predictive control is yet more popular than NMPC in industrial process, since the use of a linear model together with a quadratic objective function gives rise to a convex problem whose solution is well studied with many available methodologies (Camacho & Bordons, 2007). In addition to theoretical issues related to the main properties of NMPC, such as recursive feasibility, stability and robustness, one of the main drawbacks is the computational time for solving the optimal control problem, particularly for large-scale processes (Wolf & Marquard, 2016). Any delay in computation could lead to a loss of control performance and even instability (Findeisen & Allgöwer, 2004).

However, since there are many situations where processes with strong nonlinearities require often changes in operation regimes, and consequently, the accuracy of the model linearization is compromised, the NMPC must be employed (Camacho & Bordons, 2007). To overcome the issue of computational time, a large number of NMPC schemes have been developed, including hierarchical NMPC schemes (Ellis & Christofides, 2014; Wolf et al., 2014), distributed NMPC schemes (Scattolini, 2009), and NMPC schemes based on triggered evaluations (Zhang et al., 2014; M. Ellis & Christofides, 2015). Especially over the last fifteen years, NMPC schemes based on fast update methods, which approximate the solution of optimal control problems by means of a finite parametric nonlinear program (PNLP), may considerably reduce the computational time (Wolf & Marquard, 2016).

Together with this numerical and computational perspective, stability analysis for

NMPC is widely studied (Chuong La et al., 2017). Stability criteria have been developed for various NMPC scenarios, including infinite horizon control, receding horizon control with zero as terminal constraint (Mayne & Michalska, 1990; Michalska & Mayne, 1993), quadratic terminal costs with regional terminal constraints (Chen & Allgöwer, 1998), and general terminal costs which are control Lyapunov functions (Fontes, 2001; Rawlings et al., 2017; Grüne & Pannek, 2017). Very recent works have focused on the stability of NMPC without terminal cost and terminal constraints (Jadbabaie et al., 2001; Grüne, 2013; Müller & Worthmann, 2017; Köhler et al., 2019). When compared to MPC schemes with stabilizing constraints, MPC schemes without stabilizing constraints are easier to design, involve less computational effort in implementation, and are the popular MPC variant in industrial applications (Mehrez et al., 2020). Furthermore, MPC schemes without stabilizing constraints provide larger stability regions for a fixed prediction horizon than schemes with stabilizing constraints (Grüne & Pannek, 2017). Typically, in this type of MPC, the closed-loop stability is ensured by using bounds on the MPC value function to find a stabilizing prediction horizon length (Tuna et al., 2006; Grüne et al., 2010), or from more recent results involving economic MPC (EMPC), by holding conditions based on dissipativity and controllability properties (Grüne & Stieler, 2014).

When it comes to the latter, the primary goal of the controller is not the stabilization of a precomputed trajectory or steady state, but rather the controller's optimal performance in terms of an economic cost criterion, such as energy or time minimization (Grüne & Pirkelmann, 2020). Additionally, in EMPC, the cost functional usually reflects an economic criterion rather than just a distance to a reference, and as a result, general cost functionals that do not require any a priori structure, such as euclidean norm, can be considered. Since this thesis addresses motion control problems of underactuated vehicles directly on $\mathsf{SE}(3)$, which is a non-euclidean space, and, since it also aims to add fast motion as an economic criterion, the closed-loop stability analysis is based on dissipativity properties, that is usually found in EMPC structures. Therefore, a challenge of this work is to analyze the stability of an NMPC on $\mathsf{SE}(3)$, specially with a non-convex economic cost (or with hard constraints) related to the obstacle avoidance capability. From the best knowledge of the author, these stability analyzes are still an open research field.

2.3.2 Time-Optimal NMPC

Time-optimal control is one of the oldest classes of optimal control problems, in both continuous and discrete-time, and there is a wide literature on this subject (Verschueren et al., 2017). Classical indirect optimal control methods are based on the calculus of variations (Athans & Falb, 1966) and assume some properties on the optimal control a priori (for example, a bang-bang structure, i.e., the controls are often at their limits). Kalman (1960) has been the first to derive a time-optimal controller for linear time-

invariant (LTI) systems for problems in discrete-time, known as the dead-beat control. However, in the case of nonlinear systems, it is more complex to compute a time-optimal control law in closed form. Nesic et al. (1998) have presented a solution for some special classes of nonlinear systems. Accordingly, many recent approaches using a receding horizon technique focused on direct methods that solve the underlying optimal control problem through a finite parameter nonlinear program (Rosmann et al., 2017).

MPC with the purpose of improving the response time is called Time-Optimal MPC (TOMPC), whose goal is to drive the states/outputs of the system from a given initial condition to the target region in the shortest time steps while satisfying the input and state constraints (Ma et al., 2019). In Mayne & Schroeder (1997), a TOMPC subjected to constraints on inputs and states have been proposed for discrete-time linear systems. The achieved online computational cost is small, and the system state can be stabilized into the target region in the shortest time steps. However, its application to high order systems is limited since the method uses the Minkowski sum and the Minkowski difference. Note that the computational complexity of both operations gradually increases as the system order increases. In the application context, TOMPC has been the basis of several works. Some of them tackles point-to-point motion, while others concern the path following problem.

For the first group, Van den Broeck et al. (2011) have proposed a two-layer time-optimal MPC method for linear systems. The upper layer computes the optimal horizon length, while the lower layer is a tracking MPC with fixed horizon length. However, the horizon length can change along the system control, i.e. at each sample time the size of the OCP changes. Another straightforward type of strategy to solve the problem is to introduce a time transformation, called time scaling approach (where the horizon length is a decision variable), as proposed by Zhao et al. (2004); Afonso et al. (2020). Besides, the method requires a switch of the controller for a standard regulator NMPC when the system is close to the desired endpoint, keeping the horizon length fixed. Following a similar idea, Rösmann et al. (2015) have proposed a TONMPC scheme, where the continuous dynamics are scaled with a constant factor, such that the horizon becomes fixed. To garantee time-optimality, the scaling factor is regarded in the objective function linearly. Nonetheless, approaches using these time-scaled dynamics becomes nonlinear even for linear systems, and their stability proof is not analysed in the literature (Verschueren et al., 2017). In more recent works, a fixed horizon strategy for TONMPC, with general stability proof of the endpoint (origin) given and time-optimality established, has been proposed by Verschueren et al. (2017). The method is formulated using an exponential increase in stage costs along the horizon, based on the idea presented in Van den Broeck et al. (2010). The stage cost, defined as the l_1 norm of the stage error, has an exponential weight that encourages the motion to arrive at the end point as soon as possible, recovering therefore the time-optimality.

Conversely, in other works, the time-optimal control task does not aim to move from

one point to another, but to follow or remain within a path (Lipp & Boyd, 2014). Examples include control of computer numerical control (CNC) machines and welding robots in industrial manufacturing, where these systems must perform geometric tasks as quickly as possible in order to improve production efficiency. In addition, other important field of application is autonomous vehicle racing, where competitors must complete the geometric circuit as fast as possible. In contrast to the traditional path following, the application of driving time-optimally means to deviate largely from a nominal path (e.g. the center-line of the race track) in order to save time (Verschueren et al., 2016; Wohner et al., 2021). Due to the inherent antagonism of driving safety and fast, the MPC formulations that aim for minimum-time driving while meeting constraints, such as the limits of the race track, tend to be especially challenging (Verschueren et al., 2014). The traditional time-optimal driving solution approach consists of a two-level scheme, as presented in Liniger et al. (2015) (small-scale race cars), and Kritayakirana & Gerdes (2012) (full-scale racing car). In this kind of strategies, the dynamic optimization routine computes the optimal geometric trajectory at a higher level, while the lower level tracking controller uses the resulting trajectory as a time-dependent reference. Kehrle et al. (2011); Rucco et al. (2015) have proposed a one-level approach. A real-time NMPC scheme is presented in Verschueren et al. (2014), where the time-optimal problem has been reformulated as a path-parametric system, as proposed in Frasch et al. (2013). In contrast to Verschueren et al. (2014, 2016), Wohner et al. (2021) have solved a nonlinear economic MPC (EMPC) problem directly, taking into account a more sophisticated nonlinear vehicle dynamic model without requiring high computational complexity.

In contrast to these works, this thesis proposes an NMPC scheme in which mission time is viewed as an economic criterion, rather than the time-optimal solution. The proposed formulation is based on the exponential weighting of the stage cost, which is an adapted version of the fixed horizon strategy proposed by Verschueren et al. (2017). According to Theorem 1 of Verschueren et al. (2017), the time-optimality is guaranteed only for prediction horizons greater or equal to the time-optimal solution of the problem. Since for motion control problems the time-optimal definition mainly depends on the distance that the vehicle must travel, which can be a large value, this work does not focus on the time-optimal solution. As a result, the exponential weight is used as a tuning gain that makes the motion faster.

2.3.3 MPC for obstacle avoidance

Recently, MPC architectures have been applied to autonomous navigation systems, providing efficient collision-avoidance capability, and easily extended to robust and nonlinear systems (Hoy et al., 2015). In these cases, a trajectory planner is not necessary, and the vehicle is able of executing obstacle avoidance on-line while it autonomously navigates

in cluttered environments with unknown obstacles. Typically autonomous navigation is handled through a hierarchical combination of planning and control layers (Castillo-Lopez et al., 2018b), since this kind of strategy presents good performance and low computational cost. However, these approaches usually present inappropriate coordination between the layers, and hence, often lead to inefficient or dangerous situations (Shim et al., 2003). In addition, as MPC is able to consider non-convex constraints such as obstacles to generate feasible trajectories, the unified navigation framework is safer and less prone to local minima than hierarchical approaches (Shim et al., 2003).

One of the precursors in combining an MPC framework and obstacle avoidance has presented an NMPC scheme for multiple autonomous helicopters in complex environments (Shim et al., 2003). In this work, potential functions have been included into the optimization problem, which has been solved with a gradient-descent method. Since then, many works have been developed to improve the collision avoidance (Liu et al., 2017; Ioan et al., 2019; Castillo-Lopez et al., 2018a; Nascimento et al., 2019; Sanchez et al., 2021; Santos et al., 2021a,b), the computational cost (Dentler et al., 2016; Marzat et al., 2017; Sathya et al., 2018; Small et al., 2019; Hermans et al., 2018), the robustness against uncertainties (Alexis et al., 2016; Andersson et al., 2016; Garimella et al., 2017; Jardine & Givigi, 2019), and the application on dynamics obstacles and multi-agent scenarios (Nascimento et al., 2014; Kamel et al., 2017; Castillo-Lopez et al., 2018b; Pacheco et al., 2020; Pereira et al., 2021c).

The kind of set used to represent a motion system leads to a trade off between the object representation's accuracy and the computational burden involved to handle it for control purposes. In the case of collision avoidance, the problem usually involves just the intersection set operation. Specifically, it concerns on the conditions under the intersection between the sets occurs, as well as the existence of an algebraic condition for the intersection verification. In the NMPC with obstacle avoidance capability, the latter becomes essential since the intersection condition must be included in the optimization framework according to the predicted system states.

In this context, Liu et al. (2017) have proposed an NMPC strategy for an Autonomous Ground Vehicle (AGV) navigating in 2D environments with obstacles represented as polygons, which are detected by planar light sensor (LIDAR), based on computational geometry algorithms, to obtain linear constraints. Following this direction, Nascimento et al. (2019); Nascimento (2019) have presented an NMPC for a UAV in a 3D unknown environment. However, unlike Liu et al. (2017), the authors modeled obstacles as polyhedra, explored convex decomposition for computational simplification, and generalized the solution, allowing its application in other types of system. Ioan et al. (2019) have proposed a navigation strategy based on linear MPC with obstacle avoidance guarantees using local zonotopic approximations to cover efficiently the non-convex region of interest. In Castillo-Lopez et al. (2018a), a linear MPC has been also proposed, but with obstacles

modeled as ellipsoid, and collision avoidance defined as a hard constraint, where the framework guarantees that the UAV, modeled as a point-mass, does not belong to any obstacle set in each horizon window. Similarly, i.e., considering the UAV as a point-mass and ellipsoidal obstacles, Santos (2018); Santos et al. (2021a) designed a linear MPC controller with economic criteria for obstacle avoidance, with attraction and repulsion potential functions added in the cost functional. Local minimum is a natural limitation coming from the situations where both path following and obstacle avoidance strategies yield antagonist system reactions (Sanchez et al., 2019). Concerning this matter, Sanchez et al. (2021); Santos et al. (2021b) have proposed an NMPC framework using artificial variables and including a new forward constraint in the optimization problem.

The presence of obstacle constraints makes the MPC computation even more difficult to solve (Small et al., 2019), which can frustrate attempts at real-time implementation. As a result, some works focus on solving this limitation. Dentler et al. (2016) have presented an MPC based on a condensed multiple-shooting continuation generalized minimal residual method (CMSCGMRES) with obstacle avoidance implemented using sigmoid functions. Their experiments have shown the computational efficiency for quadrotor UAV navigation where the measured maximum computation time was less than 2 ms. Also for UAV safe navigation, Marzat et al. (2017) have developed a linear MPC used to track a reference trajectory of a UAV, where depending on the risk of collision, a new optimal control problem (OCP) is solved with an extra cost to penalize the proximity with obstacles. The authors have shown experimental results by applying the strategy to a quadrotor UAV, and consequently, demonstrating the computational capabilities. Hermans et al. (2018); Small et al. (2019); Sathya et al. (2018) have followed this same direction, but proposing nonlinear MPCs using PANOC method. This fast numerical optimization method is not sensitive to ill conditioning, involves only simple algebraic operations, and is suitable for embedded NMPC. These works have proposed a novel constraint formulation to incorporate general obstacle shapes, described as the intersection of a set of nonlinear inequalities. Then, in the optimization problem, the obstacle avoidance constraints have been written as a nonlinear equality constraint involving a smooth function which, in turn, has been relaxed by the use of a penalty function. Small et al. (2019) have applied experimentally the proposed control scheme to an inverted quadrotor, achieving a control rate of 20 Hz, while Sathya et al. (2018) have applied to a mobile robot carrying a trailer with a control rate of 10 Hz.

Other important issue is the guarantee of flight robustness against disturbances present in real–time implementations, such as sensor noises, inaccurate measurements, modeling mismatches (parametric uncertainties and unmodeled dynamic). Some recent works have proposed solutions related to stochastic trajectory optimization perspective by drawing upon techniques from machine learning. Andersson et al. (2016) have combined policy search with MPC, allowing the use of recent constrained MPC solvers while gaining the stochastic properties of policy-based methods. Heirung et al. (2019) have proposed an

MPC with active learning based on Bayesian decision theory for stochastic nonlinear systems with structural model uncertainty. In Garimella et al. (2017), a learned model has been employed in an NMPC framework, where the uncertainty of both model parameter and initial state are computed as high-confidence ellipsoids in pose space. Also, Jardine & Givigi (2019) have proposed a robust, stable, linear MPC for UAVs to perform obstacle avoidance by generating linear constraints in the XY plane by geometric calculations, considering bounded disturbances.

Although having relevant results, all these MPC schemes consider the motion system as a single point mass or a spherical set in the collision avoidance framework. Therefore, they do not explore changes in the orientation of the mechanical structure during the navigation, that is, the motion system's pose is neglected. As a result, such systems cannot perform aggressive maneuvers that necessarily require a change of their attitude.

2.3.4 MPC for underactuated systems

It is well-known that MPC has also been used to control underactuated vehicles, e.g., Raffo et al. (2010); Kunz et al. (2013); Alexis et al. (2014); Li & Yan (2017); Eskandarpour & Sharf (2020); Liang et al. (2021), due to its ability to handle constrained multiple-input multiple-output nonlinear systems regarding optimal criteria. However, most of the works found in the literature use local attitude parametrization, such as Euler-angles, and split the problem into outer and inner layers, or attitude and position control, separately (Raffo et al., 2010; Alexis et al., 2014; Eskandarpour & Sharf, 2020). Such a separation can be undesirable in complex tasks such as those involving optimal functional cost depending on position and attitude references simultaneously. Motivated by this, Murilo & Lopes (2019) have proposed a unified parameterized NMPC framework to address the attitude and position control problem of the quadrotor UAV. Nevertheless, the controller proposed by them can also suffer from singularities, and, consequently, it is just locally effective. In Wehbeh & Sharf (2022), a unified scheme has been also proposed for trajectory tracking of quadrotor UAV. Although the authors have developed a time-dependent linearization on the Lie algebra of $\mathsf{SO}(3)$, which avoids singularities, and with applicable outcomes, the feasibility and closed-loop stability of the control strategy, which are essential for practical application, are not ensured by the authors.

For simplified and linearized models, e.g., Eskandarpour & Sharf (2020), the feasibility and closed-loop stability analysis of the MPC is usually provided. However, for NMPC strategies that consider the complete nonlinear model of the underactuated vehicle, these analysis is quite limited (Liang et al., 2021). The fundamental reason is that the classical MPC with terminal constraints generally requires a locally continuous time-invariant state feedback controller to ensure system stability (Mayne et al., 2000), but according to Brockett's theorem (Brockett, 1983), there is no such feedback controller for underactuated

systems. Moving forward on solving this limitation, Li & Yan (2017) have proposed an NMPC scheme for motion control of underactuated marine vehicles that considers a transformed model with homogeneity properties obtained by introducing the homogeneous coordinates. Although such a transformation can yield a controller with exponential convergence capabilities, the NMPC law based on the converted model requires changing the control law back, which is inconvenient for implementation. In Liang et al. (2021), an NMPC with terminal constraints has been presented for tracking control of underactuated marine vehicle. The main idea has been to develop an auxiliary time-varying tracking controller to aid terminal constraint in the optimal control problem, based on Lyapunov's direct method and backstepping approach. However, the controller has been developed for underactuated vehicles moving in two dimensional Euclidean space, which is simpler than the problem in three dimensional space. Another possibility to overcome the aforementioned stability requirement, that is, a locally continuous time-invariant state feedback controller, is to work with NMPC frameworks without terminal conditions, that is, without terminal constraints and/or costs, which is one of the focus of this study.

2.3.5 MPC for UAV

MPC is a well-established method of optimal control usually for industrial applications and more recently for UAV flight control (Johansen, 2017). In addition to all the above-mentioned advantages, MPC can simply deal with multivariate underactuated systems. Therefore, it has been considered for several UAV configurations to solve flight control problems, such as unmanned helicopters (Liu et al., 2012; Kunz et al., 2013; Gong, 2019), quadrotors (Raffo et al., 2010; Nascimento et al., 2019; Small et al., 2019; Eskandarpour & Sharf, 2020; Santos et al., 2021a,b), unmanned fixed-wing (Kang & Hedrick, 2009; Rucco et al., 2016; Stastny et al., 2017; Reinhardt & Johansen, 2019; Pereira et al., 2021c), and unmanned tilt-rotors (Papachristos et al., 2013; Andrade et al., 2016; Santos et al., 2017, 2018).

2.4 Final Remarks

This chapter presented the main works related to the thesis problem. First an overview of aggressive maneuvers was presented, followed by classical obstacle-avoidance methods used in autonomous navigation. The aim of Section 2.3 was to present MPC works contextualized with motion systems, obstacle avoidance, and underactuated vehicles. In addition, a literature review on NMPC and TONMPC was presented in this section.

3 Mathematical Preliminaries

This chapter presents a mathematical background to the thesis subject. First, the characterization of rigid body systems is described on $\mathsf{SE}(3)$, providing the main properties of the $\mathsf{SE}(3)$ manifold, followed by the equations of motion of the class of underactuated vehicles that is investigated. In the second part, the most important concepts and issues involving numerical solutions of optimal control problems are described. The last part reviews dissipativity-based analysis for MPC.

3.1 Rigid Body Systems

This section is concerned with the establishment of coordinate systems to represent the position and orientation of rigid bodies, and transformations among these coordinate systems. All the presented concepts and definitions are based on Murray et al. (1994) and Lee et al. (2018).

3.1.1 Manifold concepts

Differential equations are usually used to describe dynamic systems. In most of the cases, the system variables can be viewed as elements of a finite-dimensional vector space, such as $\mathbb{R}^n$. However, some systems are better represented by different mathematical structures, specifically, by a manifold structure. This subsection introduces a summary of manifold concepts, focusing on manifolds related to rigid motion.

3.1.1.1 Manifolds

Let $\mathsf{H} \subset \mathbb{R}^n$ and $\mathsf{V} \subset \mathbb{R}^m$ be open sets. A mapping $\Phi : \mathsf{H} \to \mathsf{V}$ is a smooth map if all partial derivatives of Φ, of any order, exist and are continuous. If $m = n$, Φ is bijective, and both Φ and Φ^{-1} are smooth, then Φ is called a diffeomorphism, and H and V are said to be diffeomorphic.

Definition 3.1. A manifold of dimension m is a set M which is locally diffeomorphic to $\mathbb{R}^m$, that is, each point in a neighborhood of a point $p \in \mathsf{M}$ can be described as a point in $\mathbb{R}^m$.

Another definition states that finite-dimensional differentiable manifolds are sets with a differential geometric structure that can be analyzed using calculus. Globally, the geometry of the manifold is quite different from the linear geometry of $\mathbb{R}^m$. For this reason, although local representation is commonly used in the literature, this thesis intend to explore the global properties of the $\mathsf{SE}(3)$ manifold, which allow to represent motion systems globally and uniquely.

3.1.1.2 Tangent vectors, tangent spaces and tangent bundles

Consider a manifold M with dimension m, and a differential curve γ on M with $\gamma(0) = x \in \mathsf{M}$, where $\gamma : [-1, 1] \to \mathsf{M}$. Then, $\frac{d\gamma(s)}{ds}$, evaluated at $s = 0$, is a tangent vector to M at $x \in \mathsf{M}$. The tangent space of M at $x \in \mathsf{M}$, denoted by $\mathsf{T}_x\mathsf{M}$, is the set of all tangent vectors to M at $x \in \mathsf{M}$, which is a subspace of $\mathbb{R}^n$, and, consequently, it is a linear manifold. Therefore, the tangent space, with dimension $n - m$, is equivalent to the set of vectors in $\mathbb{R}^n$ that are orthogonal to all gradients of the functions that define the manifold. In addition, the tangent bundle of a manifold M, which has its own manifold structure, is the set of pairs $(x, \varrho) \in \mathsf{M} \times \mathsf{T}_x\mathsf{M}$. It is denoted by TM and has dimension $2(n - m)$.

To better describe these definitions, consider the unit sphere S^2, shown in Figure 3.1, as an example of a two-dimensional manifold embedded in $\mathbb{R}^3$ given by

$$\mathsf{S}^2 \triangleq \{q \in \mathbb{R}^3 : \|q\|^2 = 1\}.$$

For any $q \in \mathsf{S}^2$, the tangent space to S^2 at $q \in \mathsf{S}^2$ is a two-dimensional vector space described as

$$\mathsf{T}_q\mathsf{S}^2 \triangleq \{\varrho \in \mathbb{R}^3 : q \cdot \varrho = 0\}.$$

The tangent bundle of S^2, which is a four-dimensional vector space, is given by

$$\mathsf{TS}^2 \triangleq \{(q, \varrho) \in \mathbb{R}^3 \times \mathbb{R}^3 : q \in \mathsf{S}^2, \varrho \in \mathsf{T}_q\mathsf{S}^2\}.$$

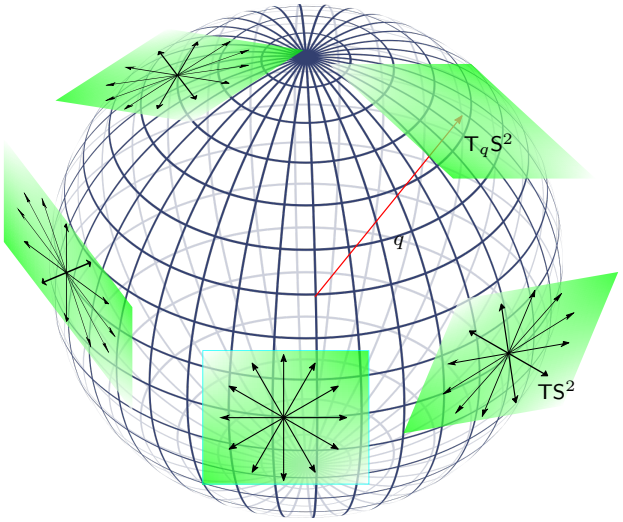


Figura 3.1: Tangent space and tangent bundle on the unit sphere S^2 manifold.

3.1.1.3 Lie Groups and Lie Algebras

Although the generality of the mathematical theory of Lie groups and Lie algebra, this thesis uses only concepts of matrix Lie groups and Lie algebras. A matrix Lie group, denoted by G, is a subset of $\mathsf{GL}(\mathsf{n})$, the set of all $n \times n$ real invertible matrices, which is also a matrix Lie group. It satisfies both group and manifold properties.

Definition 3.2. A matrix G together with matrix product operation is called group if it satisfies the following axioms:

1. *Closure*: If $\mathsf{G}_1, \mathsf{G}_2 \in \mathsf{G}$, then $\mathsf{G}_1\mathsf{G}_2 \in \mathsf{G}$.

2. *Identity*: The identity matrix, I_n, is the group identity such that $\mathsf{G}_1 I_n = I_n \mathsf{G}_1 = \mathsf{G}_1$ for every $\mathsf{G}_1 \in \mathsf{G}$.

3. *Inverse*: For each $\mathsf{G}_1 \in \mathsf{G}$, there exists an (unique) inverse, $\mathsf{G}_1^{-1} \in \mathsf{G}$, such that $\mathsf{G}_1\mathsf{G}_1^{-1} = \mathsf{G}_1^{-1}\mathsf{G}_1 = I_n$.

4. *Associativity*: If $\mathsf{G}_1, \mathsf{G}_2, \mathsf{G}_3 \in \mathsf{G}$, then $(\mathsf{G}_1\mathsf{G}_2)\mathsf{G}_3 = \mathsf{G}_1(\mathsf{G}_2\mathsf{G}_3)$.

An important subset of $\mathsf{GL}(\mathsf{n})$ is the set of real $n \times n$ orthogonal matrices with determinant $+1$, referred to as special orthogonal group, denoted by $\mathsf{SO}(n)$. In particular, the matrix Lie group $\mathsf{SO}(3)$ is usually used to describe physical objects that exist in three-dimensional space. There is a close connection between $\mathsf{SO}(3)$ and the vector space of all 3×3 skew-symmetric matrices, denoted by $\mathfrak{so}(3)$. A skew-symmetric matrix $S \in \mathbb{R}^{n \times n}$ has the property that $S + S^\top = 0$. The linear transformation map $\mathcal{S}(\cdot) : \mathbb{R}^3 \to \mathfrak{so}(3)$ is given by

$$\mathcal{S}(x) = \begin{bmatrix} 0 & -x_3 & x_2 \\ x_3 & 0 & -x_1 \\ -x_2 & x_1 & 0 \end{bmatrix},$$

such that for $x, y \in \mathbb{R}^3$, $x \times y = \mathcal{S}(x)y$. It can be verified that an orthogonal matrix can be expressed in terms of a skew-symmetric matrix. An orthogonal matrix $R \in \mathsf{SO(3)}$ can be represented in terms of the matrix exponential map

$$R = e^{\nu} = \sum_{n=0}^{\infty} \frac{\nu^n}{n!}, \tag{3.1}$$

where $\nu \in \mathfrak{so}(3)$. This relationship can also be done by the Cayley transformation

$$R = (I_3 - \nu)(I_3 + \nu)^{-1}. \tag{3.2}$$

This close association between the Lie group $\mathsf{SO(3)}$ and the vector space $\mathfrak{so}(3)$ is formalized by referring to $\mathfrak{so}(3)$ as the Lie algebra associated with the Lie group $\mathsf{SO(3)}$. Geometrically, the Lie algebra can be interpreted as the tangent space at the identity of the group. Therefore, $\mathfrak{so}(3)$ is the tangent space of $\mathsf{SO(3)}$ at the identity matrix, namely $\mathsf{T}_{I_3}\mathsf{SO(3)}$.

It can be shown that the Special Euclidean group $\mathsf{SE(3)}$, defined by an ordered pair $(R, \xi) \in \mathsf{SE(3)} \triangleq \mathsf{SO(3)} \ltimes \mathbb{R}^3$, is a six-dimensional manifold embedded in the Lie group $\mathsf{GL(4)}$. For any $(R, \xi) \in \mathsf{SE(3)}$, the tangent space, denoted by $\mathsf{T}_{(R,\xi)}\mathsf{SE(3)}$, is given by

$$\mathsf{T}_{(R,\xi)}\mathsf{SE(3)} \triangleq \{(R\nu, y) \in \mathbb{R}^{3\times 3} \times \mathbb{R}^3 : \nu \in \mathfrak{so}(3)\}.$$

The tangent bundle of $\mathsf{SE(3)}$ is defined as

$$\mathsf{TSE(3)} \triangleq \{(R, x, R\nu, y) \in \mathsf{SE(3)} \times \mathbb{R}^{3\times 3} \times \mathbb{R}^3\},$$

which is a twelve-dimensional manifold, with $R\nu$ being a three-dimensional subspace. As a result, the tangent bundle of $\mathsf{SE(3)}$ can also be written as

$$\mathsf{TSE(3)} \triangleq \{(R, x, \nu, y) \in \mathsf{SE(3)} \times \mathbb{R}^3 \times \mathbb{R}^3\}.$$

The vector space $\mathfrak{se}(3) \triangleq \mathfrak{so}(3) \times \mathbb{R}^3$ is the tangent space of $\mathsf{SE(3)}$ at I_4, that is, considering $R = I_3$ and $\xi = \mathbf{0}_{3\times 1}$. Thus, $\mathfrak{se}(3)$ is the Lie algebra associated with the Lie group $\mathsf{SE(3)}$. Locally, the analysis on both $\mathsf{SO(3)}$ and $\mathsf{SE(3)}$ can be translated into the analysis on the associated Lie algebra, $\mathfrak{so}(3)$ and $\mathfrak{se}(3)$ respectively.

3.1.2 Rigid transformation

A rigid body can be interpreted as a body with fixed dimensions, where deformations never occur. From a more formal perspective, a *rigid body* is defined as a collection of particles such that the distance between any two particles remains fixed, regardless of any motion of the body or forces exerted on the body. When a rigid body moves from one location to another, via rotation and translation movements in the space, the terms *rigid*

motion (continuous movement) and *rigid displacement* (point-to-point movement) come out. In order to mathematically characterize the *rigid motion*, the definition of *rigid body transformation* as a mapping from $\mathbb{R}^3$ to $\mathbb{R}^3$ is presented.

Definition 3.3. (Murray et al., 1994). Given an object that is described as a set $\mathcal{O} \subseteq \mathbb{R}^3$, and two points $p, q \in \mathcal{O}$. A mapping $g : \mathbb{R}^3 \to \mathbb{R}^3$ is a *rigid body transformation* if it satisfies the following properties:

1. Length is preserved: $\|g(p) - g(q)\| = \|p - q\|$ for all points $p, q \in \mathbb{R}^3$.
2. The cross product is preserved: $g_*(v \times w) = g_*(v) \times g_*(w)$ for all vectors $v, w \in \mathbb{R}^3$, where vectors transform according to $g_*(v) = g(q) - g(p)$.

The *configuration* of a rigid body is represented by a Cartesian coordinate frame attached to some point on the rigid body, from which the motion of this rigid body coordinate frame relative to a fixed frame can be tracked. All coordinate frames are required to be *right-handed*: given three orthonormal vectors $x, y, z \in \mathbb{R}^3$ which define a coordinate frame, they must satisfy $z = x \times y$. Therefore, if the configuration of a rigid body is a right-handed frame, given by the vectors v_1, v_2, v_3 attached to a point p, then the configuration of the rigid body, after the rigid body transformation g, is given by the right-handed frame of vectors $g_*(v_1), g_*(v_2), g_*(v_3)$ attached to the point g(p).

3.1.3 Rotation motion in $\mathbb{R}^3$

In this section, just pure rotation is considered as a rigid motion. The orientation of the body is given by the relative orientation between a coordinate frame attached to the body and an inertial coordinate frame. Let $\mathcal{I}$ be the inertial frame, $\mathcal{B}$ the body frame, and $x_{\mathcal{B}}^{\mathcal{I}}, y_{\mathcal{B}}^{\mathcal{I}}, z_{\mathcal{B}}^{\mathcal{I}} \in \mathbb{R}^3$ the coordinates of the principal axes of $\mathcal{B}$ relative to $\mathcal{I}$, as exemplified in Figure 3.2, concatenating horizontally these coordinate vectors. Thus, the rotation matrix[1] $R_{\mathcal{B}}^{\mathcal{I}} \in \mathsf{SO(3)}$ is defined as

$$R_{\mathcal{B}}^{\mathcal{I}} = \begin{bmatrix} x_{\mathcal{B}}^{\mathcal{I}} & y_{\mathcal{B}}^{\mathcal{I}} & z_{\mathcal{B}}^{\mathcal{I}} \end{bmatrix}.$$

3.1.3.1 Representational singularities

Representational singularities or mathematical singularities are related to the multiple solution regions at the inverse transformation problem, not concerning to physical limitations of the rigid body (Lee, 2015). A fundamental topological fact is that representational singularities can never be eliminated in any local representation of $\mathsf{SO(3)}$. Euler angles are an example of a local parameterization of $\mathsf{SO(3)}$. As in the case of the equivalent axis representation, singularities in the parameterization (as it is also known) referred to the

[1] For more information on rotation matrices, see Appendix A.

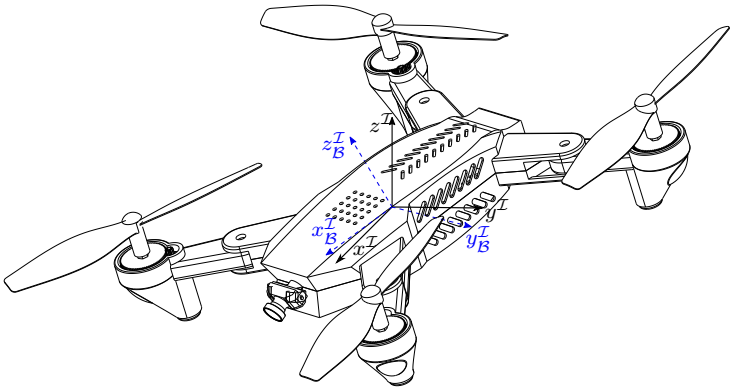


Figura 3.2: Rotation of a rigid body about a point.

lack of existence of global, smooth solutions to the inverse problem of determining the parameters from the rotation. In the case of equivalent axis representation, the singularity occurs for $R = I_3$, alluding to the fact that is not possible to find an equivalent axis as a function of the orientation R at this condition. Although Euler angle parameterizations have the advantage of not having singularity at the identity orientation, they do contain singularities at other, different, orientations. For example, the ZYX Euler angles, given by

$$R^{\mathcal{I}}_{\mathcal{B}} = R_z(\psi)R_y(\theta)R_x(\phi) = e^{\hat{z}\psi}e^{\hat{y}\theta}e^{\hat{z}\phi},$$

are singular when $\theta = -\pi/2$. In addition, they are undesirable because there are some orientations in space where infinite rotational rates are required to produce finite angular velocity and acceleration of the rigid body (Paul, 1981). This behavior can be seem when it is necessary to obtain the derivative of the Euler angles from the angular velocity of the rigid body, for instance given by

$$\begin{bmatrix} \dot{\phi} \\ \dot{\theta} \\ \dot{\psi} \end{bmatrix} = \begin{bmatrix} 1 & \sin(\phi)\tan(\theta) & \cos(\phi)\tan(\theta) \\ 0 & \cos(\phi) & -\sin(\phi) \\ 0 & \sin(\phi)\sec(\theta) & \cos(\phi)\sec(\theta) \end{bmatrix} \begin{bmatrix} p \\ q \\ r \end{bmatrix},$$

where the mapping is discontinuous and gives infinite rotational rates when θ is near to $\pi/2$.

3.1.3.2 Attitude error function on $\mathsf{SO}(3)$

Although a system modeled by a rotation matrix $R \in \mathsf{SO}(3)$ does not have representational singularities, choosing a positive definite error function that measures the difference between two configurations is a critical step in the control design. Consider the i-th configuration error function is defined as (Lee, 2015)

$$\Psi_i(R, R_d) = \frac{1}{2}\|Re_i - R_d e_i\|^2 = 1 - Re_i \cdot R_d e_i, \tag{3.3}$$

where $e_i \in \mathsf{S}^2 \triangleq \{q \in \mathbb{R}^3 : \|q\|^2 = 1\}$ is a unit-vector starting from the mass center of the rigid body. Let e_1, e_2 be normal to each other. Then, for positive constants $k_i > 0$, the complete configuration error function is given by (Lee, 2015)

$$\Psi(R, R_d) = k_1 \Psi_1(R) + k_2 \Psi_2(R). \tag{3.4}$$

It can be noticed that $\Psi_i(R, R_d)$ represents the geometric projection between Re_i and $R_d e_i$, and $\Psi_i(R, R_d)$ is positive definite about $Re_i = R_d e_i$. Therefore, the complete configuration error $\Psi(R, R_d)$, given by (3.4), is positive definite about $R = R_d$, that is, $\Psi(R, R_d) \geq 0$, and $\Psi(R, R_d) = 0$ if only if $R = R_d$.

3.1.4 Rigid motion in $\mathbb{R}^3$

In general, rigid motions are composed by rotations and translations. The previous subsection concerned about pure rotational movements. The representation of pure translational motion is simpler: choose a point in the body and keep tracking the coordinates of this point relative to some known frame. Nevertheless, there is more involvement in the representation of general rigid motion when both translation and rotation occur. The attitude and position of the motion system illustrated in Figure 3.3 are described by a coordinate frame $\mathcal{B}$ attached to the body relative to an inertial frame $\mathcal{I}$. Let $\xi^{\mathcal{I}} \in \mathbb{R}^3$ be the position vector of the origin of frame $\mathcal{B}$ from the origin of frame $\mathcal{I}$, and let $R^{\mathcal{I}}_{\mathcal{B}} \in \mathsf{SO(3)}$ be the attitude of frame $\mathcal{B}$ relative to frame $\mathcal{I}$. Thus, the pair $(R^{\mathcal{I}}_{\mathcal{B}}, \xi^{\mathcal{I}}) \in \mathsf{SE(3)}$ composes the configuration of the motion system.

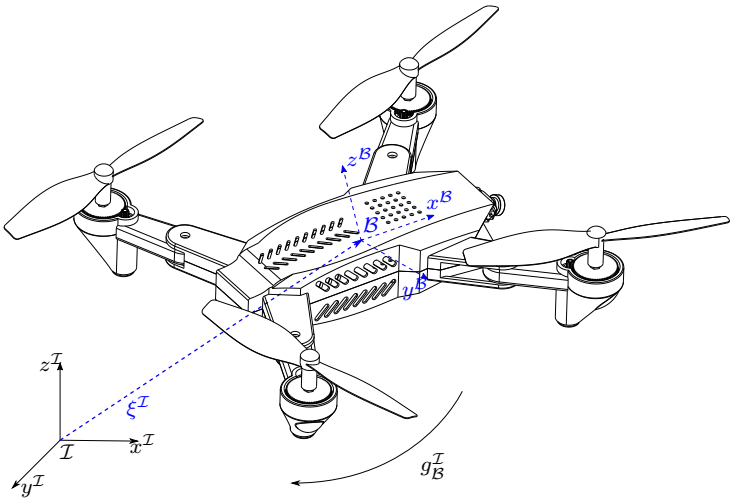


Figura 3.3: Coordinate frames for rigid motion specification.

Analogously to the rotational motion, an element $(R^{\mathcal{I}}_{\mathcal{B}}, \xi^{\mathcal{I}}) \in \mathsf{SE(3)}$ is used for both definition of rigid body configuration and transformation of a point from one frame to another. Let $q^{\mathcal{I}}, q^{\mathcal{B}} \in \mathbb{R}^3$ be the coordinates of a point q relative to frames $\mathcal{I}$ and $\mathcal{B}$, respectively. Given $q^{\mathcal{B}}$, the coordinate $q^{\mathcal{I}}$ can be found by a transformation of coordinates,

as follows

$$q^{\mathcal{I}} = \xi^{\mathcal{I}} + R^{\mathcal{I}}_{\mathcal{B}} q^{\mathcal{B}},$$

where $g^{\mathcal{I}}_{\mathcal{B}} = (R^{\mathcal{I}}_{\mathcal{B}}, \xi^{\mathcal{I}}) \in \mathsf{SE}(3)$ is the configuration of frame $\mathcal{B}$ relative to frame $\mathcal{I}$.

3.2 Dynamics of Underactuated Motion System on SE(3)

This section details the mathematical model of a class of underactuated vehicles that is investigated in this work. In these underactuated systems, the control force vector is applied in a body-fixed direction, with full attitude control and only one translational force input, that is, with four independent control inputs for the six DOF of translational and rotational motions in three dimensional Euclidean space. This actuation model formulated on $\mathsf{SE}(3)$ covers a wide range of vehicles such as helicopters, multi-propeller helicopters, ducted fans, underwater vehicles, and satellites.

The configuration manifold is represented by the ordered pair $(R^{\mathcal{I}}_{\mathcal{B}}, \xi^{\mathcal{I}}) \in \mathsf{SE}(3)$, where the rotation matrix $R^{\mathcal{I}}_{\mathcal{B}} \in \mathsf{SO}(3)$ describes the rigid body's attitude and $\xi^{\mathcal{I}} \in \mathbb{R}^3$ is a vector describing the position of center of mass of the vehicle. The state space of the system is $\mathsf{TSE}(3)$, which is the tangent bundle of $\mathsf{SE}(3)$. Thus, the dynamics[2] of the motion system can be viewed through the evolution of the states $x \triangleq (R^{\mathcal{I}}_{\mathcal{B}}, \xi^{\mathcal{I}}, \omega^{\mathcal{B}}, v^{\mathcal{I}}) \in \mathsf{TSE}(3)$. The continuous-time equations of motion are (Kobilarov, 2013)

$$\dot{\xi}^{\mathcal{I}} = v^{\mathcal{I}}, \tag{3.5}$$

$$m\dot{v}^{\mathcal{I}} = f^{\mathcal{I}} = R^{\mathcal{I}}_{\mathcal{B}} e^{\mathcal{B}} T + f^{\mathcal{I}}_e(\xi^{\mathcal{I}}, v^{\mathcal{I}}), \tag{3.6}$$

$$\dot{R}^{\mathcal{I}}_{\mathcal{B}} = R^{\mathcal{I}}_{\mathcal{B}} \mathcal{S}(\omega^{\mathcal{B}}), \tag{3.7}$$

$$J\dot{\omega}^{\mathcal{B}} = -\omega^{\mathcal{B}} \times J^{\mathcal{B}}\omega^{\mathcal{B}} + \tau^{\mathcal{B}} + \tau^{\mathcal{B}}_e(x), \tag{3.8}$$

where $T \in \mathbb{R}$ is a control force applied in a body-fixed direction defined by the unit vector $e^{\mathcal{B}} \in \mathbb{R}^3$, $\tau^{\mathcal{B}} \in \mathbb{R}^3$ is the control torque expressed in the body frame $\mathcal{B}$, both applied in the center of mass of the motion system, $v^{\mathcal{I}} \in \mathbb{R}^3$ is the linear velocity of the center of mass, $\omega^{\mathcal{B}} \in \mathbb{R}^3$ is the angular velocity of the body with respect to $\mathcal{I}$, expressed in $\mathcal{B}$, $\mathcal{S}(\omega^{\mathcal{B}}) \in \mathfrak{so}(3)$, m is the total mass of the motion system, and J is the inertia tensor. The vehicle is subjected to known external forces and torques given by the functions $f^{\mathcal{I}}_e : \mathbb{R}^3 \times \mathbb{R}^3 \to \mathbb{R}^3$ and $\tau^{\mathcal{B}}_e : \mathrm{TSE}(3) \to \mathbb{R}^3$, respectively.

[2]For more information on Newton-Euler dynamics equations for a single rigid body on $\mathsf{SE}(3)$, see Appendix B.

3.2.1 System discretization

The Euler method is used to discretize the dynamic equations (3.5) and (3.6) considering that the predicted time $t_p = jT_s$, resulting in

$$\xi^{\mathcal{I}}(j+1) = \xi^{\mathcal{I}}(j) + T_s v^{\mathcal{I}}(j), \tag{3.9}$$

$$v^{\mathcal{I}}(j+1) = v^{\mathcal{I}}(j) + T_s \left(\frac{R^{\mathcal{I}}_{\mathcal{B}}(j) e^{\mathcal{B}} T(j) + f^{\mathcal{I}}_e(j)}{m} \right). \tag{3.10}$$

However, the traditional Euler method does not ensure that the predicted $R^{\mathcal{I}}_{\mathcal{B}}(j+1)$ is on $\mathsf{SO(3)}$. As a result, specific geometric integration methods for numerical integration of (3.7) and (3.8) have been developed (Ortolan, 2011). The majority of them are founded on the geometric relationship between $\mathsf{SO(3)}$ and $\mathfrak{so}(3)$, where $\mathfrak{so}(3)$ can be interpreted as the tangent space of $\mathsf{SO(3)}$ at the identity $I_3 \in \mathsf{SO(3)}$. Furthermore, since $\mathfrak{so}(3)$ is the Lie algebra of the Lie Group $\mathsf{SO(3)}$, the map $\mathfrak{so}(3) \to \mathsf{SO(3)}$ corresponds to the usual exponential matrix map. Therefore, the solution of the differential equation (3.7) is the following exponential map:

$$R^{\mathcal{I}}_{\mathcal{B}}(t) = e^{t\mathcal{S}(\omega^{\mathcal{B}}(t))} = I_3 + t\mathcal{S}(\omega^{\mathcal{B}}(t)) + \frac{(t\mathcal{S}(\omega^{\mathcal{B}}(t)))^2}{2!} + \ldots,$$

which can be discretized as

$$R^{\mathcal{I}}_{\mathcal{B}}(j) = R^{\mathcal{I}}_{\mathcal{B}}(jT_s) = e^{jT_s\mathcal{S}(\omega^{\mathcal{B}}(jT_s))}.$$

Thus, given the current configuration at the j-th sample time $(R^{\mathcal{I}}_{\mathcal{B}}(j),\ \omega^{\mathcal{B}}(j))$, the next configuration $(R^{\mathcal{I}}_{\mathcal{B}}(j+1),\ \omega^{\mathcal{B}}(j+1))$ is defined by the following iteration rule (Simo & Vu-Quoc, 1988):

$$\omega^{\mathcal{B}}(\bar{j}) = \omega^{\mathcal{B}}(j) + \frac{T_s}{2} J^{-1}(J\omega^{\mathcal{B}}(j) \times \omega^{\mathcal{B}}(j) + \tau^{\mathcal{B}}(j) + \tau^{\mathcal{B}}_e(j)), \tag{3.11}$$

$$R^{\mathcal{I}}_{\mathcal{B}}(j+1) = R^{\mathcal{I}}_{\mathcal{B}}(j)\mathrm{cay}(T_s\omega^{\mathcal{B}}(\bar{j})), \tag{3.12}$$

$$\omega^{\mathcal{B}}(j+1) = \omega^{\mathcal{B}}(\bar{j}) + \frac{T_s}{2} J^{-1}(J\omega^{\mathcal{B}}(\bar{j}) \times \omega^{\mathcal{B}}(\bar{j}) + \tau^{\mathcal{B}}(j) + \tau^{\mathcal{B}}_e(j)), \tag{3.13}$$

where $\mathrm{cay}(\cdot)$ is the Cayley map, which is the second-order approximation of the matrix exponential function defined by

$$\mathrm{cay}(\nu) \triangleq (I_3 + \frac{1}{2}\mathcal{S}(\nu))(I_3 - \frac{1}{2}\mathcal{S}(\nu))^{-1} \approx \mathrm{expm}(\mathcal{S}(\nu)). \tag{3.14}$$

3.3 Model Predictive Control without Terminal Conditions

Consider a finite-dimensional nonlinear system of the form

$$\dot{x}(t) = g(x(t), u(t)), \tag{3.15}$$

for some state-transition map $g : X \times U \to X$, with X and U normed spaces that denote the state and control spaces, respectively. Additionally, $x \in \mathbb{X} \subseteq X$ represents the states, and $u \in \mathbb{U} \subseteq U$ the inputs, with $\mathbb{X}$ and $\mathbb{U}$ designating, respectively, the set of admissible states and inputs.

By considering a nonlinear discrete-time invariant model obtained from (3.15)

$$x(j+1) = g_d(x(j), u(j)), \tag{3.16}$$

with $t = jT_s$, where T_s is the sampling time, the discrete-time optimal control problem (OCP) to be solved at the time instants k, with $t = kT_s$, is posed as

$$\begin{aligned} & \min_{x,u} \sum_{j=0}^{N_p} \ell(x(k+j), u(k+j)) \\ \text{s.t.} \quad & x(j+1) = g_d(x(j), u(j)), && x_0 = x(k), \\ & x \in \mathbb{X}, && \forall j \in \mathbb{N}_p, \\ & u \in \mathbb{U}, && \forall j \in \mathbb{N}_p, \end{aligned} \tag{3.17}$$

where $\ell : X \times U \to \mathbb{R}_0^+$ is the stage cost, x_0 is the current state, and $\mathbb{N}_p$ represents the non-negative integers bounded by the prediction horizon N_p. The optimization variables are given by the sequences $x \triangleq (x(0), x(1), \ldots, x(N_p))$ and $u \triangleq (u(0), u(1), \ldots, u(N_p - 1)$.

At each time instant k, the feedback law is defined by the following MPC iteration:

1. Measure the current state x_0.
2. Solve the OCP (3.17), and define the resulting optimal control sequence $u^\star$.
3. Apply the first element of $u^\star$, that is $u^\star(0)$, until the next time instant.

3.4 Optimal Control Problem Solution

The purpose of this section is to describe some of important concepts and issues involving the numerical solution of optimal control problems, which is the core of every NMPC implementation since the choices made in the algorithms have a strong impact on its reliability and performance. The content of this section is based on Rawlings et al. (2017).

The main idea of MPC is to compute a numerical approximation of the optimal feedback control for a given current state. Usually, the optimal control sequence is not exact since the system model is an approximation, the horizon length is finite, the system model is discretized, and the optimization problem is not solved exactly. This section focuses on the last two presented facts, which are related with the numerical solution of the NMPC. To justify why the finite horizon MPC is not usually solved exactly, there are some reasons. The first one is related to the finite precision arithmetic and finite computational time which usually cause numerical errors. The second one is related to the trade-off between accuracy and computational cost that might lead to large and impractical feedback delays. Third, errors due to an inexact numerical solution do not significantly change the closed-loop performance, as they are smaller than the errors introduced by the system uncertainties (modeling, sensor inaccuracy, etc). Therefore, evaluating the features and issues of numerical methods for NMPC solutions is a crucial design stage.

3.4.1 Convex versus nonconvex MPC

MPC schemes repeatedly solve, in each time step, an optimization problem, which can be convex or nonconvex, depending on the cost function and the feasible set characteristics. By definition, an optimization problem is convex if its feasible set is a convex set and if its objective function is a convex function.

Definition 3.4. (Rawlings et al., 2017). A set $S \in \mathbb{R}^n$ is said to be convex if, for any $x_1, x_2 \in S$ and $\lambda \in [0,1], (\lambda x_1 + (1-\lambda)x_2) \in S$.

Definition 3.5. (Rawlings et al., 2017). A function $f : \mathbb{R}^n \to \mathbb{R}$ is said to be convex if, for any $x_1, x_2 \in \mathbb{R}^n$ and $\lambda \in [0,1]$, $f(\lambda x_1 + (1-\lambda)x_2) \leq \lambda f(x_1) + (1-\lambda)f(x_2)$.

Within the optimization context, be convex results finding the globally optimal solution in polynomial time since every local minimum is also a global one. Conversely, if a problem is not convex the globally optimal solution cannot be guaranteed, and just locally optimal points are found. Moreover, when a nonconvex problem faces with infeasibility, it is not possible to determine if this occurs due to the problem being infeasible, or the optimization algorithm is simply unable to find points in the feasible set. Hence, in order to design correctly an optimization algorithm, it is crucial to determine if the problem is convex or not, as it impacts in all solution strategies.

Regarding the MPC, usually the objective function is convex, for example the sum of quadratic functions. Also, most of the constraints in the MPC optimization problem usually can be chosen to be convex sets. Nevertheless, the constraints $x(j+1) = g_d(x(j), u(j)), \quad x_0 = x(k)$, that reflect the system dynamics, might or might not describe a convex set. If the system model is linear or affine, then such a set is convex. This affirmation cannot be done when the system model is nonlinear, which represents most likely a nonconvex set.

Therefore, the division between convex and nonconvex optimization problems usually coincides with the division between linear and nonlinear system models. Thus, in the literature, the term linear MPC usually means *convex linear MPC* and the term nonlinear MPC nearly always coincides with *nonconvex nonlinear MPC* (Rawlings et al., 2017).

3.4.2 Simultaneous versus sequential approach

Observing the optimal control problem (3.17), the optimization variables are given by both the state, x, and control, u, trajectories. Hence, both the model simulation, represented by constraints, and the optimization problem are computed simultaneously by the optimization scheme, which is called as *simultaneous approach to optimal control*. Conversely, another possibility is to use the constraints to find the unique feasible state trajectory, x, for any given control trajectory, u. In each iteration, the OCP is solved by a sequence of two steps. First, for a given u, the simulation routine computes the state trajectory x, and second, the optimization routine updates the control variables u to iterate toward an optimal solution. In this context, due to this sequential evaluation, this approach is called *sequential approach to optimal control*.

For linear MPC, the computational cost for both formulations depends on the number of states, controls, and constraints, the specific sparsity structures, and the horizon length N_p. However, for nonlinear MPC, the sequential approach is preferable if the optimization solver cannot exploit sparsity and the system is stable, while the simultaneous approach is preferable for unstable nonlinear systems, for problems with state constraints, and for systems which need implicit simulation routines.

3.4.3 Direct optimal control parameterizations

Most of the recent approaches focus on direct methods to solve optimal control problems through a finite parameter nonlinear program. In contrast to classical indirect optimal control methods that rely on the calculus of variations, direct methods finitely represent continuous functions, i.e. discretize them, and then transform optimal control problems into a finite-dimensional optimization frameworks of the general form

$$\min_{w \in \mathbb{R}^{n_w}} \quad F(w) \tag{3.18a}$$

$$\text{s.t.} \quad G(w_0, w) = 0, \tag{3.18b}$$

$$H(w) \leq 0, \tag{3.18c}$$

where w is the optimization variable.

Direct methods are divided into two common strategies: *direct single-shooting*, when the sequential approach is regarded, and *direct multiple-shooting*, when the simultaneous approach (3.17), considered in this thesis, is regarded. In summary, the single-shooting

method treats all intermediate state values computed in the numerical integration routine as hidden variables, and solves the nonlinear program with respect to discretized control inputs. The direct multiple-shooting method considers the same piecewise control discretization, but it keeps the states at the interval boundary time as decision variables in the finite-dimensional optimization problem. Another way to define multiple-shooting is considering it as a lifted single-shooting, i.e., the problem is reformulated with more variables so as to make it less nonlinear. When comparing the two methods, although multiple-shooting presents a higher problem dimension, it is faster and exhibits better convergence properties due to its sparse structure, in particular for nonlinear and unstable systems over a long prediction horizon.

3.4.4 Nonlinear optimization

After the finite-dimensional optimization problem (3.18) is formulated, it needs to be solved. There are many nonlinear optimization strategies in the literature, depending on whether the problem is convex or not, whether there are equality or inequality constraints, or both. In the special case, when the optimization problem is convex, the first-order necessary conditions for optimality, known as the Karush-Kuhn-Tucker (KKT) conditions, can be shown to be a necessary and sufficient for global optimality. These conditions are given by the following theorem.

Theorem 3.1. (Adapted from Rawlings et al. (2017)) (KKT conditions). If w^* is a local minimizer of the optimization problem (3.18) and the linear independence constraint qualification (LICQ) holds at w^*, i.e. the gradients of all active inequalities and equalities constraints at w^* form a linearly independent set of vectors, then there exist multiplier vectors λ^* and μ^* such that

$$\nabla \mathcal{L}(w^*, \lambda^*, \mu^*) = 0, \tag{3.19a}$$

$$G(w_0, w^*) = 0, \tag{3.19b}$$

$$0 \geq H(w^*) \perp \mu^* \geq 0, \tag{3.19c}$$

where $\mathcal{L}$ is the Lagrangian function defined by

$$\mathcal{L}(w_0, w, \lambda, \mu) = F(w) + \lambda^\top G(w_0, w) + \mu^\top H(w). \tag{3.20}$$

For the general case, additional conditions on the second order derivatives of the related functions need to be computed in order to reach at sufficient conditions for local optimality. Before state these conditions, some definitions are stated. Firstly, the linearization of functions $H(w)$ and $G(w)$ at a point $\bar{w}$ obtained from the first-order Taylor series, are

defined as follows

$$H_L(w;\bar{w}) \triangleq H(\bar{w}) + H_w(\bar{x})(w-\bar{w}), \tag{3.21}$$

$$G_L(w_0,w;\bar{w}) \triangleq G(w_0,\bar{w}) + G_w(\bar{x})(w-\bar{w}). \tag{3.22}$$

Moreover, the inequality constraint $H(w)$ is divided into strictly active $H^+(w)$ ($\mu > 0$), weakly active $H^0(w)$ ($\mu = 0$), and inactive constraints $H^-(w)$ ($\mu < 0$). Based on this separation, the linear space $\mathcal{Z} \subset \mathbb{R}^{n_w}$ is defined as the null space of the following matrix:

$$A \triangleq \begin{bmatrix} G_w(w) \\ H_w^+(w) \end{bmatrix} \in \mathbb{R}^{n_A \times n_w}. \tag{3.23}$$

Thus, the columns of an orthogonal basis matrix $Z \in \mathbb{R}^{n_w \times (n_w - n_A)}$ of $\mathcal{Z}$ that satisfies $AZ = 0$ and $Z^\top Z = I$ span $\mathcal{Z}$. This $\mathcal{Z}$ space can be interpreted as the linear space of directions in which the strictly active constraints and the equality constraints remain constant up to first order. As a result, it plays an important role in the second-order sufficient conditions for optimality, as stated in the following theorem.

Theorem 3.2. (Rawlings et al., 2017) (Strong second-order sufficient conditions for optimality). If (w^*, λ^*, μ^*) is a KKT point and if the Hessian of its Lagrangian is positive definite on the corresponding space $\mathcal{Z}$, i.e., if

$$Z^\top \nabla_w^2 \mathcal{L}(w^*, \lambda^*, \mu^*) Z > 0, \tag{3.24}$$

then the point w^* is a local minimizer of (3.18).

For the NMPC formulated by the simultaneous approach (3.17), the constraint sets $\mathbb{X}$ and $\mathbb{U}$ are replaced by equivalent inequality constraints, which define an inherently nonsmooth set in the primal-dual variable space. Consequently, the Newton-type method or its variants can be applied only after some important modifications. Newton-type algorithms are numerical nonlinear root-finding problem solvers, that is, they find solutions to the KKT complementary system (3.19) by iterating on the triple

$$v^i \triangleq (w^i, \lambda^i, \mu^i) \quad \text{(at iteration i)},$$

until a solution is reached, regarding some accuracy. The two widely methods applied to these classes of problems are namely sequential quadratic programming (SQP) and nonlinear interior point (IP) methods. Since the latter is computationally cheaper and it fully exploit the sparsity structure of the optimization problem, the IP solver known as IPOPT (Wächter & Biegler, 2006), is chosen to be used in this work.

3.4.4.1 Nonlinear interior point methods

Nonlinear interior point (IP) methods are based on transforming inequality constrained optimization problems into approximate equality constrained ones, removing the nonsmoothness of the KKT conditions and allowing the use of smooth root-finding methods. The first step is to reformulate the nonlinear inequalities $H(w) \leq 0$ into equality constraints $H(w) + s = 0$ by the introduction of slack variables $s \in \mathbb{R}^{n_H}$. Since s is required to be positive, the equivalent new problem has bounds of the form $s \geq 0$, which is only inequality constraints. In barrier methods, as IP methods are also known, a barrier function is added to the optimization cost in order to replace these bounds defined by the variable s. For the IPOPT method (Wächter & Biegler, 2006), the barrier function is logarithmic, and the constrained optimization problem is given by

$$\min_{w,s} \quad F(w) - \tau \sum_{i=1}^{n_H} \log s_i \tag{3.25a}$$

$$\text{s.t.} \quad G(w_0, w) = 0, \tag{3.25b}$$

$$H(w) + s = 0, \tag{3.25c}$$

with $\tau > 0$. For $\tau \to 0$, the barrier term $-\tau \log s_i$ becomes zero for any strictly positive $s_i > 0$, while it always grows to infinity for $s_1 \to 0$, that is, on the boundary of the feasible set. Therefore, the solution of the modified problem (3.25) tends to be the solution of (3.18) for $\tau \to 0$. Denoting the multipliers for the equalities $H(w) + s = 0$ by $\mu \in \mathbb{R}^{n_H}$, and keeping the original definition of the Lagrangian (3.20), the necessary optimality conditions of problem (3.25), which are a smooth set of equations, can be formulated as

$$\nabla_w \mathcal{L}(w, \lambda, \mu) = 0, \tag{3.26a}$$

$$G(w_0, w) = 0, \tag{3.26b}$$

$$H(w) + s = 0, \tag{3.26c}$$

$$\mu_i s_i = \tau \quad \text{for} \quad i = 1, \ldots, n_H. \tag{3.26d}$$

The condition (3.26d) is a smooth version of $0 \leq s \perp \mu \geq 0$ that would correspond to the KKT conditions of the original problem with the variable s. The IPOPT algorithm (Wächter & Biegler, 2006) basically computes an approximate solution to the barrier problem (3.25) for a fixed value of τ, solving the corresponding root-finding problem (3.26). Then, the barrier parameter τ is decreased, and the solution of the next barrier problem, which is initialized with the solution of the previous one, is computed iteratively until a settable optimality error parameter is reached.

3.4.5 CasADi for optimization

CasADi (Andersson et al., 2018) is an open-source software tool for numerical optimization in general and optimal control. The project has been started by Joel Andersson and Joris Gillis while PhD students at the Optimization in Engineering Center (OPTEC) of the KU Leuven under supervision of Moritz Diehl. CasADi implements algorithmic differentiation (AD) on user-defined symbolic expressions, that is, it numerically evaluates the derivative of user-defined functions applying the chain rule concept repeatedly. Moreover, it has standardized optimization interfaces that automatically provide the necessary derivatives to numerical solvers without additional user input, independently of the user-defined CasADi function. CasADi is written in C++, but it allows user input to be provided from Python, Octave, and Matlab. The solvers IPOPT (Wächter & Biegler, 2006), described in the previous section, and qpOASES (Ferreau et al., 2014) interface to casADi, which is automatically provided in the standard CasADi installation (see `http://casadi.org` for more informations).

3.5 MPC stability based on strict dissipativity

The main dissipativity-based stability result for MPC schemes without terminal conditions presented in Grüne & Stieler (2014) is reviewed in this section (see also Grüne & Pannek (2017) for further details). Before state the main theorem developed by them, some definitions and assumptions are recalled in the discrete-time setting.

Definition 3.6. *Consider $x^e \in \mathbb{X}$ be an equilibrium for the closed-loop system. The equilibrium is said to be practically asymptotically stable w.r.t. $\rho \geq 0$ on a set $S \subseteq \mathbb{X}$ with $x^e \in S$ if there exists $\beta \in \mathcal{KL}$ such that*

$$\|x - x^e\| \leq \max\{\beta(\|x_0 - x^e\|, j), \rho\} \tag{3.27}$$

holds for all $x_0 \in S$ and all $j \in \mathbb{N}$. The equilibrium is globally practically asymptotically stable w.r.t. $\rho \geq 0$ if (3.27) holds on $S = \mathbb{X}$.

Assumption 3.1. *The OCP (3.17) is strictly dissipative with respect to the equilibrium $(x^e, u^e) \in \mathbb{X} \times \mathbb{U}$, that is, there is a non-negative storage function $\lambda : \mathbb{X} \to \mathbb{R}_0^+$, and a function $\alpha_\ell \in \mathcal{K}_\infty$ such that*

$$\lambda(g_d(x, u)) - \lambda(x) \leq \ell(x, u) - \ell(x^e, u^e) - \alpha_\ell(\|x - x^e\|), \tag{3.28}$$

holds for all $x_0 \in \mathbb{X}$, $u \in \mathbb{U}$, $j \in \mathbb{N}$.

Assumption 3.2. *The state and control constraint set $\mathbb{X}$ and $\mathbb{U}$ are compact, the functions g_d, ℓ and λ are continuous, and λ is Lipschitz continuous on a ball $\mathcal{B}_\epsilon(x^e) \triangleq \{x \in \mathbb{X} | \|x - x^e\| <$*

$\epsilon\}$ *for* $\epsilon > 0$.

Assumption 3.3. *The system* (3.16) *is local controllable on* $\mathcal{B}_\epsilon(x^e)$*, that is, there is* $\epsilon > 0$*,* $j \in \mathbb{N}$*,* $C > 0$ *such that* $\forall x_0 \in \mathcal{B}_\epsilon(x^e)$ $\exists u_1 \in \mathbb{U}^J(x_0)$*,* $\exists u_2 \in \mathbb{U}^J(x^e)$ *with*

$$x_{u_1}(J, x_0) = x^e, \quad x_{u_2}(J, x^e) = x_0,$$

where $x_{u_i}(J, x_0)$ *denotes the solution of* (3.16) *for a control sequence* $u_1 \in \mathbb{U}^J(x_0)$ *emanating from the initial value* $x_0 \in \mathbb{X}$*, and* $\mathbb{U}^J(x_0)$ *represents the set of all admissible control sequences which holds both* $u \in \mathbb{U}$ *and* $x_u(j, x_0) \in \mathbb{X}$ $\forall j \in \mathbb{I}_{0:J}$*. Moreover,*

$$\text{máx}\{\|x_{u_1}(J, x_0) - x^e\|, \|x_{u_2}(J, x^e) - x^e\|, \|u_1 - u^e\|, \|u_2 - u^e\|\}$$

$$\leq C\|x_0 - x^e\| \quad \forall j \in \mathbb{I}_{0:J-1}$$

Assumption 3.4. *The system* (3.16) *is finite time controllable into* $\mathcal{B}_\epsilon(x^e)$*, that is, for* $\epsilon > 0$ *from Assumption 3.3 there is* $J \in \mathbb{N}$ *such that for each* $x_0 \in \mathbb{X}$ *there is* $j \leq J$ *and* $\mathbb{U}^J(x_0)$ *with* $x_u(j, x_0) \in \mathcal{B}_\epsilon(x^e)$*.*

Theorem 3.3 (Adapted from Grüne & Stieler (2014))**.** *Consider the economic MPC problem without terminal conditions arisen from the receding horizon solution to OCP* (3.17) *satisfying Assumptions 3.1-3.4. Then, there exists a sufficiently large horizon* $N_p \in \mathbb{N}$*, such that the closed-loop system defined by* (3.16) *is practically asymptotically stable w.r.t* $\epsilon \to 0$ *as* $N_p \to \infty$*.*

Proposition 3.1 (Adapted from Grüne & Pannek (2017))**.** *Let Assumptions 3.1-3.4 hold. If, for the horizon* $N_p \in \mathbb{N}$*, the OCP* (3.17) *is feasible for* $j = 0$ *and* $x_0 \in \mathbb{X}$*, then it is feasible for all* $j \in \mathbb{N}$*.*

3.6 Final Remarks

This chapter provided a mathematical background to the thesis subject. The main concepts of rigid motion on $\mathsf{SE}(3)$ were described in Section 3.1, which are important to comprehend the motion equations of underactuated vehicles detailed in Section 3.2. An overview of numerical optimal control was presented in Section 3.4. The Section 3.5 reviewed the main theorem involving MPC dissipativity-based stability.

4

Point-to-point Motion Control Problem

This chapter addresses the stabilization control problem of underactuated motion systems. Also known as second-order nonholonomic dynamic systems, these vehicles have completely nonintegrable accelerations constraints, which means that some acceleration directions cannot be integrated instantaneously during movement. In addition, the vehicle's model is formulated on $\mathsf{SE}(3)$ manifold, which describes the configuration of rigid bodies globally and uniquely, allowing aggressive maneuvers. To solve this nontrivial control problem, two NMPC schemes without terminal conditions are proposed with closed-loop stability and recursive feasibility demonstration. The fundamental distinction between these two NMPC schemes is that, in the second formulation, the mission time is regarded as an economic criterion, while in the first one the cost function does not take the mission time into account. The second formulation is based on the exponential weight in the stage cost that pursues the time-optimality indirectly, which is an adapted version of the fixed horizon strategy proposed by (Verschueren et al., 2017).

The optimal control problem definition of each proposed NMPC schemes is presented in Sections 4.2.1 and 4.2.2. Thereafter, Section 4.3 provides the closed-loop stability and feasibility analysis. Numerical experiments are presented in Section 4.4, where the proposed controllers are corroborated when applied to a quadrotor UAV. Section 4.5 draws the main conclusions of the chapter.

4.1 Problem Statement

The following problems are addressed in this chapter:

Problem 4.1. *Design a stabilizing NMPC scheme without terminal conditions for motion control of underactuated vehicles modeled on* $\mathsf{SE}(3)$

Problem 4.2. *Design a stabilizing NMPC scheme without terminal conditions for motion control of underactuated vehicles modeled on* $\mathsf{SE}(3)$*, in which the mission time is regarded as an economic criterion.*

Assumption 4.1. *All system states are available to the controller.*

4.2 Control Strategies

This section describes the proposed control strategies for the presented problems.

4.2.1 NMPC for motion control of underactuated vehicles on $\mathsf{SE}(3)$

Considering the discrete-time system, g_d, given by (3.9)-(3.13), the NMPC scheme without terminal conditions, generally described in Section 3.3, repeatedly solves, in each sample time k, the following optimal control problem:

$$\begin{aligned} &\min_{x,u} \sum_{j=0}^{N_p} \|\bar{x}(k+j)\|^2_{Q_{\bar{x}}} + \|\bar{u}(k+j)\|^2_{Q_{\bar{u}}} \\ \text{s.t.} \quad & x(j+1) = g_d(x(j), u(j)), \quad x_0 = x(k), \\ & x \in \mathbb{X}, \qquad\qquad\qquad \forall j \in \mathbb{N}_p, \\ & u \in \mathbb{U}, \qquad\qquad\qquad \forall j \in \mathbb{N}_p, \end{aligned} \tag{4.1}$$

where $\bar{x} \triangleq \begin{bmatrix} (\xi^{\mathcal{I}})^\top & (v^{\mathcal{I}})^\top & \Psi(R^{\mathcal{I}}_{\mathcal{B}}, R_d) & (\omega^{\mathcal{B}})^\top \end{bmatrix}^\top \in \mathbb{R}^{10}$ and $\bar{u} \triangleq \begin{bmatrix} \|f^{\mathcal{I}}\| & (\tau^{\mathcal{B}})^\top \end{bmatrix}^\top \in \mathbb{R}^4$, with $Q_{\bar{x}} > 0$ being defined such that $\|\bar{x}\|^2_{Q_{\bar{x}}} = k_p\|\xi^{\mathcal{I}}\|^2 + k_v\|v^{\mathcal{I}}\|^2 + k_\omega\|\omega^{\mathcal{B}}\|^2 + k_R\Psi^2(R^{\mathcal{I}}_{\mathcal{B}})$, and $Q_{\bar{u}} > 0$ being defined such that $\|\bar{u}\|^2_{Q_{\bar{u}}} = k_f\|f^{\mathcal{I}}\|^2 + k_\tau\|\tau^{\mathcal{B}}\|^2$.

Remark 4.1. *Without loss of generality the position equilibrium is chosen as the origin, that is,* $(\xi^{\mathcal{I}})^e = \begin{bmatrix} 0 & 0 & 0 \end{bmatrix}^\top$*, and* R_d *is chosen as an attitude equilibrium, which depends on the system characteristics. Thus, considering the system at the equilibrium,* $\ell(x^e, u^e) = 0$*.*

4.2.2 NMPC for fast motion control of underactuated vehicles on SE(3)

Considering the discrete-time system, g_d, given by (3.9)-(3.13), the economic NMPC scheme repeatedly solves, in each sample time k, the following optimal control problem:

$$\begin{aligned} \min_{x,u} \quad & \sum_{j=0}^{N_p} \zeta^j \|\bar{x}(k+j)\|^2_{Q_{\bar{x}}} + \|\bar{u}(k+j)\|^2_{Q_{\bar{u}}} \\ \text{s.t.} \quad & x(j+1) = g_d(x(j), u(j)), \quad x_0 = x(k), \\ & x \in \mathbb{X}, \qquad\qquad \forall j \in \mathbb{N}_p, \\ & u \in \mathbb{U}, \qquad\qquad \forall j \in \mathbb{N}_p, \end{aligned} \tag{4.2}$$

where $\zeta > 1$ is an exponential weight in the stage cost that encourages the system to arrive at equilibrium as soon as possible (Verschueren et al., 2017), and the other variables are defined as the previous NMPC formulation. It is worth highlighting that the only difference between the OCPs (4.1) and (4.2) is the exponential weight, ζ.

Remark 4.2. *According to Theorem 1 of Verschueren et al. (2017), if N_p is greater or equal to the time-optimal solution of the problem, then there exists a number ζ_1 such that, for all $\zeta > \zeta_1$, the solution of (4.2) is time-optimal. Since for motion control problems the time-optimal definition mainly depends on the distance that the vehicle must travel, which can be a large value, this work does not focus on the time-optimal solution. As a result, ζ is used as a tuning gain that makes the motion faster.*

4.3 Feasibility and Stability Analysis

This section provides theoretical results ensuring the closed-loop stability and recursive feasibility of the proposed controllers.

4.3.1 NMPC for motion control of underactuated vehicles on SE(3)

The underactuated motion systems defined by (3.5)-(3.8) are not linearly controllable by a continuous time-invariant feedback control law (Brockett, 1983), implying that the conventional Kalman rank condition (Kalman et al., 1963) to evaluate the system controllability cannot be used. Therefore, the N-controllability of the system is verified.

Definition 4.1. *A linearized discrete-time system defined by matrices A and B is said to be N step controllable if the N-controllability matrix*

$$C_{o_N} \triangleq \begin{bmatrix} A^{N-1}B & \cdots & AB & B \end{bmatrix}$$

has rank greater or equal to the dimension of the system state vector x, i.e., rank$(C_{o_N}) \geq n$. This means that there exists a sequence $\{u(0), u(1), \cdots, u(N-1)\}$ that can transfer the system from any x_0 to x^e in N steps.

Lemma 4.1. *The system (3.5)-(3.8) is four step controllable.*

Demostración. Due to the state variable $R_{\mathcal{B}}^{\mathcal{I}} \in \mathsf{SO(3)}$, the conventional Jacobian linearization method cannot be used. Thus, from the exponential map (3.1) and the isomorphism between $\mathfrak{so}(3)$ and $\mathbb{R}^3$, the infinitesimal variation principle of the rotational motion is applied, satisfying (Lee et al., 2018)

$$\delta R_{\mathcal{B}}^{\mathcal{I}} = R_{\mathcal{B}}^{\mathcal{I}} \mathcal{S}(\eta), \tag{4.3}$$

$$\delta \omega^{\mathcal{B}} = \mathcal{S}(\omega^{\mathcal{B}})\eta + \dot{\eta}, \tag{4.4}$$

where a differentiable curve, $\eta \in \mathbb{R}^3$, is used to represent $\delta R_{\mathcal{B}}^{\mathcal{I}}$. Thus, the linearized equations of (3.5)-(3.8) in $\mathsf{TSE(3)}$ can be formulated as

$$\dot{\delta x} = A\delta x + B\delta u, \tag{4.5}$$

where $\delta x \triangleq \begin{bmatrix} \delta\xi^{\mathcal{I}} & \delta v^{\mathcal{I}} & \eta & \delta\omega^{\mathcal{B}} \end{bmatrix} \in \mathbb{R}^{12}$, and $\delta u \triangleq \begin{bmatrix} \delta T & \delta\tau^{\mathcal{B}} \end{bmatrix}$. The matrices $A \in \mathbb{R}^{12\times 12}$ and $B \in \mathbb{R}^{12\times 4}$ are computed as

$$A = \begin{bmatrix} \mathbf{0}_3 & I_3 & \mathbf{0}_3 & \mathbf{0}_3 \\ \mathbf{0}_3 & \mathbf{0}_3 & -\frac{T}{m} R_{\mathcal{B}}^{\mathcal{I}} \mathcal{S}(e^{\mathcal{B}}) & \mathbf{0}_3 \\ \mathbf{0}_3 & \mathbf{0}_3 & -\mathcal{S}(\omega^{\mathcal{B}}) & I_3 \\ \mathbf{0}_3 & \mathbf{0}_3 & \mathbf{0}_3 & J^{-1}(\mathcal{S}(J\omega^{\mathcal{B}}) - \mathcal{S}(\omega^{\mathcal{B}})J) \end{bmatrix},$$

$$B = \begin{bmatrix} \mathbf{0}_{3\times 1} & \mathbf{0}_3 \\ \frac{1}{m} R_{\mathcal{B}}^{\mathcal{I}} e^{\mathcal{B}} & \mathbf{0}_3 \\ \mathbf{0}_{3\times 1} & \mathbf{0}_3 \\ \mathbf{0}_{3\times 1} & J^{-1} \end{bmatrix}.$$

It can be verified that, considering $N = 4$,

$$\text{rank}\left(\begin{bmatrix} A^3B & A^2B & AB & B \end{bmatrix}\right) = 12,$$

which is equal to the dimension of the state vector δx. Therefore, the system (3.5)-(3.8) is four step controllable.

■

Remark 4.3. *Lemma 4.1 guarantees local controllability on a ball $\mathcal{B}_\epsilon(x_i^e) \triangleq \{x \in \mathbb{X} | \|x - x_i^e\| < \epsilon\}$ for $\epsilon > 0$. Additionally, as the proposed linearization (4.5) is continuous in $\mathsf{TSE(3)}$, it can be defined for any $x_i^e \in \mathsf{TSE(3)}$. Thus, considering a desirable equilibrium x_d^e that defines*

the ball $\mathcal{B}_\epsilon(x_d^e)$, for each $x_0 \in \mathbb{X}$ there is a finite sequence of κ intermediate targets $x(k) \in \mathbb{X}$, with $k = 1, \ldots, \kappa$, $x(k) \in \mathcal{B}_\epsilon(x_{k-1}^e) \cap \mathcal{B}_\epsilon(x_k^e)$, $x_\kappa^e \in \mathcal{B}_\epsilon(x_d^e)$, and $4 \leq j \leq J \in \mathbb{N}$ such that the trajectory initiating in $x_0 \in \mathbb{X}$, $x_u(j, x(k))$ pass through $\mathcal{B}_\epsilon(x_i^e) \cap \mathcal{B}_\epsilon(x_{i+1}^e) \cap \cdots \cap \mathcal{B}_d(x_d^e)$; that is, for each $x_0 \in \mathbb{X}$ there exists a finite control sequence that steers the system (3.5)-(3.8) into $\mathcal{B}_\epsilon(x_d^e)$. Therefore, the system is finite-time controllable into $\mathcal{B}_\epsilon(x_d^e)$.

Lemma 4.2. *If $k_v k_f \geq 0{,}25$ and $k_\omega k_\tau \geq 0{,}25$, then the OCP (4.1) is strictly dissipative with respect to the equilibrium $(x^e, u^e) \in \mathbb{X} \times \mathbb{U}$.*

Demostración. Consider the continuous time storage function candidate $\lambda : \mathsf{TSE(3)} \to \mathbb{R}$, defined as

$$\lambda(x) = \frac{1}{2}(\omega^{\mathcal{B}})^T J \omega^{\mathcal{B}} + \frac{1}{2}\|v^{\mathcal{I}}\|^2 - \mathcal{P}(R_{\mathcal{B}}^{\mathcal{I}}, \xi^{\mathcal{I}}), \tag{4.6}$$

which is the Lagrangian of the system on $\mathsf{TSE(3)}$, where $\mathcal{P}(R_{\mathcal{B}}^{\mathcal{I}}, \xi^{\mathcal{I}})$ is the potential energy that depends on the configuration $(R_{\mathcal{B}}^{\mathcal{I}}, \xi^{\mathcal{I}}) \in \mathsf{SE(3)}$.

It can be verified that, for a rotating and translating rigid body in three dimensions under the action of constant external forces and torques, the derivative of (4.6) is the mechanical power of the system, given by

$$\frac{d}{dt}(\lambda(x)) = (\omega^{\mathcal{B}})^\top \tau^{\mathcal{B}} + (v^{\mathcal{I}})^\top f^{\mathcal{I}}. \tag{4.7}$$

In addition, inequality (3.28) can equivalently be rewritten in the infinitesimal form as

$$\frac{d}{dt}\lambda(x(t)) \leq \ell(x, u) - \ell(x^e, u^e) - \alpha_\ell(\|x - x^e\|). \tag{4.8}$$

Thus, for $\ell(x, u)$ defined by OCP (4.1), with $\ell(x^e, u^e) = 0$, and considering (4.7), the inequality (4.8) becomes

$$(\omega^{\mathcal{B}})^\top \tau^{\mathcal{B}} + (v^{\mathcal{I}})^\top f^{\mathcal{I}} \leq \|\bar{x}\|_{Q_{\bar{x}}}^2 + \|\bar{u}\|_{Q_{\bar{u}}}^2 - \alpha_\ell(\|x - x^e\|). \tag{4.9}$$

The inequality (4.9) is equivalent to

$$h_1(x) + h_2(x) \leq k_p\|\xi^{\mathcal{I}}\|^2 + k_R(\Psi(R_{\mathcal{B}}^{\mathcal{I}}))^2 - \alpha_\ell(\|x - x^e\|), \tag{4.10}$$

where

$$h_1(x) = (v^{\mathcal{I}})^\top f^{\mathcal{I}} - k_v\|v^{\mathcal{I}}\|^2 - k_f\|f^{\mathcal{I}}\|^2, \tag{4.11}$$

$$h_2(x) = (\omega^{\mathcal{B}})^\top \tau^{\mathcal{B}} - k_\omega\|\omega^{\mathcal{B}}\|^2 - k_\tau\|\tau^{\mathcal{B}}\|^2. \tag{4.12}$$

For convenience, (4.10) will be analyzed by parts. First, by using the basic concept of quadratic difference between two real numbers, we can write that

$$(\sqrt{k_v}\|v^{\mathcal{I}}\| - \sqrt{k_f}\|f^{\mathcal{I}}\|)^2 \geq 0,$$

which can be rewritten as

$$2\sqrt{k_v k_f}\|v^{\mathcal{I}}\|\|f^{\mathcal{I}}\| - k_v\|v^{\mathcal{I}}\|^2 - k_f\|f^{\mathcal{I}}\|^2 \leq 0.$$

Additionally, Cauchy-Schwarz inequality yields

$$(v^{\mathcal{I}})^\top f^{\mathcal{I}} \leq \|v^{\mathcal{I}}\|\|f^{\mathcal{I}}\|.$$

Thus, if $k_v k_f \geq 0{,}25$, then

$$(v^{\mathcal{I}})^\top f^{\mathcal{I}} \leq k_v\|v^{\mathcal{I}}\|^2 + k_f\|f^{\mathcal{I}}\|^2 \implies h_1(x) \leq 0 \;\forall\; x \in \mathsf{TSE(3)}. \tag{4.13}$$

Second, by following similar steps approach, it can be verified that, for $k_\omega k_\tau \geq 0{,}25$, $h_2(x) \leq 0 \;\forall\; x \in \mathrm{TSE}(3)$. Thus,

$$h_1(x) + h_2(x) \leq 0 \;\forall\; x \in \mathsf{TSE(3)}. \tag{4.14}$$

Finally, if $k_v k_f \geq 0{,}25$, $k_\omega k_\tau \geq 0{,}25$, and assuming a function $\alpha_\ell \in \mathcal{K}_\infty$ such that

$$k_p\|\xi^{\mathcal{I}}\|^2 + k_R(\Psi(R_{\mathcal{B}}^{\mathcal{I}}))^2 \geq \alpha_\ell(\|x - x^e\|),$$

then, the inequality (4.10) holds, and, therefore, the OCP (4.1) is strictly dissipative with respect to the equilibrium (x^e, u^e).

■

The following Theorem is based on the main dissipativity-based stability result for MPC schemes without terminal conditions presented by Grüne & Stieler (2014), and provides a minimum stabilizing horizon for OCP (4.1).

Theorem 4.1. *The NMPC scheme defined by the OCP (4.1) is practically asymptotically stable for a sufficiently large horizon $N_p \in \mathcal{N} \triangleq \{n_p \in \mathbb{N} : n_p \geq 4\}$.*

Demostración. Lemmas 4.1 and 4.2 guarantee that Assumptions 3.1-3.4 are satisfied. Therefore, Theorem 3.3 can be applied and the NMPC scheme defined by the OCP (4.1) is practically asymptotically stable for a sufficiently large horizon $N_p \in \mathcal{N} \triangleq \{n_p \in \mathbb{N} : n_p \geq 4\}$. ■

Proposition 4.1. *Assuming that, for horizon $N_p \in \mathcal{N}$, the OCP (4.1) is feasible for $k = 0$, then the it is recursively feasible, i.e., it is feasible for all $k \in \mathbb{N}$.*

Demostración. The recursive feasibility follows from Proposition 3.1. ■

4.3.2 NMPC for fast motion control of underactuated vehicles on SE(3)

In this subsection, the closed-loop stability and recursive feasibility of the NMPC scheme described on Section 4.2.2 are evaluated. Firstly, the following Lemma specifies the conditions under which the OCP (4.2) is strictly dissipative.

Lemma 4.3. *If $k_v k_f \geq 0{,}25$ and $k_\omega k_\tau \geq 0{,}25$, then the OCP (4.2) is strictly dissipative with respect to the equilibrium $(x^e, u^e) \in \mathbb{X} \times \mathbb{U}$.*

Demostración. Consider (4.6) as a continuous time storage function candidate. The dissipation inequality (4.8) considering the continuous time version of OCP (4.2) yields

$$(\omega^{\mathcal{B}})^\top \tau^{\mathcal{B}} + (v^{\mathcal{I}})^\top f^{\mathcal{I}} \leq \zeta^t \|\bar{x}\|^2_{Q_{\bar{x}}} + \|\bar{u}\|^2_{Q_{\bar{u}}} - \alpha_\ell(\|x - x^e\|). \tag{4.15}$$

The inequality (4.15) can be rewritten as

$$h_3(x) + h_4(x) \leq \zeta^t (k_p \|\xi^{\mathcal{I}}\|^2 + k_R(\Psi(R^{\mathcal{I}}_{\mathcal{B}}))^2) - \alpha_\ell(\|x - x^e\|), \tag{4.16}$$

where

$$h_3(x) = (v^{\mathcal{I}})^\top f^{\mathcal{I}} - \zeta^t k_v \|v^{\mathcal{I}}\|^2 - k_f \|f^{\mathcal{I}}\|^2, \tag{4.17}$$

$$h_4(x) = (\omega^{\mathcal{B}})^\top \tau^{\mathcal{B}} - \zeta^t k_\omega \|\omega^{\mathcal{B}}\|^2 - k_\tau \|\tau^{\mathcal{B}}\|^2. \tag{4.18}$$

From (4.13), if $k_v k_f \geq 0{,}25$, then

$$(v^{\mathcal{I}})^\top f^{\mathcal{I}} \leq k_v \|v^{\mathcal{I}}\|^2 + k_f \|f^{\mathcal{I}}\|^2. \tag{4.19}$$

Since, for $\zeta > 1$, $\zeta^t \in \mathcal{K}_\infty$, then

$$(v^{\mathcal{I}})^\top f^{\mathcal{I}} \leq \zeta^t k_v \|v^{\mathcal{I}}\|^2 + k_f \|f^{\mathcal{I}}\|^2 \implies h_3(x) \leq 0 \ \forall \ x \in \mathsf{TSE(3)}. \tag{4.20}$$

Following the same steps approach, it can be verified that, for $k_\omega k_\tau \geq 0{,}25$, $h_4(x) \leq 0 \ \forall \ x \in$ TSE(3). Thus,

$$h_3(x) + h_4(x) \leq 0 \ \forall \ x \in \mathsf{TSE(3)}. \tag{4.21}$$

Finally, if $k_v k_f \geq 0{,}25$, $k_\omega k_\tau \geq 0{,}25$, and assuming a function $\alpha_\ell \in \mathcal{K}_\infty$ such that

$$\zeta^t (k_p \|\xi^{\mathcal{I}}\|^2 + k_R(\Psi(R^{\mathcal{I}}_{\mathcal{B}}))^2) \geq \alpha_\ell(\|x - x^e\|),$$

then, the inequality (4.16) holds, and, therefore, the OCP (4.2) is strictly dissipative with respect to the equilibrium (x^e, u^e). ■

The following Theorem specifies a minimum stabilizing horizon for OCP (4.2).

Theorem 4.2. *The NMPC scheme defined by the OCP (4.2) is practically asymptotically stable for a sufficiently large horizon $N_p \in \mathcal{N}$.*

Demostración. Assumptions 3.1-3.4 are held by Lemma 4.1 and Lemma 4.3. Therefore, from Theorem 3.3, the NMPC scheme defined by the OCP (4.2) is practically asymptotically stable for a sufficiently large horizon $N_p \in \mathcal{N}$. ■

Proposition 4.2. *Assuming that, for a horizon $N_p \in \mathcal{N}$, the OCP (4.2) is feasible for $k = 0$, then the it is recursively feasible, i.e., it is feasible for all $k \in \mathbb{N}$.*

Demostración. The recursive feasibility follows from Proposition 3.1. ■

4.4 Numerical Example: a Quadrotor UAV

In this section, the proposed NMPC schemes are corroborated using a quadrotor UAV in numerical experiments performed in the ProVANT simulator[1], which is a virtual simulation environment based on Gazebo (Koenig & Howard, 2004) and Robot Operating System (ROS) (Quigley et al., 2009) platforms. The objective of the experiments is illustrated in Figure 4.1, where the UAV has to accomplish a point-to-point motion, steering the vehicle to a desired set-point x^e from an initial configuration x_0. Firstly, the NMPC scheme (4.1) is verified through four different initial configurations. In the second part of the experiments, the NMPC scheme (4.2) is tested through these initial configurations to verify, beyond the controller efficiency, if the mission time is indeed reduced.

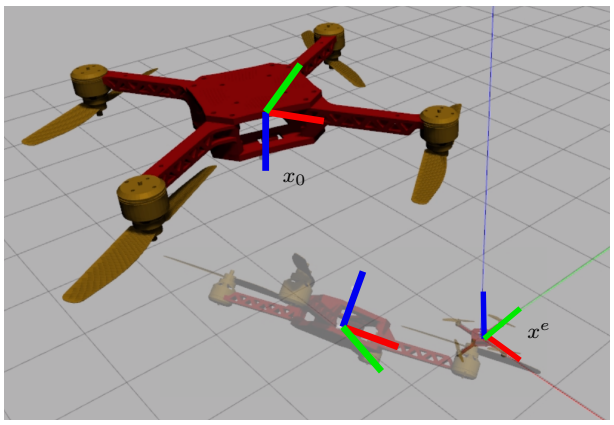


Figura 4.1: Experiment illustration. The NMPC steers the quadrotor UAV to a desired set point x^e from an initial configuration x_0.

4.4.1 Experiment setting

All experiments are performed considering the quadrotor UAV model characterized by (3.5)-(3.8), where $e^{\mathcal{B}} = e_3$ and $f_e^{\mathcal{I}} = -a_g e_3$, with $e_3 = \begin{bmatrix} 0 & 0 & 1 \end{bmatrix}^\top$, and a_g is the gravity

[1] https://github.com/Guiraffo/ProVANT-Simulator

acceleration. Because each propeller has a limited thrust, the following expression is used to map this thrust limitation to the input vector:

$$u = \begin{bmatrix} T \\ \tau_\phi \\ \tau_\theta \\ \tau_\psi \end{bmatrix} = \begin{bmatrix} 1 & 1 & 1 & 1 \\ 0 & l & 0 & -l \\ -l & 0 & l & 0 \\ c_{\tau f} & -c_{\tau f} & c_{\tau f} & -c_{\tau f} \end{bmatrix} \begin{bmatrix} f_1 \\ f_2 \\ f_3 \\ f_4 \end{bmatrix}, \tag{4.22}$$

where l is the distance from the quadrotor's center of mass to the center of each rotor, and $c_{\tau f}$ is the constant that determines the torque produced by each propeller. The quadrotor UAV's parameters were obtained from (Raffo, 2011) and reproduced in Table 4.1.

Cuadro 4.1: Quadrotor UAV parameters.

Parameter	**Value**
Mass of the quadrotor (m)	2.24 Kg
Distance between the rotors and the vehicle's center of gravity (l)	0.332 m
Maximum UAV height (h)	0.18 m
Drag coefficient of the rotors (k_τ)	1.7×10^{-7}Nms^2
Thrust coefficient of the rotors (b)	9.5×10^{-6} Ns^2
Gravitational acceleration (a_g)	9.81 m/s^2
Coeficiente de conversão Torque/força ($c_{\tau f}$)	0.018 m
Moment of inertia around the x-axis (I_x)	0.0363 Kg.m^2
Moment of inertia around the y-axis (I_y)	0.0363 Kg.m^2
Moment of inertia around the z-axis (I_z)	0.0615 Kg.m^2
Minimum thrust force of each propeller	0 N
Maximum thrust force of each propeller	12.3 N

For all the results presented in the following subsection, the controller is running at 100 Hz with a prediction horizon set to $N_p = 40$. In addition, the equilibrium set-point is defined as $x^e = (I_3, \begin{bmatrix} 0 & 0 & 4 \end{bmatrix}^\top, 0_{3\times1}, 0_{3\times1})$. From Lemmas 4.2 and 4.3, the gains for both schemes are tuned as $k_p = 150$, $k_v = 30$, $k_R = 10$, $k_1 = 10$, $k_3 = 1$, $k_\omega = 0{,}85$, $k_f = 5e^{-2}$, $k_\tau = 0{,}3$, and $\zeta = 1{,}2$. The initial configurations are given by $x_{01} = (R_{01}, \xi_{01}, 0_{3\times1}, 0_{3\times1})$, $x_{02} = (R_{02}, \xi_{02}, 0_{3\times1}, 0_{3\times1})$, $x_{03} = (R_{03}, \xi_{03}, 0_{3\times1}, 0_{3\times1})$, and $x_{04} = (R_{04}, \xi_{04}, 0_{3\times1}, 0_{3\times1})$, where

$$R_{01} = \begin{bmatrix} 0{,}1543 & 0{,}9880 & 0 \\ 0{,}1954 & -0{,}0305 & -0{,}9802 \\ -0{,}9685 & 0{,}1512 & -0{,}1978 \end{bmatrix}, \quad \xi_{01} = \begin{bmatrix} 4 \\ 5 \\ 7 \end{bmatrix},$$

$$R_{02} = \begin{bmatrix} -0{,}3045 & 0{,}2837 & 0{,}9093 \\ -0{,}4447 & 0{,}8019 & -0{,}3990 \\ -0{,}8424 & -0{,}5258 & -0{,}1180 \end{bmatrix}, \quad \xi_{02} = \begin{bmatrix} -4 \\ -5 \\ 2 \end{bmatrix},$$

$$R_{03} = \begin{bmatrix} 0{,}5175 & -0{,}3541 & -0{,}7790 \\ 0{,}8168 & 0{,}4755 & 0{,}3266 \\ 0{,}2548 & -0{,}8053 & 0{,}5353 \end{bmatrix}, \quad \xi_{03} = \begin{bmatrix} -4 \\ 5 \\ 7 \end{bmatrix},$$

$$R_{04} = \begin{bmatrix} 0{,}8660 & -0{,}5000 & 0 \\ -0{,}5000 & -0{,}8660 & 0 \\ 0 & 0 & -1 \end{bmatrix}, \quad \xi_{04} = \begin{bmatrix} 3 \\ -4 \\ 9 \end{bmatrix}.$$

Remark 4.4. *The prediction horizon N_p is determined from a trade-off between computational cost and control performance. It is possible, for example, to tune the controllers with $Np = 4$. However, to use a low stabilizing prediction horizon will require a more conservative behavior of the vehicle, with slow and smooth rotational and translational movements.*

Regarding the OCP solution, the so-called direct method, introduced in (Bock & Plitt, 1984), is used to evaluate solutions of (4.1)-(4.2) at each sample time. This method is based on finitely parameterizing infinite-dimensional decision variables in order to approximate the original OCP, given by (4.1)-(4.2), by a finite-dimensional nonlinear program (NLP) (Rawlings et al., 2017). The direct multiple-shooting technique is used, which holds both piecewise control discretization and the states at interval boundary time points as decision variables in a finite-dimensional optimization problem. The toolbox CasADI (Andersson et al., 2018) solves this NLP, interfacing with the IPOPT solver (Wächter, 2002). The experiment server used in this work is a general purpose notebook computer with an Intel Core i7 4500U, with two physical and four logical cores, running at 1.8 GHz, 8 GB of RAM and a NVidia GT 750M GPU. This computer uses the Ubuntu Linux version 18.04 operational system.

4.4.2 Results

Figures 4.2 and 4.3 present the position and attitude trajectories performed by the UAV along the experiments. In Figure 4.2, the NMPC scheme (4.1) is considered. In Figure 4.3, the fast motion NMPC scheme (4.2), which for simplicity will be denominated as FMNMPC, is employed. The same parameter values are used in both set of experiments, such as gains, prediction horizon, initial conditions, and equilibrium set point. It is considered four distinct initial conditions, where non-equilibrium configurations are applied. In the initial condition x_{04}, for example, the UAV must recover from a initial upside down position. Controllers based on non singularity-free parametrizations cannot perform this type of maneuver. Additionally, since only positive values for propeller thrust can be applied, the stabilization of the UAV is a big challenge in a such situation.

From Figures 4.4-4.7, it is noteworthy that the equilibrium point x^e is accurately reached by both NMPC schemes and for all considered initial conditions. For the sake of clarity,

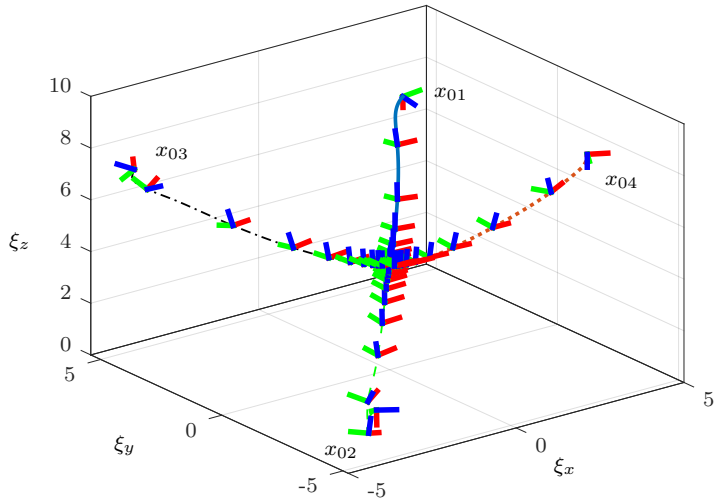


Figura 4.2: Position and attitude trajectories obtained from the experiments considering the NMPC scheme (4.1).

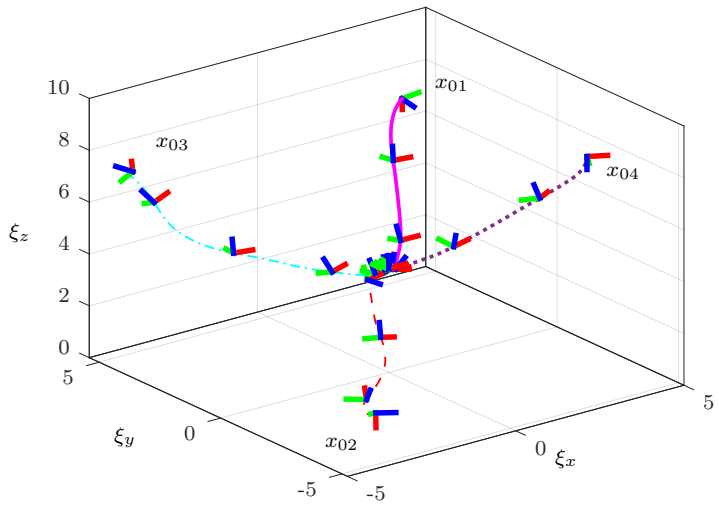


Figura 4.3: Position and attitude trajectories obtained from the experiments considering the NMPC scheme (4.2).

the UAV attitude is illustrated in Figure 4.6 by using the Euler angles representation in degree unit. In all tested situations the UAV stabilized in $I_3 \in \mathsf{SO}(3)$, which is equivalent to stabilize the roll, pitch, and yaw angles in zero degrees. Regarding the comparison between the proposed NMPC schemes, it is worth highlighting that the UAV achieved the origin faster when the FMNMPC was considered. Despite the fact that the exponential weight in the stage cost encourages all states to reach the equilibrium as soon as possible, the system underactuation requires to decide which states are priority in terms of being fast. The controller gains definition performs this prioritization. In these experiments, because the position gain, k_p, is much greater than the other gains, the faster behavior in the translational movement is clearer, that is, when FMNMPC is used, the setting time for the position vector, ξ, is significantly reduced. Also, as expected, the motion of the vehicle is more aggressive for the FMNMPC scheme, with large angular excursions (see Figure

4.6) and higher maximum velocities achieved (see Figures 4.5 and 4.7).

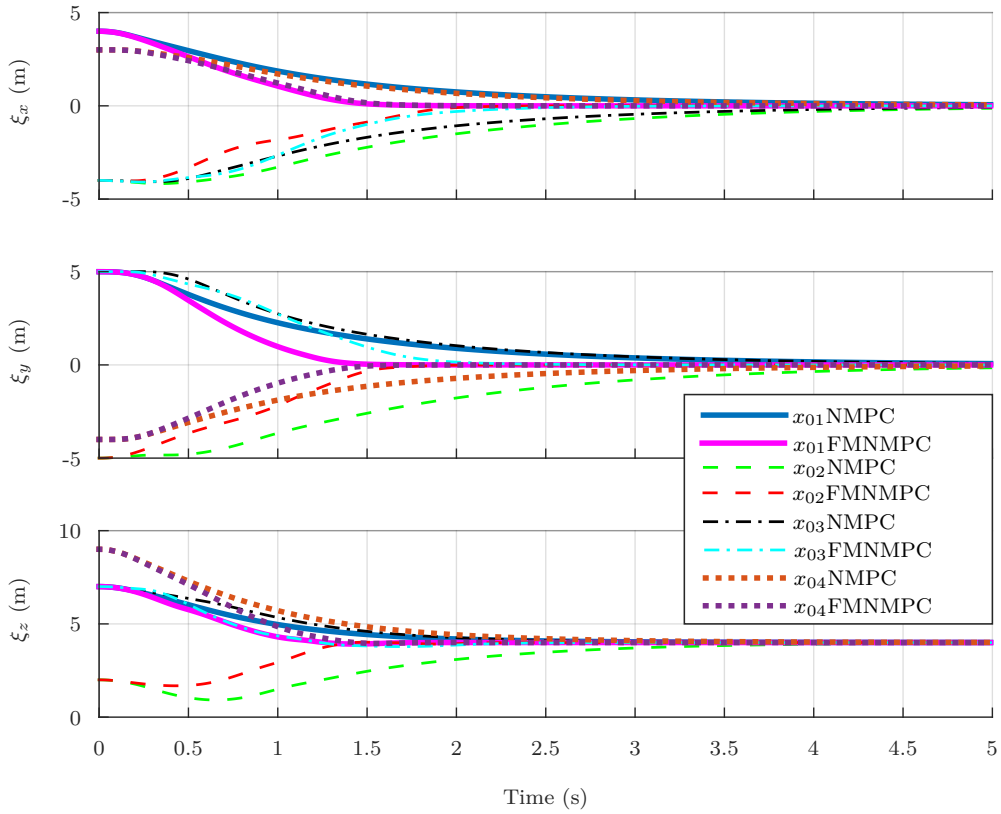


Figura 4.4: UAV position, ξ.

The proposed NMPC schemes complied with all system constraints considered in the control design. Figure 4.8 shows the propeller forces which are mapped on the input signals. Note that the input limits, given in Table 4.1, are satisfied by the controllers, which demonstrated the ability of the proposed controllers to deal with constrained control problems. Furthermore, the FMNMPC reachs the inputs limits more frequently than the NMPC scheme (4.1), which also indicates its aggressiveness.

Lastly, to clearly assess the influence of the exponential weight on the stage cost, Figures 4.9 and 4.10 are depicted. Figure 4.9 shows that the index $\|\bar{x}\|^2_{Q_{\bar{x}}}$ for FMNMPC presents a faster decay in all tested situations, which is expected since the exponential weight included in the FMNMPC encourages $\bar{x}$ to approximate the equilibrium point as soon as possible at each prediction horizon. In addition, Figure 4.10 highlights the faster behavior in the translational movement. Moreover, it is worth highlighting that the settling time is 48 % shorter on average for FMNMPC, showing that the mission time is indeed reduced. As mentioned in Remark 4.2, the parameter ζ is used as a tuning gain in this work, which allows to tune the OCP (4.2) for a larger ζ in order to reduce the setting time.

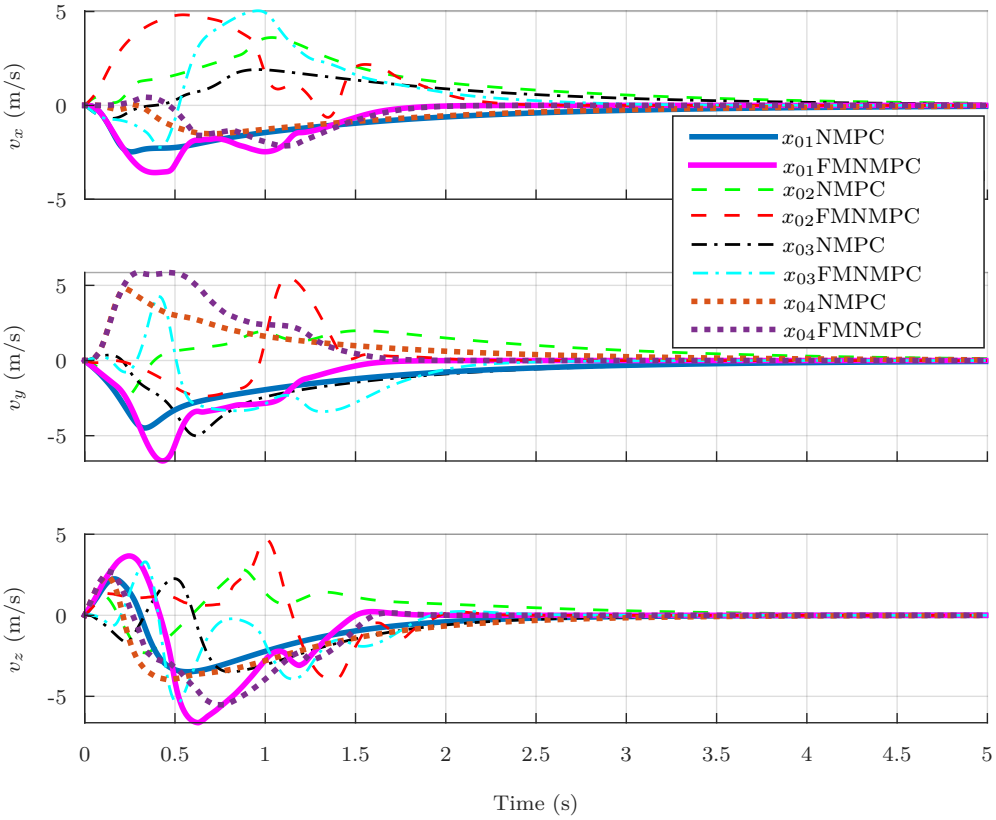


Figura 4.5: UAV velocity, v.

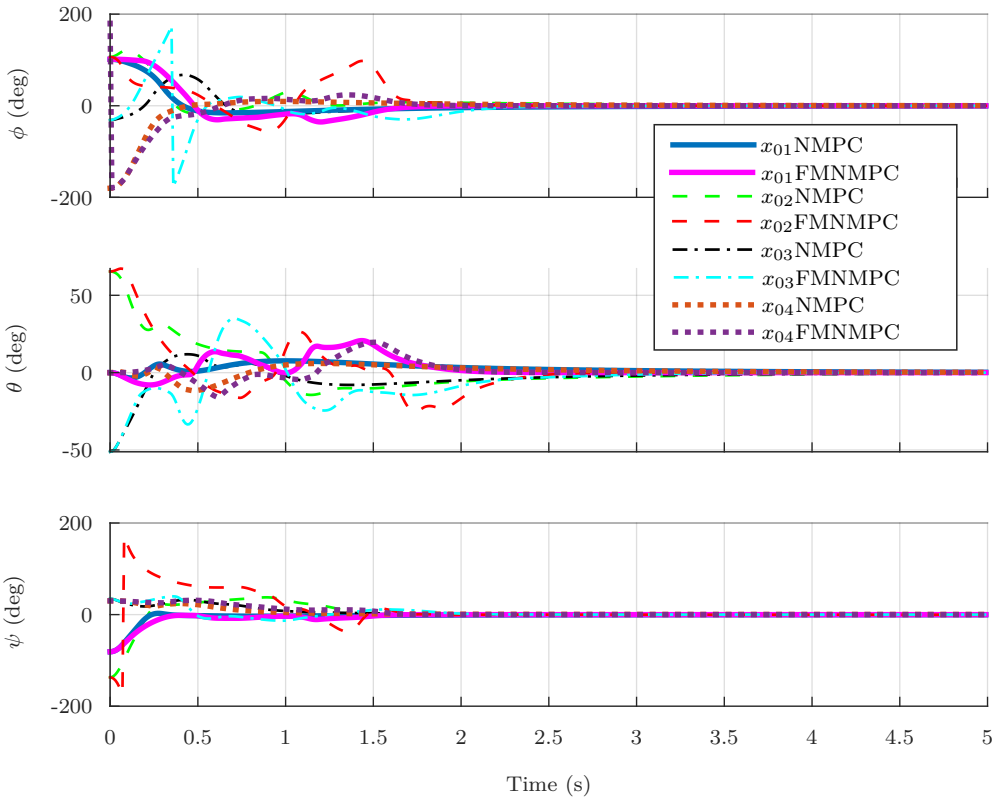


Figura 4.6: UAV Euler angles.

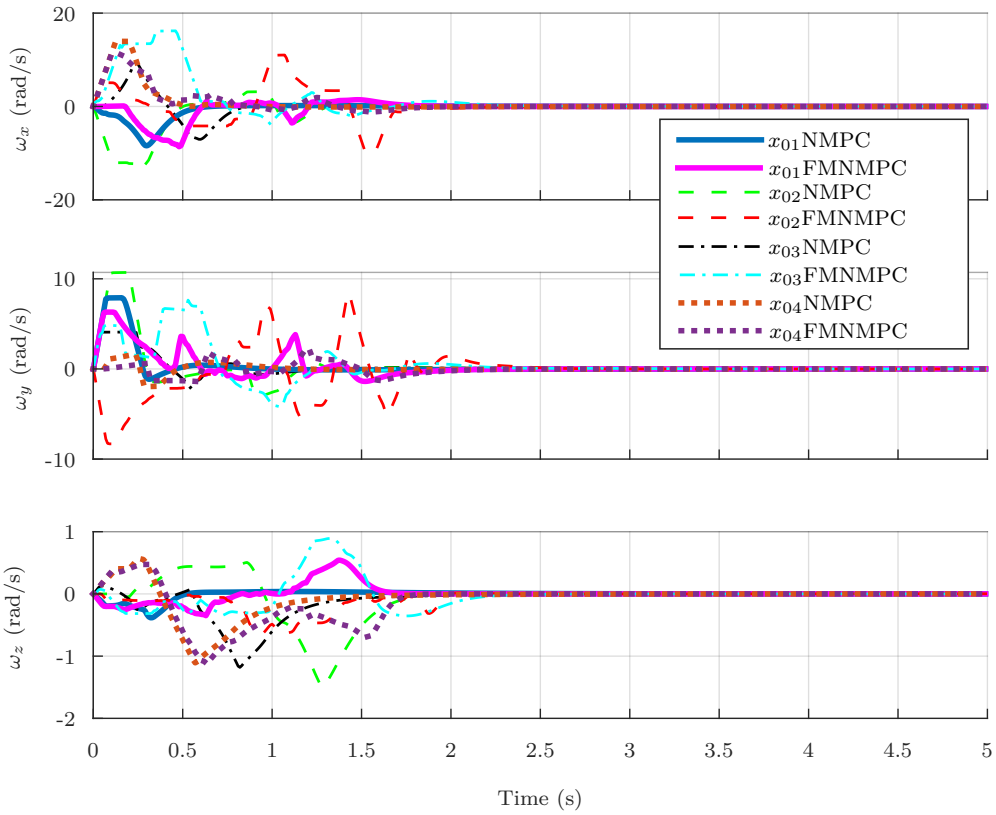


Figura 4.7: UAV Angular Velocities.

4.5 Final Remarks

Two practically asymptotically stable NMPC schemes without terminal conditions for the motion control of a class of underactuated vehicles are presented. The controllers are formulated on $\mathsf{SE}(3)$ manifold, which allows to represent the vehicle motion globally and uniquely. This singularity-free feature is demonstrated on the experiments, where the quadrotor UAV recovers from an upside down situation without any additional controller or optimization layer. The closed-loop stability and recursive feasibility are rigorously evaluated based on recent theories involving strict dissipativity and MPC schemes without terminal conditions. In addition, the proposed fast motion NMPC scheme steers the vehicle to a desirable equilibrium point by considering the mission time reduction as an economic criterion. Numerical experiments confirm the theoretical findings, in which both controllers reached the equilibrium point accurately for different initial conditions. Moreover, the effect of the exponential weight on the closed-loop performance was investigated in detail, demonstrating that with a simple tuning parameter it is possible to obtain a fast and stable response of the system.

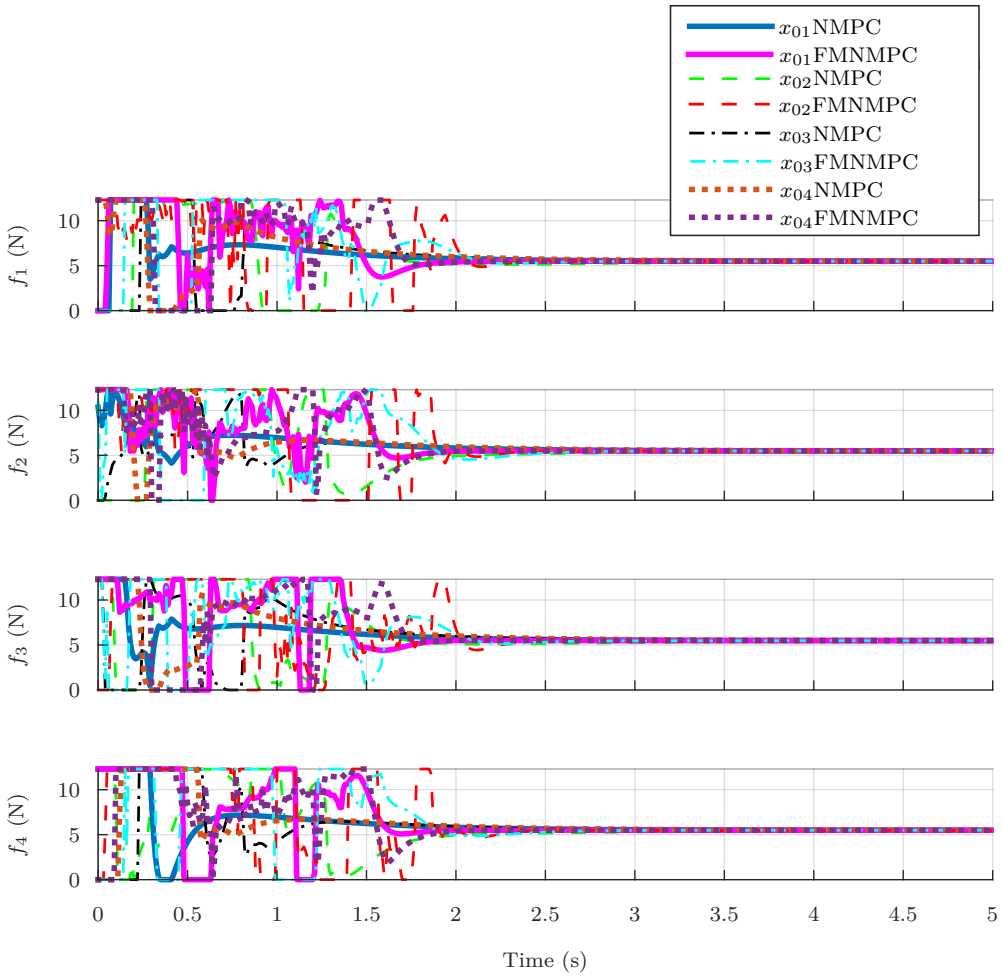


Figura 4.8: UAV propeller forces. The input bounds are correctly respected by the controller.

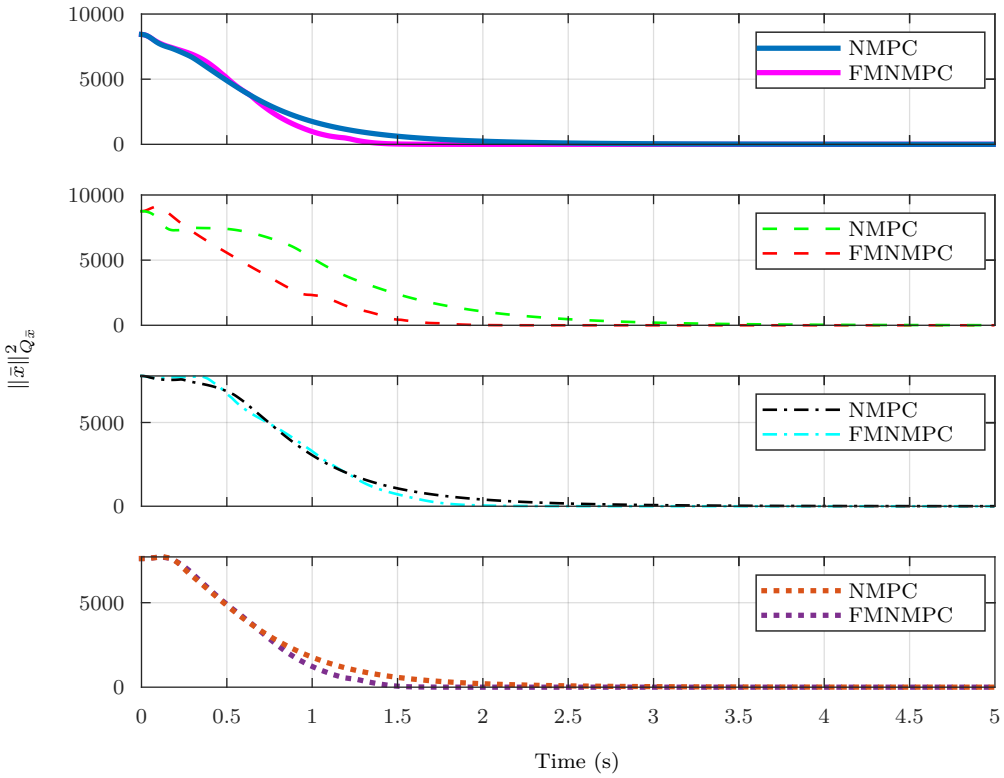


Figura 4.9: Variation of $\|\bar{x}\|^2_{Q_{\bar{x}}}$ for each initial condition and for each proposed NMPC scheme.

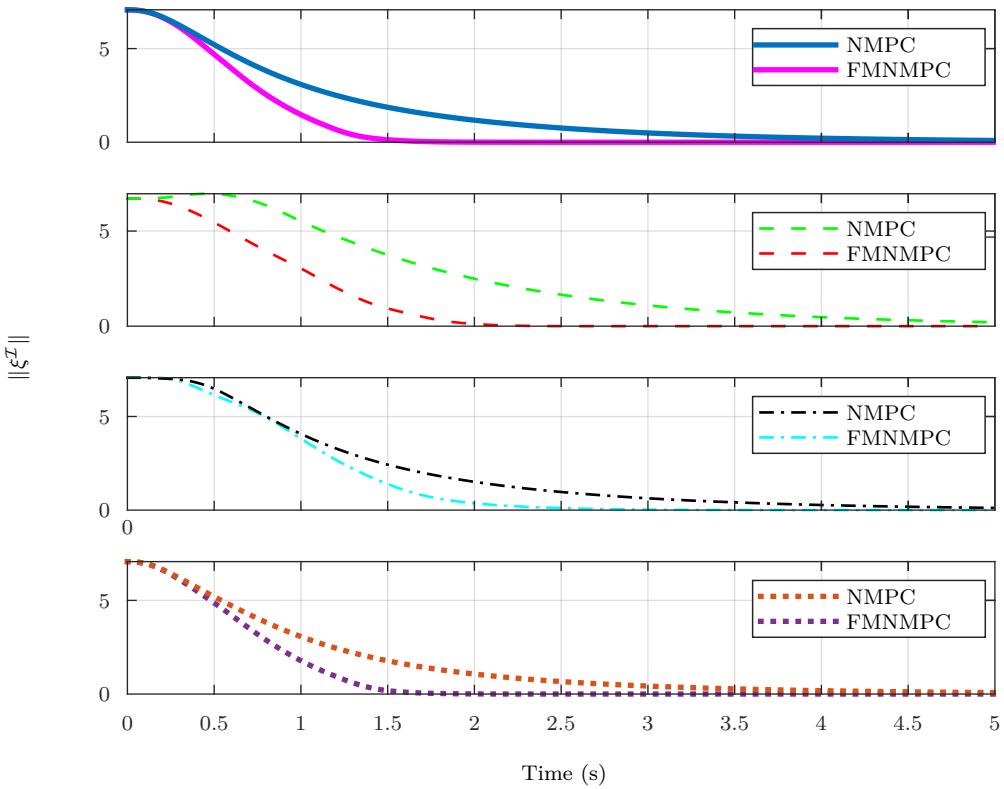
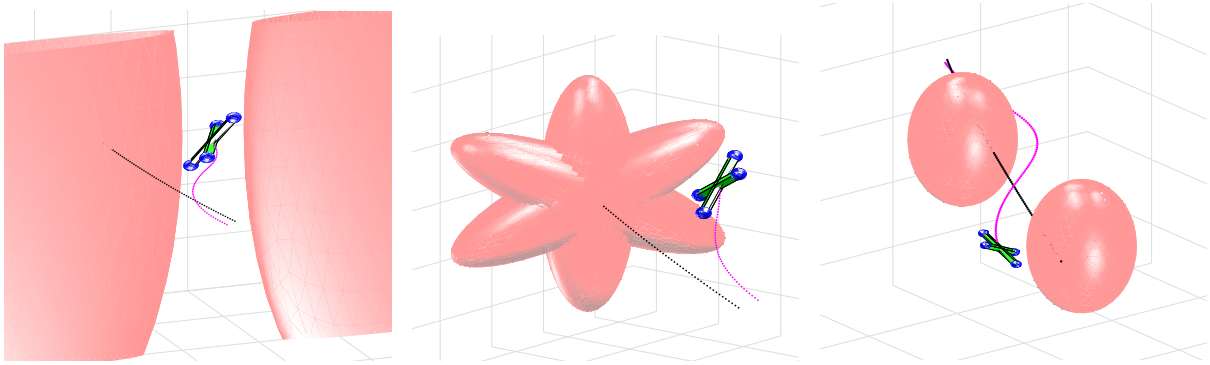


Figura 4.10: Variation of $\|\xi^{\mathcal{I}}\|$ for each initial condition and for each proposed NMPC scheme.

5

Trajectory Tracking with Obstacle Avoidance

This chapter introduces an enhanced concept of aggressive maneuvers by considering the motion system as an ellipsoidal set that characterizes both vehicle position and attitude. Also, obstacles are described by ellipsoidal sets in $\mathbb{R}^3$. The proposed method can handle the vehicle attitude as an optimization variable within the control problem, including it in the collision check. Consequently, the proposed NMPC scheme in this chapter allows the vehicle pass through narrow gaps (Figure 5.1(a)), interacts with non-convex obstacles gaps (Figure 5.1(b)), and performs fast trajectories with slalom movements, that is, executing roll and pitch movements in order to reduce the obstacle deviation time (Figure 5.1(c)).



(a) Throughing narrow gaps. (b) Non-convex obstacle deviation. (c) Slalom Movement.

Figura 5.1: Examples of aggressive maneuvers as a result of obstacle avoidance and fast flights.

The proposed NMPC is also formulated on the Special Euclidean group $\mathsf{SE}(3)$, now for trajectory tracking, considering constraints in the states and inputs, with constant disturbance rejection and aggressive maneuvers capabilities in order to improve the obstacle avoidance performance.

5.1 Problem Statement

Problem 5.1. *Design an NMPC scheme without terminal conditions able to perform trajectory tracking while avoiding obstacles with aggressive maneuver capability.*

Assumption 5.1. *The vehicle and obstacles are approximated by ellipsoidal sets;*

Assumption 5.2. *While the vehicle moves along cluttered environments with unknown obstacles, an external obstacle detector algorithm sends to the controller the parameters of the nearest obstacles;*

Assumption 5.3. *All system states are available to the controller.*

5.2 Control Strategy

This section describes the proposed control strategy. Firstly, the ellipsoidal collision check approach is presented, followed by the optimal control problem formulation. The section finishes with the proposed solution to the optimal control problem.

Figure 5.2 shows a block diagram representation of the control structure with four main blocks: the Obstacle Detector, whose operation description is beyond the scope of this work; the User which defines the desirable references; the NMPC scheme; and the underactuated vehicle.

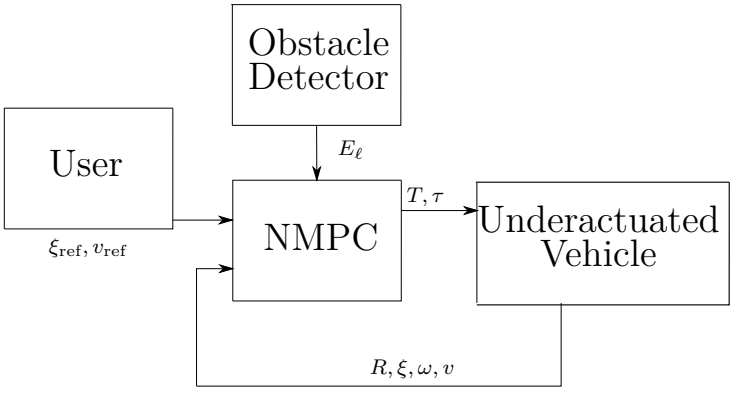


Figura 5.2: NMPC structure.

5.2.1 Ellipsoidal collision check approach

The main advantage of using ellipsoids to envelop vehicles and obstacles, for obstacle avoidance strategies, is their capacity to incorporate the body attitude and position algebraically under affine transformations while preserving their physical parameters. The vehicle, which is assumed to be a rigid body, can therefore be modeled as an ellipsoidal set $\mathcal{V}$, with radius r_x, r_y, and height h, given by

$$\mathcal{V} \triangleq \left\{ q \in \mathbb{R}^3 : \frac{x^2}{r_x^2} + \frac{y^2}{r_y^2} + \frac{z^2}{h^2} - 1 \leq 0 \right\}. \tag{5.1}$$

As the vehicle moves, it is possible to determine the time varying set $\bar{\mathcal{V}}(t)$ given the rotation matrix R, the position ξ, and a matrix $Q(t) \in \mathbb{R}^{4\times4}$, from the following affine transformation:

$$\bar{\mathcal{V}}(t) \triangleq \left\{ \bar{q} = \begin{bmatrix} x & y & z & 1 \end{bmatrix}^\top \in \mathbb{R}^4 : \bar{q}^\top Q(t) \bar{q} \leq 0 \right\}, \tag{5.2}$$

where,

$$Q(t) = S(t)^{-\top} Q_p S(t)^{-1}, \quad S(t) = \begin{bmatrix} R(t) & \xi(t) \\ \mathbf{0}_{1\times3} & 1 \end{bmatrix}, \quad Q_p = \begin{bmatrix} 1/\bar{r}_x^2 & 0 & 0 & 0 \\ 0 & 1/\bar{r}_y^2 & 0 & 0 \\ 0 & 0 & 1/\bar{h}^2 & 0 \\ 0 & 0 & 0 & -1 \end{bmatrix},$$

with $\bar{r}_x = (r_x + \epsilon_x)$, $\bar{r}_y = (r_y + \epsilon_y)$ and $\bar{h} = (h + \epsilon_h)$ being parameters considering safety distance margins, $\epsilon_x > 0$, $\epsilon_y > 0$ and $\epsilon_h > 0$, related to the collision avoidance.

Each obstacle can also be approximated by an ellipsoidal set $\mathcal{E}$ characterized by a coefficient matrix $E \in \mathbb{R}^{4\times4}$, which is defined by the external obstacle detector. The parameters of E are calculated from the problem of enclosing the obstacle by the minimum volume ellipsoid that fits it. Thus, $\mathcal{E}$ is given by

$$\mathcal{E} \triangleq \{ e = \begin{bmatrix} x & y & z & 1 \end{bmatrix}^\top \in \mathbb{R}^4 : e^\top E e \leq 0 \}. \tag{5.3}$$

To evaluate algebraically whether the ellipsoidal sets overlap or are disjoint, the roots of the following characteristic polynomial are analyzed:

$$f(\lambda) = \det(\lambda Q(t) + E). \tag{5.4}$$

This analysis is performed by using the following theorem.

Theorem 5.1 (Adapted from Wang et al. (2001)). *Consider $f(\lambda)$ given in (5.4), where $E \in \mathbb{R}^{4\times4}$ and $Q(t) \in \mathbb{R}^{4\times4}$ define the sets $\mathcal{E}$, for the obstacle, and $\bar{\mathcal{V}}$, for the vehicle, respectively. The following algebraic conditions are verified:*

1. *The characteristic equation $f(\lambda) = 0$ always has at least two negative roots;*

2. *The two ellipsoids $\bar{\mathcal{V}}$ and $\mathcal{E}$ are separated if and only if $f(\lambda) = 0$ has two distinct positive roots;*

3. *The two ellipsoids $\bar{\mathcal{V}}$ and $\mathcal{E}$ touch each other externally if and only if $f(\lambda) = 0$ has a positive double root;*

4. *The two ellipsoids $\bar{\mathcal{V}}$ and $\mathcal{E}$ overlap if and only if $f(\lambda) = 0$ has no positive root.*

The authors in [4] propose a direct way to characterize the collision condition by using Theorem 1. They denoted the monic representation of (5.4) and proposed the following theorem.

Theorem 5.2 (Caravantes & Gonzalez-Vega (2018))**.** *Let $\bar{\mathcal{V}}$ and $\mathcal{E}$ be two ellipsoids with characteristic equation*

$$f(\lambda) = \lambda^4 + a\lambda^3 + b\lambda^2 + c\lambda + d = 0. \tag{5.5}$$

$\bar{\mathcal{V}}$ and $\mathcal{E}$ overlap if and only if $\Delta(f) < 0$, where

$$\Delta(f) = -27d^2a^4 - 4a^3c^3 + 18a^3dcb + a^2c^2b^2 - 6a^2c^2d \\ - 4a^2b^3d + 144a^2bd^2 - 192ad^2c - 80ab^2cd. \tag{5.6}$$

The advantage of Theorem 5.2 is related to its better numerical performance with respect to the conditions proposed in Theorem 5.1, which justifies the use of Theorem 5.2 in this work.

5.2.2 Nonlinear model predictive control formulation

A fundamental task in the NMPC formulation consists in designing the cost functional and the constraints that affect the system, considering the particular characteristics that the controller must deal with.

5.2.2.1 Integral action for disturbance rejection

At first, state variables are determined from equations (3.5)-(3.8). Due to the vehicle underactuation, the control objective is specified as the tracking of ξ and the stabilization of the other states. However, for an effective trajectory tracking in the presence of constant disturbances and parametric uncertainties, an integral action on the error of the tracked states is required. One suitable approach, presented in Raffo et al. (2010), is to describe an augmented system where the integral of tracking errors appears in the state variables as follows

$$\tilde{x} \triangleq (R_{\mathcal{B}}^{\mathcal{I}}, \xi^{\mathcal{I}}, \omega^{\mathcal{B}}, v^{\mathcal{I}}, \iota) \in \mathsf{TSE}(3) \times \mathbb{R}^3, \tag{5.7}$$

where $\iota \triangleq \int(\xi - \xi_{\text{ref}})dt \in \mathbb{R}^3$, with ξ_{ref} being the position reference trajectory.

5.2.2.2 Relaxed collision constraint for obstacle avoidance

As was mentioned before, to perform safe navigation, it is necessary to ensure that collisions do not occur during the trajectory tracking. Therefore, constraints are imposed to ensure that the predicted set at each time instant k, $\bar{\mathcal{V}}(k)$, given by equation (5.2) after discretization, does not come in space positions that are obstructed by obstacles, that is,

$$\bar{\mathcal{V}}(k+j) \subseteq \underbrace{\left(\mathbb{R}^3 - \bigcup_{l=1}^{N_o} \mathcal{E}_\ell\right)}_{\text{free space}}, \quad \forall \ell = 1, \cdots, N_o, \quad \forall j = 0, \cdots, N_p. \tag{5.8}$$

From Theorem 5.2,

$$\bar{\mathcal{V}} \cap \mathcal{E} \neq \emptyset \iff \Delta(f) < 0.$$

Hence,

$$\bar{\mathcal{V}} \subseteq \underbrace{\left(\mathbb{R}^3 - \bigcup_{l=1}^{N_o} \mathcal{E}_\ell\right)}_{\text{free space}} \iff \bar{\mathcal{V}} \cap \mathcal{E}_\ell = \emptyset \iff \Delta_\ell(f) > 0, \quad \forall \ell = 1, \cdots, N_o.$$

Therefore, the condition (5.8) is guaranteed if

$$\Delta_\ell(f(k+j)) > 0, \quad \forall \ell = 1, \cdots, N_o, \quad \forall j = 0, \cdots, N_p. \tag{5.9}$$

However, due to the numerical complexity of computing the admissible state set from $\Delta(f)$, the use of such a function may lead to the violation of the imposed constraints and, consequently, to an unfeasible optimization procedure. Therefore, aiming to improve the computational performance, this work replaces the constraint (5.9) by soft constraints, considering penalty functions at the cost functional. The proposed relaxation is given by

$$\varphi_\ell(\Delta(f(k+j))) = \frac{K_n[d_s - d_\ell]_+}{1 + K_d[\Delta_\ell(f(k+j))]_+^{K_e}}, \tag{5.10}$$

where d_ℓ is the Euclidean distance between the vehicle's position prediction and the ℓ-th obstacle's center, K_n, K_d and K_e are tuning parameters, and d_s is a safe distance parameter adjusted by the designer.

5.2.2.3 Optimal control problem

Considering the discrete-time system g_d given by (3.9)-(3.13), the NMPC scheme repeatedly solves, in each sample time, the following optimal control problem:

$$\begin{aligned}\min_{x,u} \sum_{j=0}^{N_p} \|\hat{x}(k+j) - \hat{x}_{\text{ref}}(k+j)\|^2_{Q_{\tilde{x}}} + \|u(k+j)\|^2_{Q_u} + \sum_{\ell=1}^{N_o}\sum_{j=0}^{N_p} \varphi_\ell(\Delta f(k+j))^2 \\ \text{s.t.} \quad x(j+1) = g_d(x(j), u(j)), \quad x_0 = x(k), \\ x \in \mathbb{X}, \qquad\qquad \forall j \in \mathbb{N}_p, \\ u \in \mathbb{U}, \qquad\qquad \forall j \in \mathbb{N}_p,\end{aligned} \tag{5.11}$$

where $\hat{x} \triangleq \begin{bmatrix}(\xi^{\mathcal{I}})^\top & (v^{\mathcal{I}})^\top & \Psi(R^{\mathcal{I}}_{\mathcal{B}}, I_3) & (\omega^{\mathcal{B}})^\top & \iota^\top\end{bmatrix} \in \mathbb{R}^{13}$, the attitude error $\Psi(R, I_3)$ is given by (3.4), and $\hat{x}_{\text{ref}} \triangleq \begin{bmatrix}(\xi^{\mathcal{I}})^\top_{\text{ref}} & (v^{\mathcal{I}})^\top_{\text{ref}} & 0 & \mathbf{0}_{3\times1} & \mathbf{0}_{3\times1}\end{bmatrix} \in \mathbb{R}^{13}$. The desirable rotation matrix, R_d, is the identity matrix, while aggressive maneuvers should occur with minimal angles. After the aggressive maneuver execution, the controller must stabilize the attitude error as close to zero as possible.

5.3 Numerical Example: a Quadrotor UAV

In this section, the proposed NMPC scheme is corroborated using a quadrotor UAV through numerical experiments[1]. An eight-shaped trajectory in $\mathbb{R}^3$ is required to be tracked, which is described as follows

$$\xi_{\text{ref}} = \begin{bmatrix} 8\cos(\pi t/10)\ \text{m} \\ 8\sin(\pi t/5)\ \text{m} \\ 3 - \cos(\pi t/10)\ \text{m}. \end{bmatrix} \tag{5.12}$$

Besides the trajectory tracking, obstacles are positioned requiring aggressive maneuvers from the vehicle to accomplish the circuit with minimal deviation from the reference. Additionally to the three situations described in Figure 5.1, the UAV is evaluated for the standard convex obstacle deviation. Although the obstacles are predefined in the proposed test circuit, the controller does not know any information about them.

5.3.1 Experiment setting

All experiments are performed considering the quadrotor UAV model characterized by (3.5)-(3.8), where $e^{\mathcal{B}} = e_3$ and $f^{\mathcal{I}}_e = -a_g e_3$, with $e_3 = \begin{bmatrix}0 & 0 & 1\end{bmatrix}^\top$, and a_g is the gravity acceleration. Because each propeller has a limited thrust, the expression (4.22) is used to map this thrust limitation to the input vector. The quadrotor UAV's parameters were obtained from Raffo (2011) (see Table 4.1).

The parameters of obstacles at each zone, which are positioned along the trajectory, are defined in Table 5.1. Figure 5.3 shows the top view of the test circuit, where the S

[1] A video of the performed experiments is available in https://youtu.be/1JG-xxsLKyg.

(Slalom), N (Non-convex Obstacle composed by the union of ellipsoids 4.1, 4.2, and 4.3), G (Narrow Gap), and C (Convex Obstacle) zones identify specific required maneuvers.

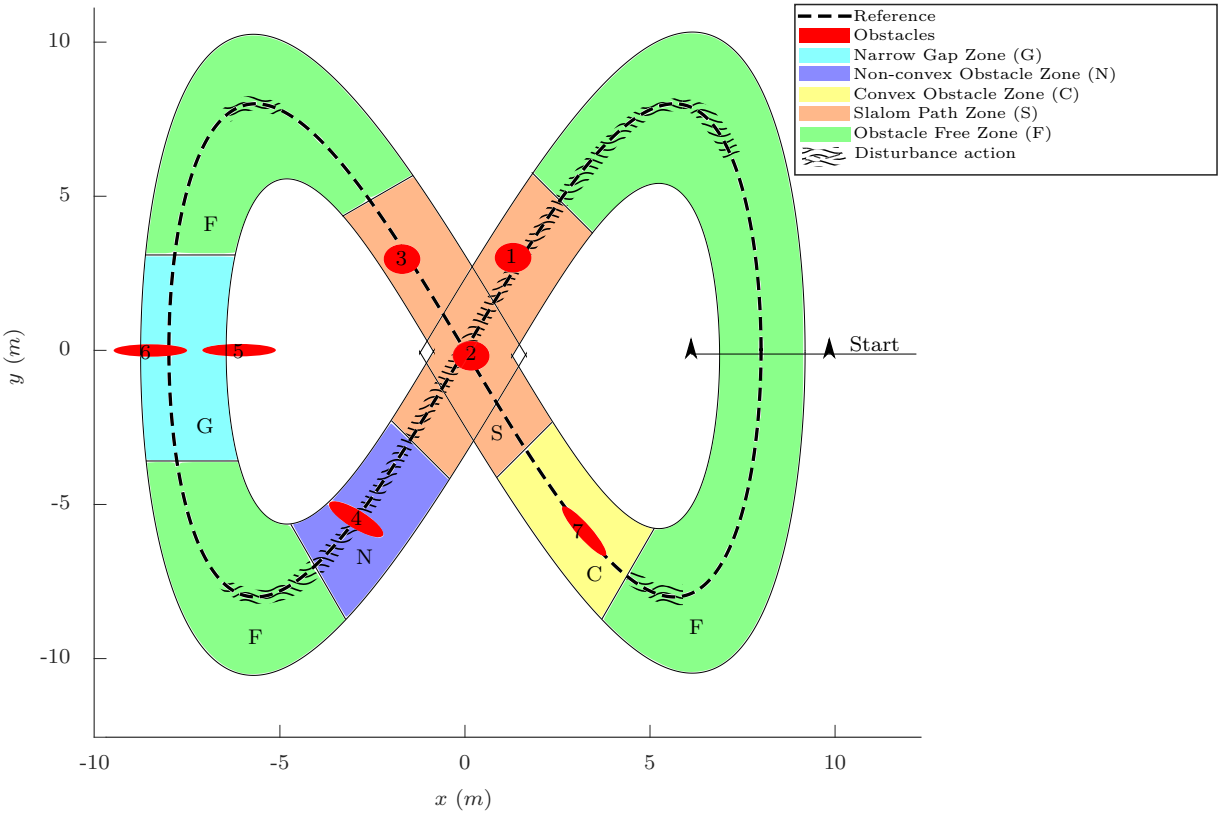


Figura 5.3: Proposed test circuit illustration.

Cuadro 5.1: Obstacles parameters at each test circuit zone shown in Figure 5.3.

Zone	Obs.	Elipsoidal Parameters								
		Physical Dimensions (m)			Center (m)			Orientation (ZYX) (rad)		
		w_x	w_y	w_z	c_x	c_y	c_z	ψ	θ	ϕ
S	1	0.5	0.5	1	1.3	3	2.8	0	0	0
	2	0.5	0.5	1	0.2	-0.2	3	0	0	0
	3	0.5	0.5	1	-1.8	2.97	3.19	0	0	0
N	4.1	0.3	0.3	1	-2.92	-5.44	3.36	$\pi/3$	$\pi/5$	$\pi/5$
	4.2	0.3	0.3	1	-2.92	-5.44	3.36	$-\pi/3$	$-\pi/5$	$-\pi/5$
	4.3	0.3	0.3	1	-2.92	-5.44	3.36	0	0	0
G	5	1	0.2	3	-6	0	4	0	0	0
	6	1	0.2	3	-8.5	0	4	0	0	0
C	7	0.2	1	0.2	3.2	-5.86	2.59	$-\pi/5$	0	0

In addition, the UAV is affected by exogenous forces, $T_{\text{dist}} = \begin{bmatrix} \eta_x & \eta_y & \eta_z \end{bmatrix}^\top$, in the three directions in order to corroborate the disturbance rejection capability of the proposed controller. These forces can be interpreted as unexpected aerodynamic forces caused by, for example, persistent wind, which vary according to Table 5.2. For instance, assuming a

wind gust speed of $v = 40km/h$ affecting laterally the UAV, the air density $\rho = 1{,}2kg/m^3$, the lateral area of the UAV of approximately $A = 0{,}07\text{m}^2$, then the drag force, $F_w = \frac{1}{2}\rho v^2 A$, caused by the wind gust is approximately $5N$. In addition, it is highlighted in Figure 5.3 where the disturbances occur along the test circuit. To simulate an external obstacle detector, Algorithm 5.1 is implemented in the main simulation structure.

Cuadro 5.2: Disturbance parameters considered in the simulation.

Period t (s)	T_{dist}(N)		
	η_x	η_y	η_z
$2 < t < 8$	-5	5	5
$12 < t < 13$	5	-5	5
$17 < t < 18$	5	5	-5
other	0	0	0

Algorithm 5.1 Simulation of an external obstacle detector.

$C_i \leftarrow$ center of the i-th obstacle
$E_i \leftarrow$ ellipsoidal set parameter that represents the i-th obstacle
$\mathbb{E}_c \leftarrow$ set of matrices that are considered by the NMPC
$\gamma \leftarrow$ sensor range
for each time step k **do**
  for each i-th obstacle specified in Table 1 **do**
    if $\|C_i - \xi\|_2 < \gamma$ **then**
      $\mathbb{E}_c \leftarrow \{\mathbb{E}_c; E_i\}$
    else
      $\mathbb{E}_c \leftarrow \{\mathbb{E}_c; \mathbf{0}_{4\times 4}\}$
    end
  end
end

The initial conditions for this scenario are zero for all states except for $\xi_0 = \begin{bmatrix} 8 & 0 & 2 \end{bmatrix}^\top$ and $R_0 = I_3$. Both the input and state limits are presented in Table 5.3. For all the results presented below, the controller is running at 100 Hz with a prediction horizon set to $N_p = 120$, which is defined from a trade-off between computational cost and tracking performance. In the obstacle-avoidance context, the prediction horizon's length is defined by considering the time required to perform an unexpected deviation trajectory since the UAV knows only the obstacles within the sensor range. If the prediction horizon is insufficient, the UAV may collide with obstacles due to its inertia and its accelerations that are limited. For the cost functional, the weighting matrices and constants are defined as $Q_y = \texttt{diag}\{170I_3, 40I_3, 60I_3\}$, $Q_u = 0{,}02I_4$, $K_n = 157{,}5$, $K_d = 1{,}5$, $K_e = 0{,}08$, $\epsilon_r = 0{,}15r$, $\epsilon_h = 0{,}15h$, $K_R = k_1 = k_2 = k_3 = 1$, $d_s = \max\{\delta_x, \delta_y, \delta_z\}$, where δ_x, δ_y, and δ_z are the width ellipsoidal parameters of each obstacle.

Cuadro 5.3: Input/State Constraints.

Variable	Minimum value	Maximum value
f_1	0 N	12.3 N
f_2	0 N	12.3 N
f_3	0 N	12.3 N
f_4	0 N	12.3 N
v_x	-13 m/s	13 m/s
v_y	-13 m/s	13 m/s
v_z	-13 m/s	13 m/s
a_x	-30 m/s^2	30 m/s^2
a_y	-30 m/s^2	30 m/s^2
a_z	-30 m/s^2	30 m/s^2
ω_p	-18 rad/s	18 rad/s
ω_q	-18 rad/s	18 rad/s
ω_r	-8 rad/s	8 rad/s

5.3.2 Results

Following the design of experiments, Figures 5.4 to 5.11 are depicted in order to evaluate the performance of the controller with respect to the main objectives pursued in this chapter. As described in Section 5.1 (problem statement), three states, ξ, are chosen as tracked variables. Moreover, an integral action, included in the augmented system with the integral of tracking errors, is considered in the control design. From Figures 5.4 and 5.5, observe that the reference trajectory is accurately tracked in all numerical experiments, that is, with nominal parameters and with uncertainty of $\pm 10\,\%$ in the elements of the mass and inertia. Note that sharpest oscillations occur when obstacles are avoided, which are more evident in Figure 5.5. All disturbances affecting the system (see Table 5.2) are rejected efficiently, as shown in the highlighted regions of Figure 5.6. The proposed control strategy, therefore, robustly fulfilled the requirements for trajectory tracking in the presence of uncertainties, disturbance, and obstacles.

In addition to the obstacle avoidance capability, other important feature of the proposed control strategy is the ability to perform aggressive maneuvers mainly as a result of a more efficient obstacle deviation. Figure 5.7 shows the ellipsoidal set $\bar{\mathcal{V}}(t)$ which varies according to both the UAV position and attitude. It is worth highlighting that the aircraft (green ellipsoid) satisfactorily executes the required maneuvers, that is, throwing a narrow gap, passing by a non-convex obstacle gap, avoiding a convex obstacle, and performing slalom movements.

To verify the collision avoidance performance throughout the entire flight, after the experiments, the minimum distance σ_ℓ between the UAV set $\bar{\mathcal{V}}(t)$ (see (5.2)) and the ℓ-th

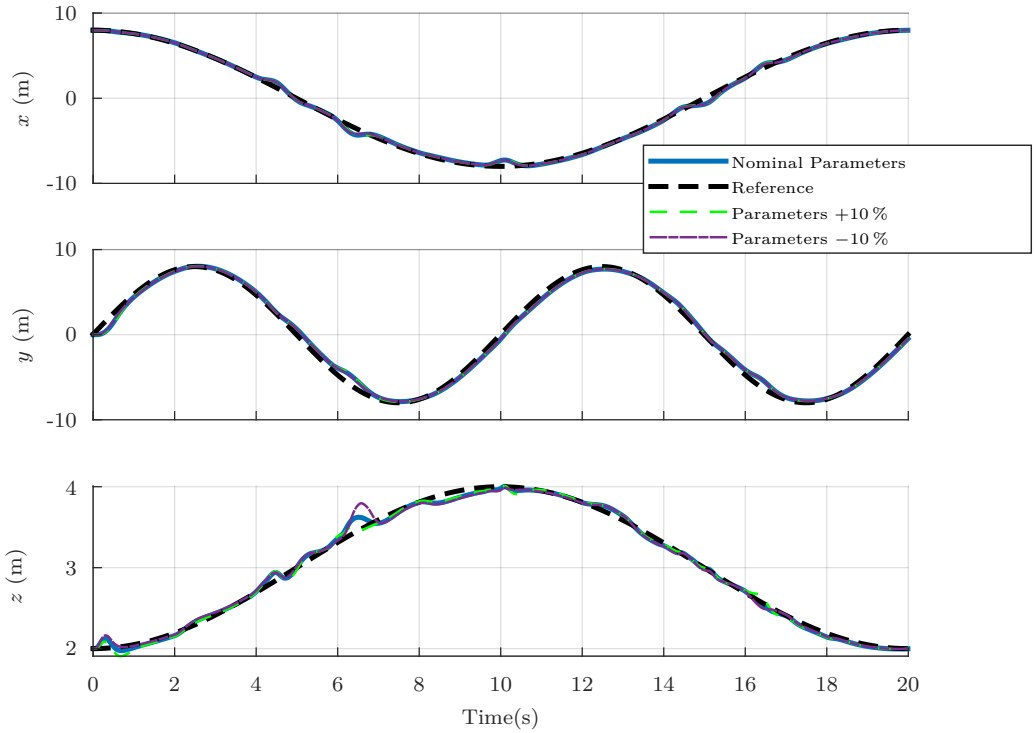


Figura 5.4: UAV Position, ξ, during the numerical experiments. The reference is defined by (5.12).

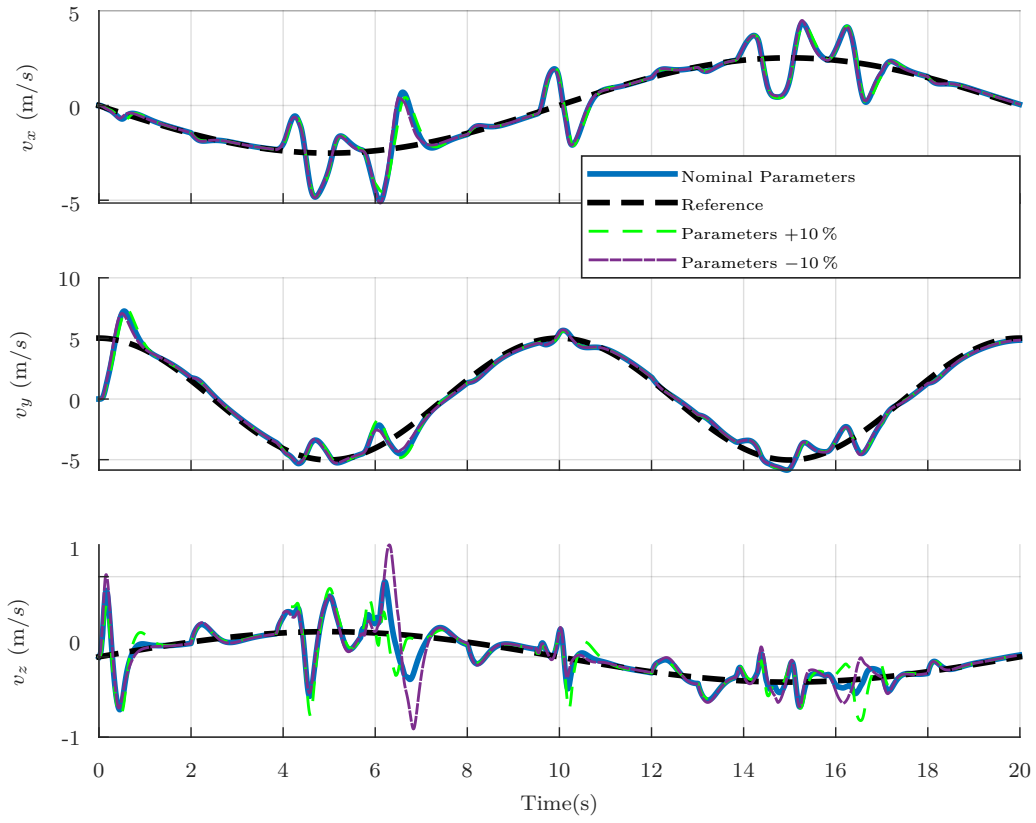


Figura 5.5: UAV Velocity, $\dot{\xi}$, during the numerical experiments. The sharpest oscillations are due to the aggressive reaction to obstacles with fast deviation movements.

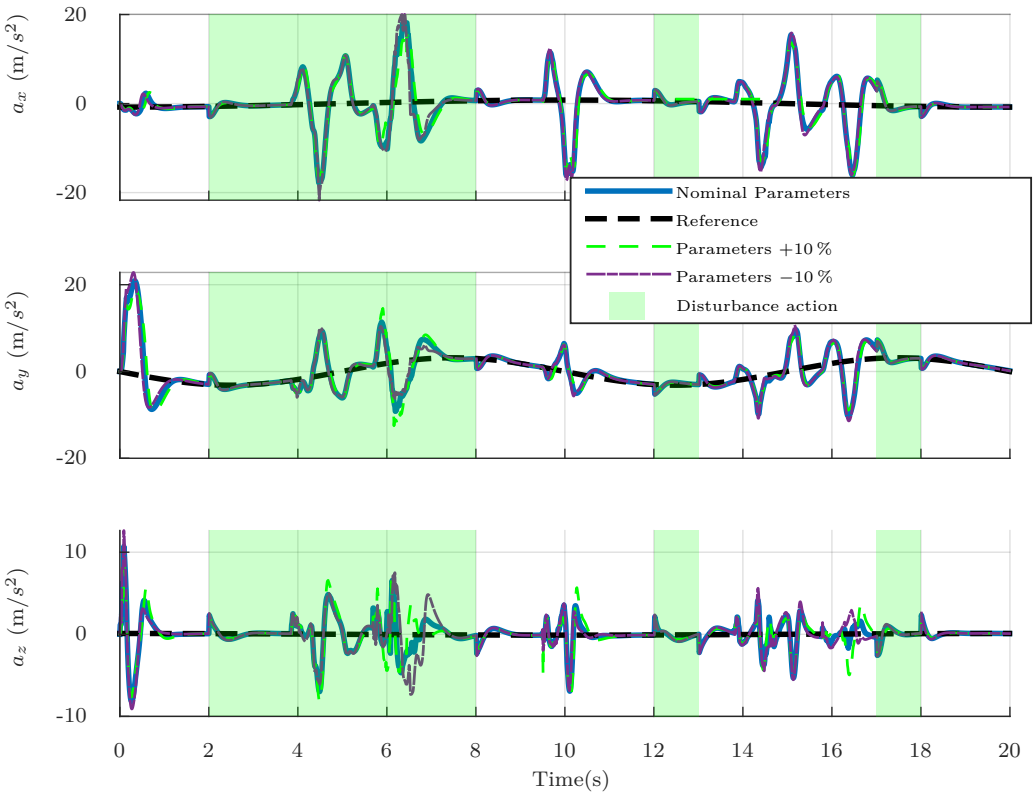
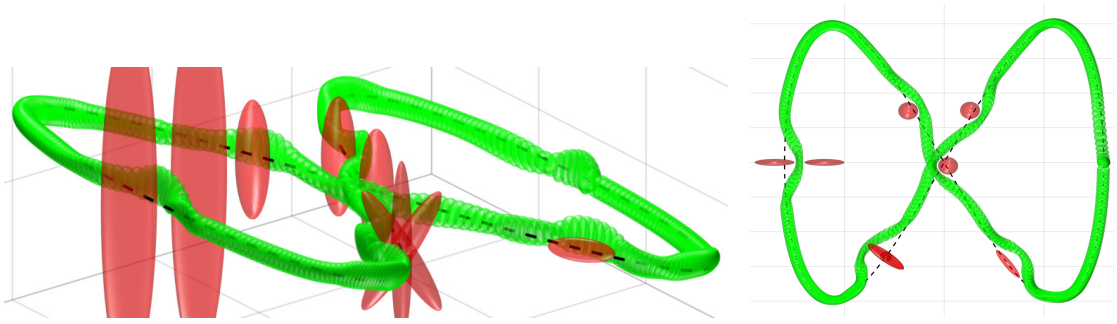


Figura 5.6: UAV acceleration behavior, $\ddot{\xi}$, during the numerical experiments. Highlighted areas show the rejection of disturbances applied to the system, which are presented in Table 5.2. In addition, high accelerations required in some situations indicate aggressive flight execution.



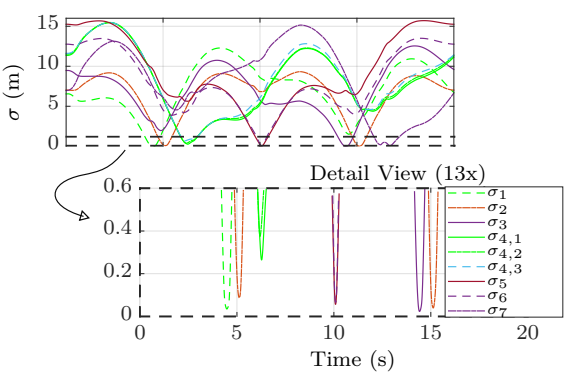
(a) Isometric View. (b) Top View.

Figura 5.7: Ellipsoidal set $\bar{\mathcal{V}}$(t) during the numerical experiment. The UAV attitude parameterization, considered in the set modeling, allows the aggressive maneuver execution by the NMPC controller.

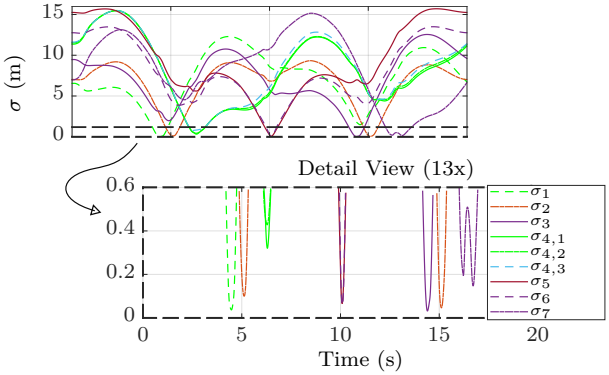
obstacle set (see (5.3)) are calculated from the following optimization problem:

$$\begin{aligned} \sigma_\ell(t) = \quad & \text{mín} \quad \|q(t) - e\|_2, \qquad \forall \ell = 1, \cdots, N_o, \\ & \text{s.t.} \qquad q(t) \in \bar{\mathcal{V}}(t), \quad e \in \mathcal{E}_\ell. \end{aligned} \tag{5.13}$$

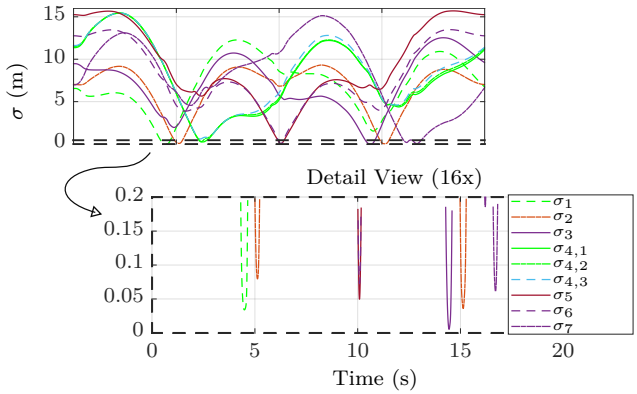
Figure 5.8 shows the calculated σ_ℓ for all simulated cases. As mentioned in Section 5.2.1, the condition given by $\Delta(f)$ (see (5.6)) only guarantees the separation between the ellipsoids, but there is no relation with distance. Therefore, the safety margins ϵ_r and ϵ_h, considered in the definition of the set $\bar{\mathcal{V}}(t)$ (see (5.2)), are used as design parameters allowing to perform the trajectory tracking safely when model uncertainties can cause unexpected behavior. Such parameters are thus specified on the basis of the maximum and minimum system uncertainties and, then, adjusted according to the performance of the numerical experiments. From Figure 5.7, the term σ_ℓ presents small values when avoiding obstacles due to the aggressive maneuvering capability that allows minimum deviation of the tracked trajectory, even with the model mismatch due to parametric uncertainties. Additionally, it is always greater than 0 for all cases, which validates the collision avoidance capability of the proposed NMPC.



(a) Nominal Parameters.



(b) Parameters +10 %.



(c) Parameters −10 %.

Figura 5.8: Minimum distance between the UAV and obstacles along all the numerical experiments, i.e. nominal parameters and with uncertainty of ±10 % in the parameters of mass and inertia tensor. The term σ_ℓ is always greater than 0 for all cases, which validates the collision avoidance capability of the proposed NMPC.

For the sake of clarity, the attitude of the UAV is illustrated in Figure 5.9 by using the Euler angles representation in degree unit. As expected, mainly during the obstacle deviation, large angular excursions are executed without any concern for representational singularity, since the proposed NMPC controller is formulated on $\mathsf{SE}(3)$. On the other hand,

the term $\Psi(R)$, considered in the cost functional, is responsible to maintain and stabilize the angles close to zero when no maneuver is required. In addition, the aggressiveness feature is corroborated by Figure 5.10, where the fast motion control demands large angular acceleration.

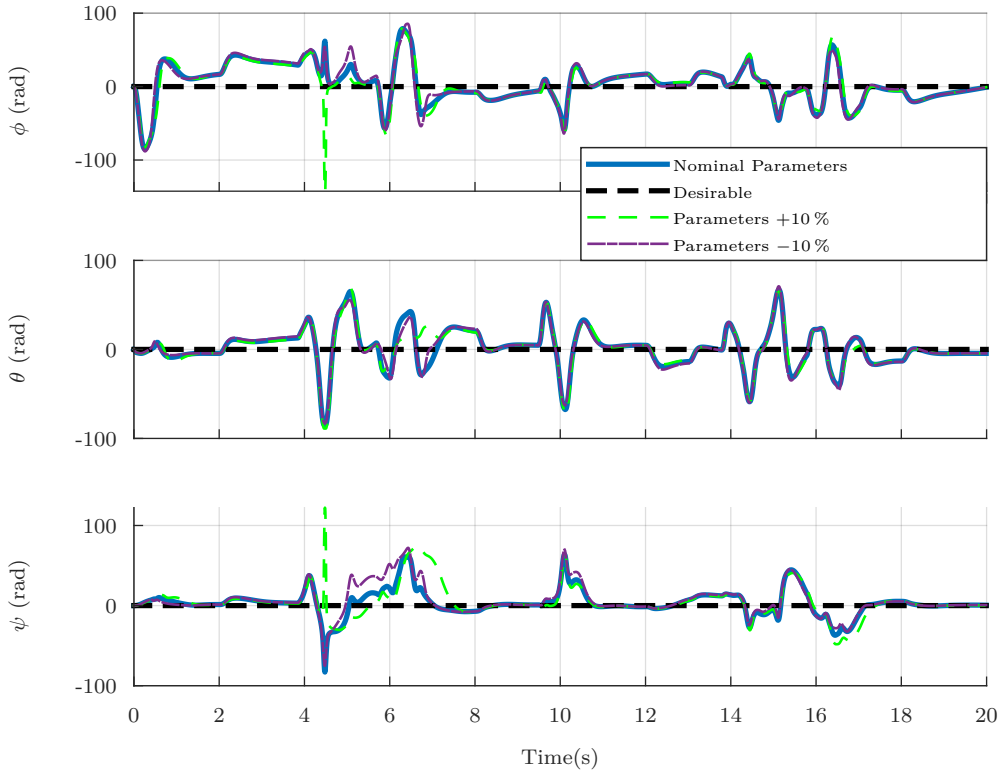


Figura 5.9: UAV Euler angles computed from the rotation matrix after the numerical experiments. Large angular excursions corroborate the aggressive maneuver capability.

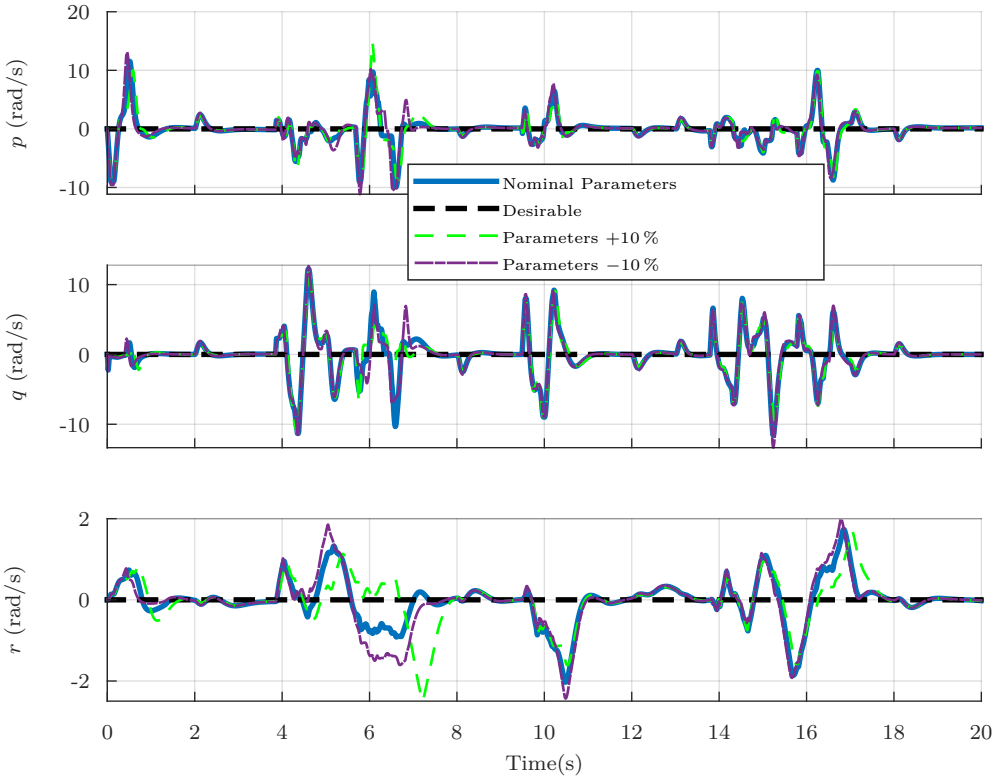


Figura 5.10: UAV Angular Velocities during the numerical experiments. Fast motion control has demanded large angular acceleration.

The proposed NMPC complied with all the system constraints considered in the control design. Figure 5.11 shows the control signals during the experiments. Such a set of input signals, found in Figure 5.11a, are mapped on the propeller forces, Figure 5.11b. It is worth remembering that the NMPC design's input constraints include the UAV propeller motors' physical characteristics. It can be noticed from Figure 5.11 that the inputs reach the limits given in Table 5.3 during almost the entire flight, which indicate the aggressiveness of the proposed controller and its ability to deal with constrained control problems. These extreme values applied in the UAV occur when aggressive maneuvers are required, or when the UAV has to overcome its inertia at the beginning of the experiments.

5.3.2.1 Aggressiveness versus tracking performance

An important feature of the proposed controller is to allow the modification of the weighting variable K_R, which multiplies the element $\Psi(R)$ in the cost functional (5.11), and to make the UAV acts more or less aggressive. To evaluate such a skill and its consequences for tracking performance, an additional numerical experiment is proposed in which the circuit illustrated in Figure 5.12b is used without considering external disturbances. This experiment involves performing slalom movements with different K_R values and different

speed trajectories, while tracking the trajectory given by

$$x_{\text{ref}} = v_{\text{ref}} t,$$
$$y_{\text{ref}} = 0,$$
$$z_{\text{ref}} = 2.$$

As stated above, the orientation error $\Psi(R)$ considers the identity matrix to be a reference. This means that when the rotation matrix is close to this condition the rotation angles are close to zero, performing little rotational movements. Hence, situations where the orientation error presents higher values are considered more aggressive. In this way, from Figure 5.12a, it can be observed that, preserving all experimental conditions and by increasing the K_R parameter, the aggressiveness has been reduced. However, when this feature is lost, the UAV has more difficulty to follow fast trajectories, as the time spent during the obstacle avoidance process is longer. Therefore, if the UAV is more aggressive, the obstacle deviation is faster and the tracking is more effective.

Experiments with different speed trajectories were performed in order to verify this behavior. The performance was analyzed by the ISE (Integral Squared Error) index, concerning both the position and attitude errors. In each case, the presented indexes were normalized as follows: the ISE position indexes were divided by the index obtained with $v_{\text{ref}} = 3$ m/s and $K_R = 1$, while the ISE attitude indexes were divided by the index obtained with $v_{\text{ref}} = 3{,}5$ m/s and $K_R = 1500$. The normalized values of ISE indexes are presented in Table 5. From this analysis, the flight tends to be more aggressive as the reference speed increases, regardless of the value of K_R. This demonstrates the ability of the proposed NMPC controller to consider the UAV attitude into the optimal control problem. Additionally, the performance improvement from the increase in aggressiveness is sustained at all simulated speeds, corroborating the advantage of the aggressive maneuver capability in the tracking problem with obstacle avoidance.

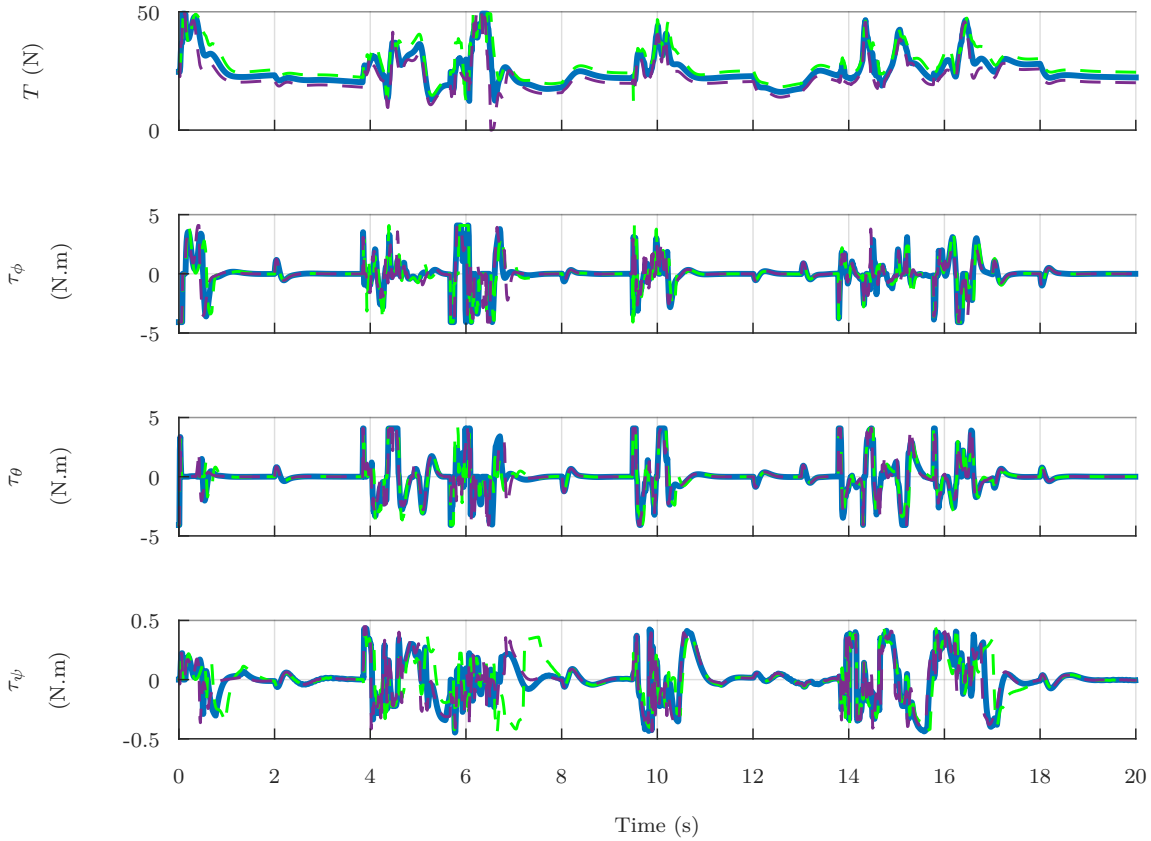
Cuadro 5.4: Normalized ISE performance indexes for K_R and v combinations.

v_{ref} (m/s)	K_R							
	1	500	1000	1500	1	500	1000	1500
	Position ISE				Attitude ISE (from $\Psi(R)$)			
3	1.02	1.22	1.46	1.69	6.88	1.66	1.22	1.00
3.5	1.00	1.19	1.49	1.80	7.73	2.26	1.64	1.36
4	1.03	1.36	1.76	2.13	10.53	3.44	2.55	2.12
4.5	1.39	1.67	2.17	2.65	19.02	5.32	3.83	3.11
5	1.89	2.18	2.85	3.43	22.07	7.30	5.18	4.24
5.5	2.44	3.25	3.82	4.54	21.24	9.82	6.87	5.50

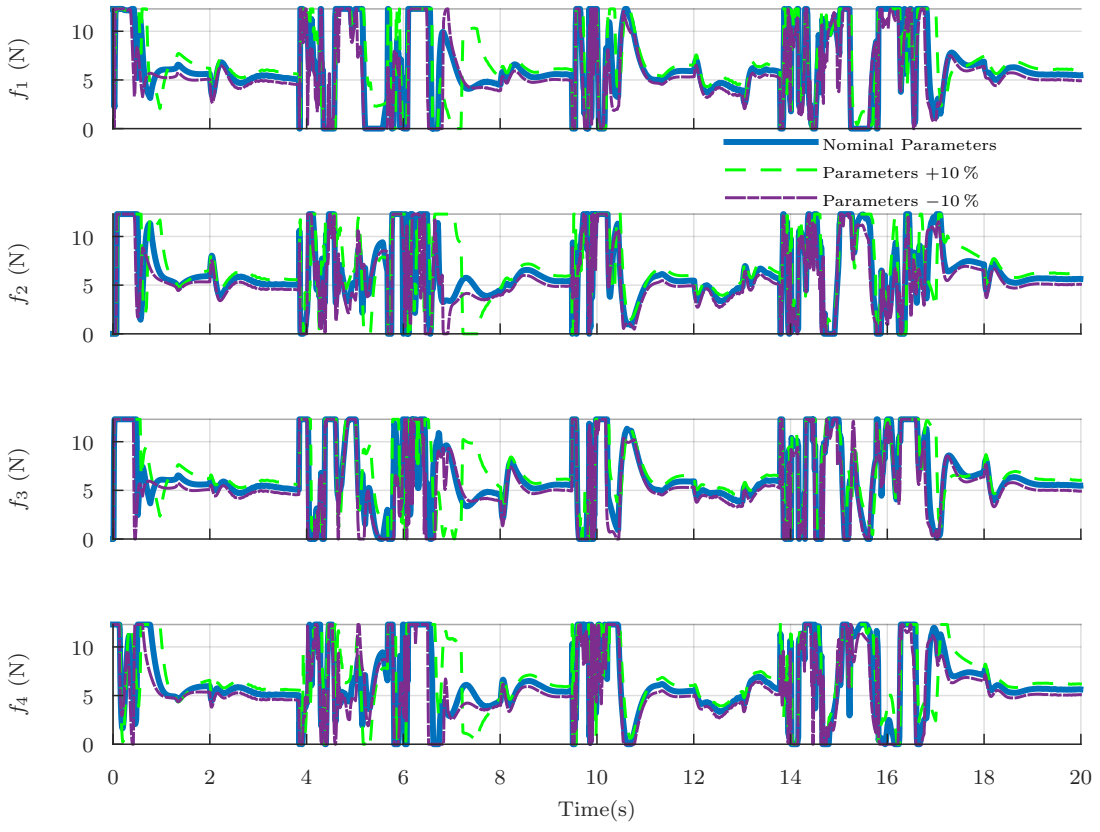
5.4 Final Remarks

A nonlinear model predictive control strategy was proposed for underactuated vehicles to perform fast motion while avoiding obstacles dynamically with aggressive maneuvers. A single optimization layer directly considers the dynamic equations of the UAV formulated in $\mathsf{SE}(3)$, without concerning representational singularities, and considering integral action in all tracked states. The algebraic ellipsoidal approach, in which the vehicle's attitude was considered into the optimal control problem, made the obstacle-avoidance process more efficient with faster deviation movements and allowed the aircraft to fly through narrow spaces, that is, when the vehicle's attitude influences the success of the deviation maneuver.

Numerical results with a quadrotor UAV corroborated the controller ability to perform aggressive maneuvers, robustly fulfilling the requirements for trajectory tracking in the presence of parametric uncertainties, external disturbance, and obstacles. In addition, it was demonstrated that flight aggressiveness improves task performance, which can be tuned from the cost functional parameterization. This feature is useful in situations where large angular accelerations are not desirable, such as autonomous air transport of human organs, allowing to achieve a trade-off between aggressiveness and performance.

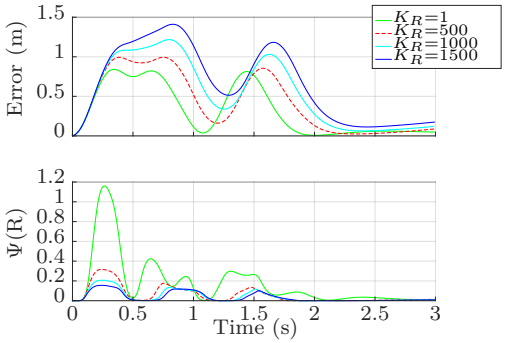


(a)

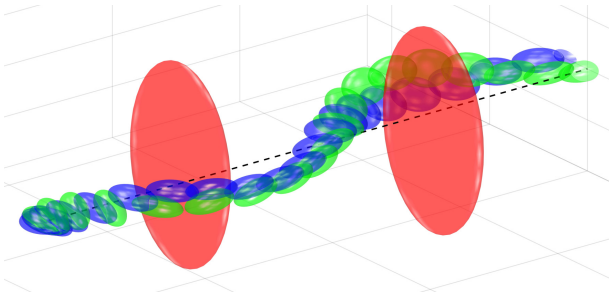


(b)

Figura 5.11: The input bounds are correctly satisfied by the controller, which applied extreme force values when aggressive maneuvers are required.



(a) Position error and Ψ(R).



(b) Ellipsoidal set $\bar{\mathcal{V}}$(t). Trajectories obtained with $K_R = 1$ (green ellipsoids) and $K_R = 1500$ (blue ellipsoids).

Figura 5.12: Performance and aggressiveness evaluation from variation of parameter K_R. As far as K_R increases, the aggressiveness and the performance decrease.

6

Point-to-point Motion with Obstacle Avoidance

The problem of aggressive motion in cluttered environments with unknown obstacles is also addressed in this chapter. However, in contrast to the previous chapter, the autonomous underactuated vehicle only receives the destination point. This means that, in addition to controlling the vehicle, the NMPC scheme must compute an optimal trajectory that performs a point-to-point motion while avoiding obstacles located between the starting and destination points. As in the previous chapter, an algebraic condition for set intersection verification must be included in the OCP. In this context, a secondary objective of the chapter is to better represent the obstacles as polytopes, which are suitable for describing asymmetric and arbitrary objects, while keeping the vehicle representation as ellipsoidal sets. Such a mixed polytopic-ellipsoidal representation of obstacles and vehicle aims to achieve a balance compromise between accuracy and computational burden. In this regard, a new ellipsoidal-polytopic approach for obstacle avoidance is proposed. This chapter also investigates a modified version of the OCP (4.2), in which fast motion control with obstacle-avoidance capability is regarded.

6.1 Problem Statement

Problem 6.1. Design an NMPC scheme without terminal conditions able to perform point-to-point motion while avoiding obstacles with aggressive maneuver capability.

Problem 6.2. Design an NMPC scheme without terminal conditions able to perform point-to-point motion while avoiding obstacles with aggressive maneuver capability, which considers the mission time reduction as an economic criterion.

Assumption 6.1. *The vehicle is approximated by an ellipsoidal set, and the obstacles are approximated by polytopic sets;*

Assumption 6.2. *While the vehicle moves along cluttered environments with unknown obstacles, an external obstacle detector algorithm sends to the controller the parameters of the nearest obstacles;*

Assumption 6.3. *All system states are available to the controller.*

6.2 Control Strategies

This section describes the proposed control strategies. First, the ellipsoidal-polytopic collision detection approach is presented, followed by the NMPC and fast motion NMPC formulations, both with obstacle-avoidance capability, which are extension versions of OCPs (4.1) and (4.2), respectively.

6.2.1 Ellipsoidal-polytopic collision check approach

For collision avoidance purposes, the shape of the vehicle is also modeled as an ellipsoidal set, $\mathcal{V}(\xi, Q)$, as defined by equation (5.1) in the previous chapter. However, now, a different affine transformation is applied to determine the time varying set $\mathcal{V}(t)$ given the rotation matrix R, the position ξ, and a matrix $\hat{Q}(t) \in \mathbb{R}^{3\times3}$

$$\mathcal{V}(\xi, \hat{Q}) \triangleq \{q \in \mathbb{R}^3 : (q - \xi(t))^\top \hat{Q}^{-1}(q - \xi(t)) \leq 1\}, \tag{6.1}$$

where,

$$\hat{Q}(t) = R_{\mathcal{B}}^{\mathcal{I}} D (R_{\mathcal{B}}^{\mathcal{I}})^\top, \qquad D = \begin{bmatrix} r_x^2 & 0 & 0 \\ 0 & r_y^2 & 0 \\ 0 & 0 & h^2 \end{bmatrix},$$

with r_x, r_y, and h physical parameters defined from the problem of enclosing the motion system by the minimum volume ellipsoid that fits it considering safety distance margins.

Each obstacle is modeled as a polytopic set. Convex polytopes are closed under linear mapping, Minkowski sum, and generalized intersection operation. Since this latter operation can only be computed efficiently in the half-space representation (in V-rep is NP-hard) (Scott et al., 2016), this work opts to model the obstacles as H-rep polytopes.

A hyperplane $\mathcal{H}_i$ in $\mathbb{R}^n$, $i = 1, \cdots, m$, given by

$$\mathcal{H}_i \triangleq \{x \in \mathbb{R}^n : a_i^\top x = b_i\},$$

with $a_i \in \mathbb{R}^n$ and $b_i \in \mathbb{R}$, defines two closed half-spaces

$$\mathcal{S}_i \triangleq \{x \in \mathbb{R}^n | a_i^\top x \leq b_i\}, \tag{6.2}$$

$$\bar{\mathcal{S}}_i \triangleq \{x \in \mathbb{R}^n | a_i^\top x > b_i\}. \tag{6.3}$$

Thus, the H-rep of a polytope $\mathcal{P}$ is given by

$$\mathcal{P} \triangleq \{x \in \mathbb{R}^n | Ax \leq b\}, \tag{6.4}$$

with $A = [a_1^\top \ \cdots \ a_m^\top]^\top \in \mathbb{R}^{m \times n}$ and $b = [b_1 \ \cdots \ b_m]^\top \in \mathbb{R}^m$.

In order to avoid linear programming to verify if the motion system, represented by the ellipsoidal set $\mathcal{V}$, intersects the obstacle, represented by the polytope $\mathcal{P}$, we make use of an algebraic approach based on geometric projection. In Kurzhanskiy & Varaiya (2006), a relation is presented to determine the distance and, consequently, a intersection condition between an Ellipsoid $\mathcal{V}(\xi, \hat{Q})$ and a hyperplane $\mathcal{H}(a_i, b_i)$. If the distance function $d(\mathcal{V}(\xi, \hat{Q}), \mathcal{H}(a_i, b_i))$, given by

$$d(\mathcal{V}(\xi, \hat{Q}), \mathcal{H}(a_i, b_i)) = \frac{|b_i - a_i^\top \xi| - (a_i^\top \hat{Q} a_i)^{\frac{1}{2}}}{(a_i^\top a_i)^{\frac{1}{2}}}, \tag{6.5}$$

is greater than zero, then the sets do not intersect each other, i.e., $\mathcal{V} \cap \mathcal{H} = \emptyset$. From (6.5), extending for half-space sets, but, for convenience, regarding just the complementary half-space set, $\bar{\mathcal{S}}_i$ (see (6.3)), the distance function between $\mathcal{V}(\xi, \hat{\mathcal{Q}})$ and $\bar{\mathcal{S}}_i(a_i, b_i)$ is given by

$$w(\mathcal{V}(\xi, \hat{Q}), \bar{\mathcal{S}}_i(a_i, b_i)) = \frac{b_i - a_i^\top \xi + (a_i^\top \hat{Q} a_i)^{\frac{1}{2}}}{(a_i^\top a_i)^{\frac{1}{2}}}. \tag{6.6}$$

As a result, if $w(\mathcal{V}(\xi, \hat{Q}), \bar{\mathcal{S}}_i(a_i, b_i)) < 0$, then $\mathcal{V} \subseteq \bar{\mathcal{S}}_i$. However, from the best knowledge of the authors, in the literature, there is no algebraic way for intersection verification between an ellipsoid and a polytope. Therefore, Theorem 6.1 is proposed.

Theorem 6.1. *Consider the polytope $\mathcal{P}$ given by (6.4), an ellipsoidal set $\mathcal{V}(\xi, \hat{Q})$ defined in (6.1), the half-space $\bar{\mathcal{S}}_i$ given by (6.3), $i = 1, \cdots, m$, and the operator $[\Upsilon]_+ = \max\{\Upsilon, 0\}$, $\Upsilon \in \mathbb{R}$. If function $\tilde{\Delta}(\mathcal{V}, \mathcal{P})$, given by*

$$\tilde{\Delta}(\mathcal{V}, \mathcal{P}) = \prod_{i=1}^{m} [w(\mathcal{V}, \bar{\mathcal{S}}_i(a_i, b_i))]_+, \tag{6.7}$$

is equal to zero, then the sets $\mathcal{V}(\xi, \hat{Q})$ and $\mathcal{P}$ are disjoint, i.e., $\mathcal{V}(\xi, \hat{Q}) \cap \mathcal{P} = \emptyset$.

Demostración. Since $\mathcal{P}$ is a convex set,

$$\bar{\mathcal{S}}_i \not\subseteq \bar{\mathcal{S}}_j \quad \forall j = 1, \cdots, m, \quad \forall i = 1, \cdots m, \quad \forall j \neq i,$$

$$\bar{\mathcal{S}}_i \not\subseteq \mathcal{S}_i \quad \forall i = 1, \cdots, m,$$

where m is the number of half-spaces that defines the polytope. Hence,

$$\begin{aligned}
\mathcal{V} \cap \mathcal{S}_i \neq \emptyset &\iff \mathcal{V} \nsubseteq \bar{\mathcal{S}}_i, \\
\mathcal{V} \cap \mathcal{S}_i = \emptyset &\iff \mathcal{V} \subseteq \bar{\mathcal{S}}_i, \\
\mathcal{V} \subseteq \bar{\mathcal{S}}_1 \vee \cdots \vee \mathcal{V} \subseteq \bar{\mathcal{S}}_m &\implies \mathcal{V} \cap \underbrace{\mathcal{S}_1 \cap \cdots \cap \mathcal{S}_m}_{\mathcal{P}} = \emptyset, \\
\mathcal{V} \subseteq \bar{\mathcal{S}}_1 \vee \cdots \vee \mathcal{V} \subseteq \bar{\mathcal{S}}_m &\implies \mathcal{V} \cap \mathcal{P} = \emptyset. \qquad (6.8)
\end{aligned}$$

Returning to (6.6),

$$\mathcal{V} \subseteq \bar{\mathcal{S}}_i \iff w(\mathcal{V}, \bar{\mathcal{S}}_i) < 0 \iff [w(\mathcal{V}, \bar{\mathcal{S}}_i)]_+ = 0,$$

$$\mathcal{V} \subseteq \bar{\mathcal{S}}_i \iff [w(\mathcal{V}, \bar{\mathcal{S}}_i)]_+ = 0.$$

Hence,

$$\begin{aligned}
\tilde{\Delta}(\mathcal{V}, \mathcal{P}) = \prod_{i=1}^{m} [w(\mathcal{V}, \bar{\mathcal{S}}_i(a_i, b_i))]_+ = 0 \\
\iff \mathcal{V} \subseteq \bar{\mathcal{S}}_1 \vee \mathcal{V} \subseteq \bar{\mathcal{S}}_2 \vee \cdots \vee \mathcal{V} \subseteq \bar{\mathcal{S}}_m.
\end{aligned}$$

Returning to (6.8)

$$\begin{aligned}
\tilde{\Delta}(\mathcal{V}, \mathcal{P}) = \prod_{i=1}^{m} [w(\mathcal{V}, \bar{\mathcal{S}}_i(a_i, b_i))]_+ = 0 \\
\implies \mathcal{V} \subseteq \bar{\mathcal{S}}_1 \vee \mathcal{V} \subseteq \bar{\mathcal{S}}_2 \vee \cdots \vee \mathcal{V} \subseteq \bar{\mathcal{S}}_m \\
\implies \mathcal{V} \cap \mathcal{P} = \emptyset
\end{aligned}$$

and, therefore,

$$\tilde{\Delta}(\mathcal{V}, \mathcal{P}) = \prod_{i=1}^{m} [w(\mathcal{V}, \bar{\mathcal{S}}_i(a_i, b_i))]_+ = 0 \implies \mathcal{V} \cap \mathcal{P} = \emptyset.$$

■

6.2.1.1 Relaxed collision constraint for obstacle avoidance

To perform safe navigation, it is necessary to ensure that collisions do not occur during the movement of the motion system. Hence, constraints are imposed to ensure that the predicted set at each time instant j, $\mathcal{V}(k+j)$, given by equation (6.1) after discretization, does not come in space positions that are obstructed by obstacles, i.e.

$$\mathcal{V}(k+j) \subseteq \underbrace{\left(\mathbb{R}^3 - \bigcup_{l=1}^{N_o} \mathcal{P}_\ell\right)}_{\text{free space}}, \forall \ell = 1, \cdots, N_o, \forall j = 0, \cdots, N_p. \qquad (6.9)$$

The condition (6.9) is guaranteed if

$$\tilde{\Delta}_\ell(\mathcal{V}(k+j),\mathcal{P}_\ell)=0,\quad \forall \ell=1,\cdots,N_o,\quad \forall j=0,\cdots,N_p. \tag{6.10}$$

Aiming to improve the computational performance, this work replaces the constraint (6.10) by soft constraints, considering penalty functions at the cost functional. The proposed relaxation is given by

$$\tilde{\varphi}_\ell(\tilde{\Delta}(\mathcal{V}(k+j),\mathcal{P}_\ell)=K_n\tilde{\Delta}_\ell(\mathcal{V}(k+j),\mathcal{P}_\ell)^2, \tag{6.11}$$

where K_n is a tuning parameter.

6.2.2 NMPC with obstacle-avoidance capability for motion control of underactuated vehicles on SE(3)

Considering the discrete-time system g_d given by (3.9)-(3.13), the NMPC scheme without terminal conditions, described generally by Section 3.3, repeatedly solves, in each sample time k, the following optimal control problem:

$$\begin{aligned}\min_{x,u}\ &\sum_{j=0}^{N_p}\|\breve{x}(k+j)\|^2_{Q_{\breve{x}}}+\|\bar{u}(k+j)\|^2_{Q_{\bar{u}}}+\sum_{\ell=1}^{N_o}\sum_{j=0}^{N_p}\tilde{\varphi}_\ell(\tilde{\Delta}(\mathcal{V}(k+j),\mathcal{P}_\ell)^2\\ \text{s.t.}\quad & x(j+1)=g_d(x(j),u(j)), && x_0=x(k),\\ & x\in\mathbb{X}, && \forall j\in\mathbb{N}_p,\\ & u\in\mathbb{U}, && \forall j\in\mathbb{N}_p,\end{aligned} \tag{6.12}$$

where $\breve{x}\triangleq\begin{bmatrix}(\xi^{\mathcal{I}}-\xi^{\mathcal{I}}_{\text{end}})^\top & (v^{\mathcal{I}})^\top & \Psi(R^{\mathcal{I}}_{\mathcal{B}},R_d) & (\omega^{\mathcal{B}})^\top\end{bmatrix}^\top\in\mathbb{R}^{10}$ and $\bar{u}\triangleq\begin{bmatrix}\|f^{\mathcal{I}}\| & (\tau^{\mathcal{B}})^\top\end{bmatrix}^\top\in\mathbb{R}^4$, with $Q_{\breve{x}}>0$, and $Q_{\bar{u}}>0$.

Remark 6.1. *The attitude error $\Psi(R^{\mathcal{I}}_{\mathcal{B}},R_d)$ is given by (3.4) considering the identity matrix as a desirable rotation matrix R_d, since the aggressive maneuvers should occur with minimal necessary angles. After the aggressive maneuver is performed, the controller must stabilize the attitude error as close as possible to zero.*

6.2.3 NMPC with obstacle-avoidance capability for fast motion control of underactuated vehicles on SE(3)

Considering the discrete-time system g_d given by (3.9)-(3.13), the economic NMPC scheme repeatedly solves, in each sample time k, the following optimal control problem:

$$\begin{aligned}\min_{x,u} \sum_{j=0}^{N_p} \zeta^j \|\breve{x}(k+j)\|^2_{Q_{\breve{x}}} + \|\bar{u}(k+j)\|^2_{Q_{\bar{u}}} + \sum_{\ell=1}^{N_o}\sum_{j=0}^{N_p} \tilde{\varphi}_\ell(\tilde{\Delta}(\mathcal{V}(k+j),\mathcal{P}_\ell)^2 \\ \text{s.t.} \quad x(j+1) = g_d(x(j),u(j)), \quad x_0 = x(k), \\ x \in \mathbb{X}, \qquad\qquad \forall j \in \mathbb{N}_p, \\ u \in \mathbb{U}, \qquad\qquad \forall j \in \mathbb{N}_p,\end{aligned} \tag{6.13}$$

where $\zeta > 1$ is an exponential weight in the stage cost that encourages the system to arrive at destination point as soon as possible, and the other variables are defined as the OCP (6.12).

Remark 6.2. *Similar to the OCP (4.2), the parameter ζ is used as a tuning gain that makes the motion faster.*

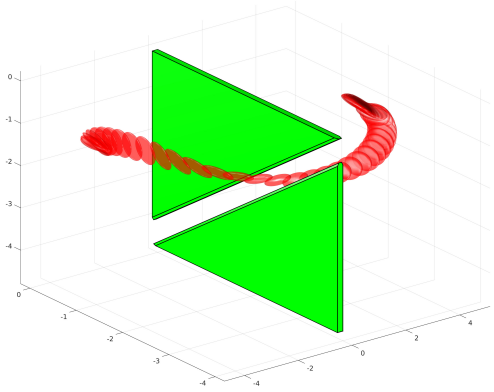
6.3 Numerical Example: a Quadrotor UAV

The proposed NMPC schemes are corroborated with a quadrotor UAV through numerical experiments. First, the objective is to demonstrate the main advantages of the ellipsoidal-polytopic approach, such as avoiding asymmetrical obstacles with long flat surfaces, and improving the computational cost compared to the ellipsoidal strategy presented in Chapter 5. In the second part, experiments are conducted to verify the NMPC scheme defined by the OCP (6.12). In the last part, the proposed approaches defined by (6.12) and (6.13) are compared under the same experimental conditions in order to verify if the exponential weight in the stage error with the included obstacle-avoidance cost indeed results in faster behavior. All experiments are performed considering the quadrotor UAV characterized by the parameters presented in Tables 4.1 and 5.3. The dynamic model is formulated on SE(3), described by (3.5)-(3.8), with $e^{\mathcal{B}} = e_3$, and $f_e^{\mathcal{I}} = -a_g e_3$, where $e_3 = \begin{bmatrix}0 & 0 & 1\end{bmatrix}^\top$ and a_g is the gravity acceleration. Because each propeller has a limited thrust, the expression (4.22) is used to map this thrust limitation to the input vector.

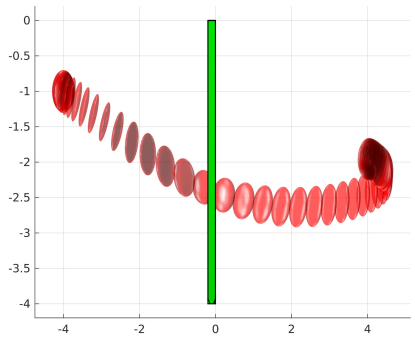
6.3.1 Ellipsoidal versus ellipsoidal-polytopic approach

The first experiment involves the maneuver illustrated in Figure 6.1, where the UAV must accomplish a point-to-point motion avoiding obstacles positioned between the start and destination points. The challenge is to performing a rolling movement defined by the available free space (tilting gap) while moving forward to the destination and keeping the

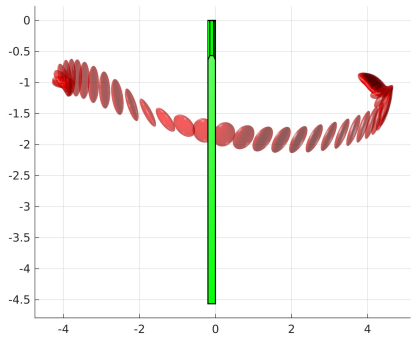
flight stability of the UAV. In this first experiment, we focus on evaluating the ellipsoidal-polytopic based approach, that is, verifying the computational cost compared to the ellipsoidal strategy presented in Chapter 5.



(a) Isometric View.



(b) X-Y plane view.



(c) X-Z plane view.

Figura 6.1: (a) The UAV performing the proposed maneuver: throwing a narrow and tilted gap. (b)-(d) Ellipsoidal set $\mathcal{V}(t)$ during the numerical experiment.

In this sense, both formulations, the ellipsoidal and ellipsoidal-polytopic approaches, are tested with the same experimental environment and under the same simulation conditions. The number of iterations required by the NLP solver to find the optimal solution for each formulation is showed in Figure 6.2. Usually, when the accuracy of the set representation increases, the complexity of the required calculations also increases. However, as can be seen from Figure 6.2, the new approach produced better results, which is less computationally costly. The arithmetic mean of the ellipsoidal representation was 96.6 iterations, with a maximum value equal to 960 iterations, while the ellipsoidal-polytopic representation shows 52.64 (45 % drop) and 298 (70 % drop) iterations, respectively, as the arithmetic mean and the maximum value.

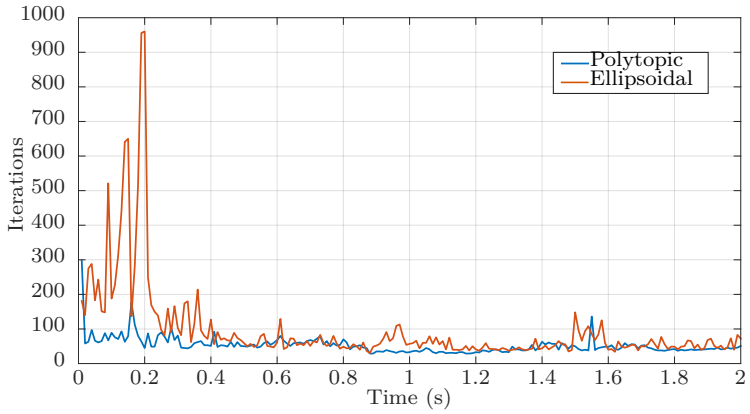


Figura 6.2: Number of iterations required by the NLP solver to find the optimal solution for both the ellipsoidal approach and ellipsoidal-polytopic approach. The latter is less computationally costly.

6.3.2 Motion control with obstacle-avoidance capability using ellipsoidal-polytopic based NMPC

In this second round of experiments[1], two obstacles are added after the tilted gap, as illustrated in Figure 6.3. The major challenge is to perform aggressive maneuvers, defined by the available free spaces, while moving forward to the destination and keeping the UAV flight stability. Additionally, it can be noticed from Figure 6.3 the presence of narrow gaps, i.e., when the distance between two obstacles is smaller than the quadrotor diameter. In this type of environment, the success of the obstacle deviation requires the UAV attitude is considered by the controller.

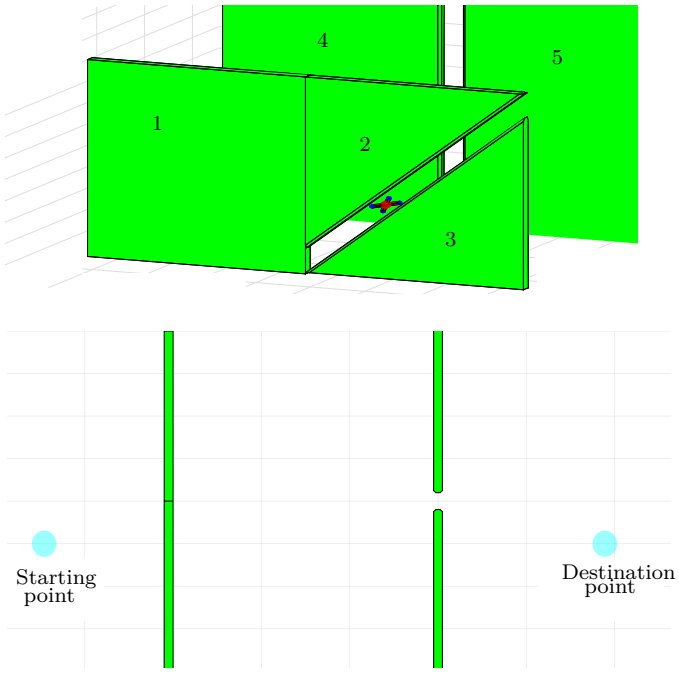


Figura 6.3: Illustration of the proposed experiment.

[1]A video of the performed experiments is available in https://youtu.be/__2jL8Bh_CZo

Moreover, similar to Chapter 5, it is assumed that, while the UAV moves along the proposed environment, an external obstacle detector algorithm sends the parameters of the nearest obstacles to the controller. Although the obstacles are predefined in the proposed test environment, the controller does not know any information about them. To simulate an external obstacle detector, Algorithm 6.1 is implemented in the main simulation structure. In this context, a LIDAR (Light Detection And Ranging) sensor with a range of 8 meters is considered.

Algorithm 6.1 Simulation of an external obstacle detector.

$C_i \leftarrow$ center of the i-th obstacle
$O_i \leftarrow$ matrix that represents the i-th obstacle
$\mathcal{F} \leftarrow$ set that represents the sensor field of view
$\mathbb{O}_c \leftarrow$ set of matrices that are considered by the NMPC
for each time step k **do**
  for each i-th obstacle specified in the proposed test environment **do**
    if $\mathcal{P}_i \cap \mathcal{F} \neq \emptyset$ **then**
      $\mathbb{O}_c \leftarrow \{\mathbb{O}_c; O_i\}$
    else
      $\mathbb{O}_c \leftarrow \{\mathbb{O}_c; \mathbf{0}\}$
    end
  end
end

For all the results presented below, the controller is running at 100 Hz with a prediction horizon set to $N_p = 150$, which is defined from a trade-off between computational cost and control performance. In the obstacle-avoidance context, the length of the prediction horizon is defined taking into account the time required to perform unexpected deviation trajectory, since the UAV knows only the obstacles within the sensor range. If the prediction horizon is insufficient, the UAV may collide with obstacles due to its inertia and limited accelerations.

Remark 6.3. *The prediction horizon is designed so that the predicted position of the UAV is always within the sensor range.*

Remark 6.4. *Since a LIDAR sensor is considered, during the simulation the sensor field of view is used. For example, obstacle four (see Figure* **??***) is only considered by the NMPC after the UAV has passed through the first gap.*

The initial conditions are zero for all states except for $\xi_0 = \begin{bmatrix}-3 & -1 & -2\end{bmatrix}^\top$ and $R_0 = I_3$. The destination point is $\xi_{\text{end}} = \begin{bmatrix}12 & -1 & -2\end{bmatrix}^\top$. For the cost functional, the weighting matrices and constants are defined as $Q_\xi = 320I_3$, $Q_u = 0{,}5I_4$, $K_n = 1{,}5e10$, $K_R = k_1 = k_2 = k_3 = 10$. Theorem 1 is then used with the dimension of the polytope, $\mathcal{P}$,

$n = 3$, and the obstacles are defined by $O_i = [A_i, b_i]$, with

$$O_1 = \begin{bmatrix} -1 & 1 & 0 & 0 & 0{,}7 & 0 & 0{,}7 \\ 0 & 0 & -1 & 0{,}7 & 0{,}5 & 0 & 0{,}5 \\ 0 & 0 & 0 & 0{,}7 & 0{,}5 & -1 & 0{,}5 \\ 0{,}2 & 0 & 4 & -3{,}2 & -2{,}2 & 4{,}6 & -2{,}3 \end{bmatrix}^\top,$$

$$O_2 = \begin{bmatrix} -1 & 1 & 0{,}7 & 0 & 0 & 0 & 0{,}7 \\ 0 & 0 & 0{,}5 & & 0 & 0{,}7 & 0{,}5 \\ 0 & 0 & 0{,}5 & 0 & & 0{,}7 & 0{,}5 \\ 0{,}2 & 0 & 2 & 0 & 0 & 2{,}8 & 2{,}1 \end{bmatrix}^\top,$$

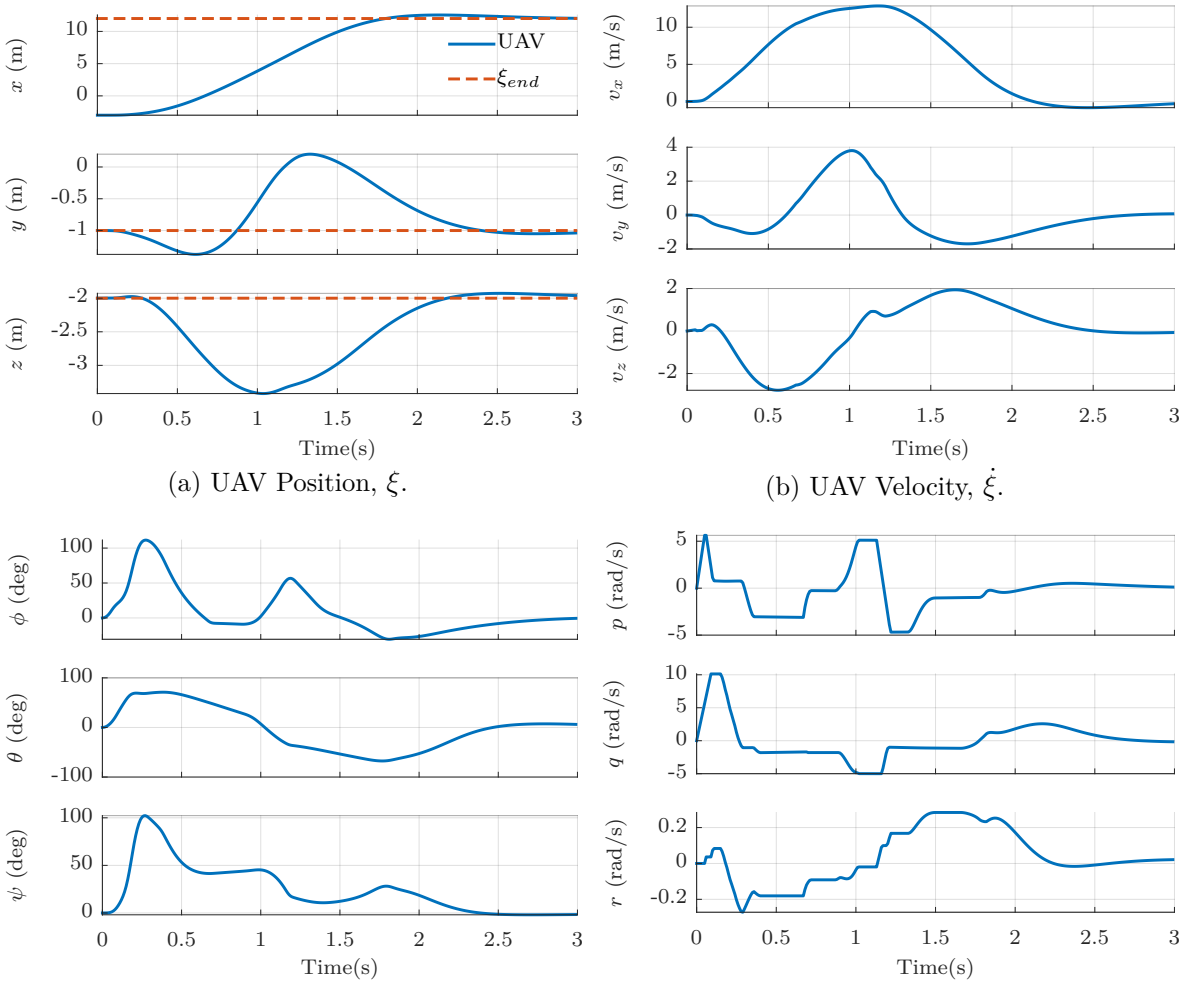
$$O_3 = \begin{bmatrix} 1 & -1 & 0 & 0 & 0 & 0 \\ 0 & 0 & 1 & -1 & 0 & 0 \\ 0 & 0 & 0 & 0 & 1 & -1 \\ 0 & 0{,}2 & 4 & 0 & 0 & 4{,}6 \end{bmatrix}^\top,$$

$$O_4 = \begin{bmatrix} 1 & -1 & 0 & 0 & 0 & 0 & -1 & 1 \\ 0 & 0 & & -1 & 0 & 0 & 1 & 1 \\ 0 & 0 & 0 & 0 & 1 & -1 & 0 & 0 \\ 6{,}1 & -5{,}9 & -0{,}2 & 4{,}2 & 2 & 6 & -6{,}1 & 5{,}8 \end{bmatrix}^\top,$$

$$O_5 = \begin{bmatrix} 1 & -1 & 0 & 0 & 0 & 0 & -1 & 1 \\ 0 & 0 & 1 & -1 & 0 & 0 & -1 & -1 \\ 0 & 0 & 0 & 0 & 1 & -1 & 0 & 0 \\ 6{,}1 & -5{,}9 & 4{,}2 & -0{,}2 & 2 & 6 & -6{,}1 & 5{,}8 \end{bmatrix}^\top.$$

Following the design of experiments, Figures 6.4a-6.4d are depicted in order to evaluate the performance of the NMPC controller. From Figure 6.4a, it is noteworthy that the destination point is accurately reached. Note that, in the velocities shown in Figure 6.4b, sharpest oscillations do not occur as the controller predicts an optimal trajectory of deviation along the prediction horizon.

Similar to Chapter 5, the attitude of the UAV is illustrated in Figure 6.4c by using the Euler angles representation in degree unit. As expected, mainly during the obstacle deviation, large angular excursions are executed without any concern for representational singularity, since the proposed NMPC controller is formulated on $\mathsf{SE}(3)$. After the destination point is reached, the term $\Psi(R)$, considered in the cost functional, is responsible to maintain and stabilize the angles close to zero, that is, with R close to I_3. In addition, the aggressiveness feature is corroborated by Figure 6.4d, where large angular velocities are performed by the UAV during the experiment.



(a) UAV Position, ξ.

(b) UAV Velocity, $\dot{\xi}$.

(c) UAV Euler angles.

(d) UAV Angular Velocities.

Figura 6.4: Data obtained in the second round of experiments: motion control with obstacle-avoidance capability using ellipsoidal-polytopic based NMPC.

The proposed NMPC complied with all the system constraints considered in the control design. Figure 6.5 shows the propeller forces which are mapped on the input signals. It can be noticed that the inputs reach the limits during almost the entire flight, which also indicates the aggressiveness of the proposed controller and its ability to deal with constrained control problems. These extreme values applied in the UAV occur when the obstacle deviation maneuvers are required, or when the UAV has to overcome its inertia at the beginning of the experiments.

Furthermore, the obstacle avoidance capability of the proposed strategy can be evaluated from Figure 6.6, which shows snapshots of the ellipsoidal set $\mathcal{V}(\xi, \hat{Q})$ during the experiment. It is possible to verify that the aircraft (blue ellipsoid) satisfactorily executes the required maneuvers, i.e., by throwing the narrow gaps in order to deviate from the obstacles and reach its destination point.

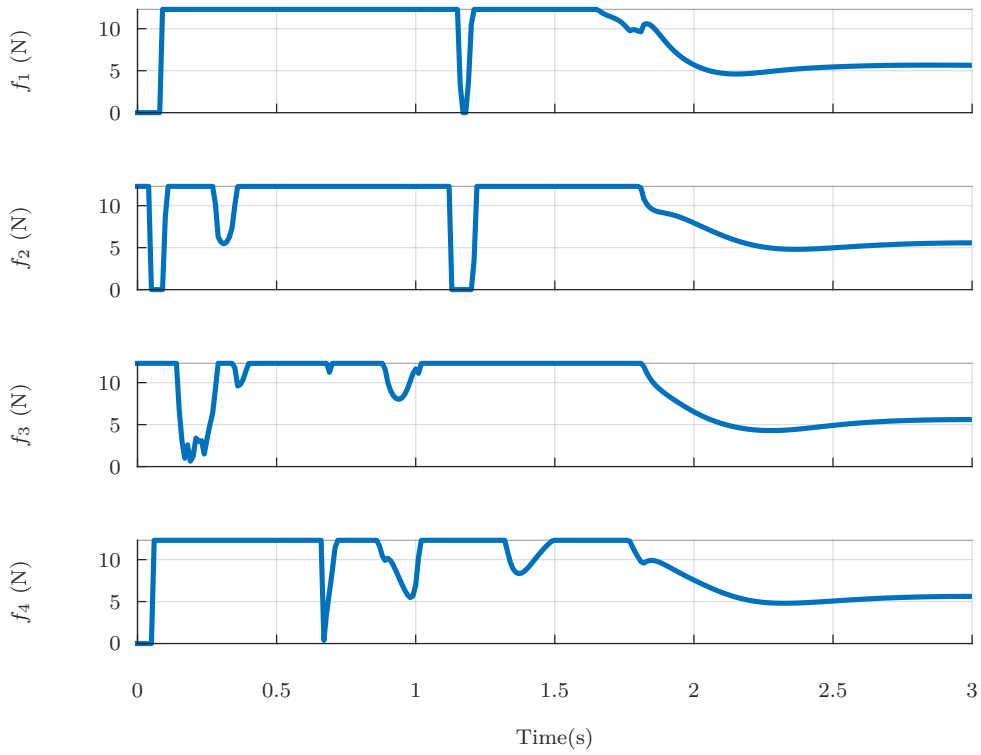


Figura 6.5: UAV propeller forces. The input bounds are correctly respected by the controller.

To verify the collision avoidance performance over the entire flight, after the experiments, similar to Chapter 5, the minimum distance σ_ℓ between the UAV set $\mathcal{V}(\xi, \hat{Q})$ (see (6.1)) and the ℓ-th obstacle set (see (6.4)) are calculated from the following optimization problem:

$$\begin{aligned} \sigma_\ell(t) = \quad & \min \quad \|q(t) - \rho\|_2, \qquad \forall \ell = 1, \cdots, N_o, \\ & \text{s.t.} \qquad q(t) \in \mathcal{V}(\xi, \hat{Q}), \quad \rho \in \mathcal{P}_\ell. \end{aligned} \tag{6.14}$$

Figure 6.7 shows the calculated σ_ℓ for all obstacles. The condition given by Theorem 6.1 only guarantees the separation between the UAV and the obstacles, but there is no relation with distance. Therefore, in situations involving model uncertainties, safe margin variables might be considered in the definition of the set $\mathcal{V}(\xi, \hat{Q})$. Additionally, note that σ_ℓ is always greater than 0 for all cases, which validates the collision avoidance capability of the proposed NMPC.

6.3.3 Fast motion control with obstacle-avoidance capability using ellipsoidal-polytopic based NMPC

The main objective of this third round of experiments is to compare the behavior of NMPC scheme given by (6.12) and the fast motion scheme given by (6.13). The experiment involves the maneuver illustrated in the Figure 6.8, where the UAV should accomplish a point-to-point motion avoiding obstacles positioned between the start and destination points. Similar to the previous experiments, the UAV performs a rolling movement, but now defined by a perpendicular and narrow gap.

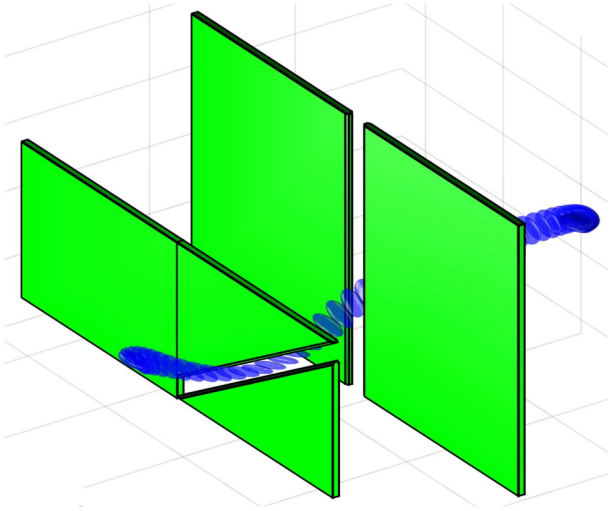


Figura 6.6: Ellipsoidal set $\mathcal{V}(t)$ during the numerical experiment.

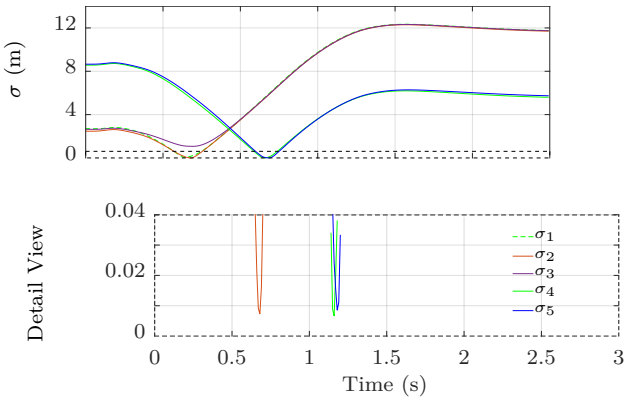


Figura 6.7: Minimum distance between the UAV and obstacles.

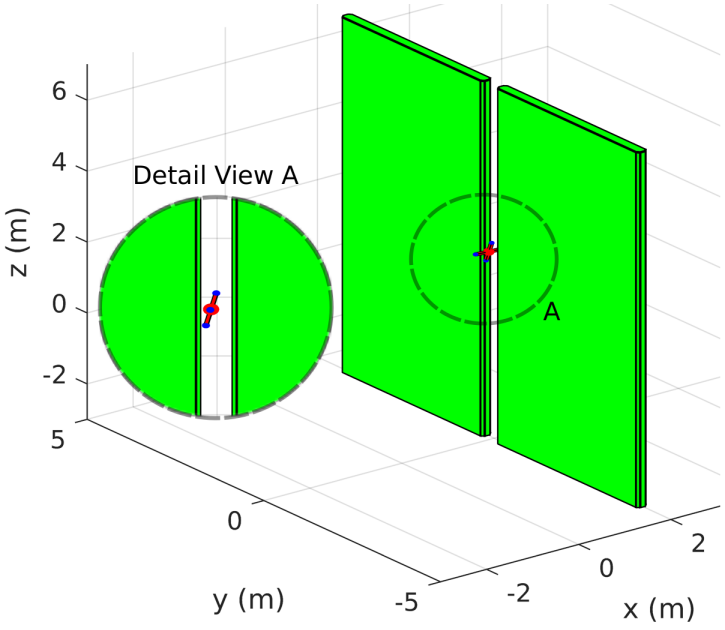


Figura 6.8: The UAV performing the proposed maneuver: throwing a narrow and perpendicular gap.

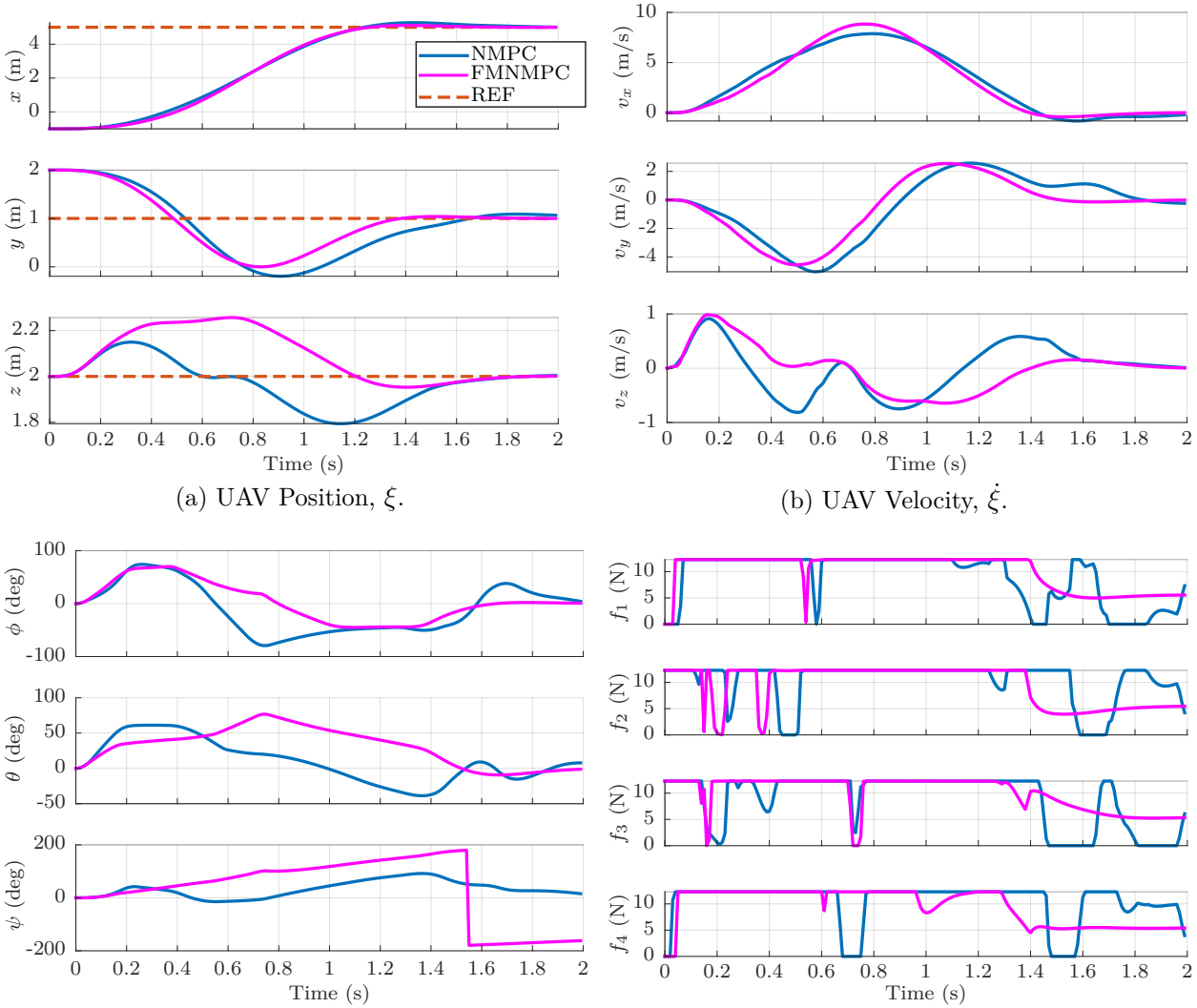
The initial conditions are zero for all states except for $\xi_0 = \begin{bmatrix} -1 & 2 & 2 \end{bmatrix}^\top$ and $R_0 = I_3$. The destination point is $\xi_{\text{end}} = \begin{bmatrix} 5 & 1 & 2 \end{bmatrix}^\top$. The obstacles are defined by

$$A_1 = \begin{bmatrix} 1 & 0 & 0 \\ -1 & 0 & 0 \\ 0 & 1 & 0 \\ 0 & -1 & 0 \\ 0 & 0 & 1 \\ 0 & 0 & -1 \\ 1 & 1 & 0 \\ -1 & 1 & 0 \\ -1 & -1 & 0 \\ 1 & -1 & 0 \end{bmatrix}, \; A_2 = \begin{bmatrix} 1 & 0 & 0 \\ -1 & 0 & 0 \\ 0 & 1 & 0 \\ 0 & -1 & 0 \\ 0 & 0 & 1 \\ 0 & 0 & -1 \\ 1 & 1 & 0 \\ -1 & 1 & 0 \\ 1 & -1 & 0 \\ -1 & -1 & 0 \end{bmatrix}, \; b_1 = \begin{bmatrix} 2{,}1 \\ -1{,}9 \\ -0{,}2 \\ 4{,}2 \\ 7 \\ 3 \\ 1{,}85 \\ -2{,}15 \\ 2{,}25 \\ 6{,}25 \end{bmatrix}, \; b_2 = \begin{bmatrix} 2{,}1 \\ -1{,}9 \\ 4{,}2 \\ -0{,}2 \\ 7 \\ 3 \\ 6{,}25 \\ 2{,}25 \\ 1{,}85 \\ -2{,}15 \end{bmatrix}.$$

For the cost functional of both formulations, the weighting matrices and constants are defined as $Q_y = 80I_3$, $Q_u = 0{,}01I_4$, and $K_R = k_1 = k_2 = k_3 = 10$. The penalty weight K_n is equal to $1e5$ for the NMPC scheme given by (6.12) and equal to $2{,}5e7$ for the fast motion scheme. Moreover, the exponential weight ζ is equal to 1,05.

The performance of each formulation can be compared from Figure 6.9. From Figures 6.9a and 6.9b, it can be verified that the destination point is precisely reached by both formulations, but as expected, the formulation with exponential weight was approximately 20 % faster. Both approaches perform large attitude angles due to the required maneuver. With regard to this matter, it is possible to notice from Figures 6.9c and 6.9d that the fast motion formulation was a bit more aggressive, which is coherent as the flight aggressiveness is also related to fast movements of the vehicle.

Furthermore, Figure 6.10 shows snapshots of the ellipsoidal set $\mathcal{V}(\xi, M)$ during the experiments. The UAV controlled by the fast motion formulation (magenta ellipsoids) satisfactorily executes the required maneuver, throwing a narrow gap (width equals to 0.4 m) and achieving its destination point. When compared with the UAV controlled by the NMPC scheme (6.12) (blue ellipsoids), it can be noted that the NMPC scheme (6.13) uses the prediction feature to compute the optimized trajectory in such a way that the recovery flight is faster after the maneuver execution. The obstacle avoidance capability is maintained by the NMPC scheme (6.13) as it can be verify from Figure 6.11, which shows σ_ℓ (see (6.14)) always greater than 0 for both formulations.



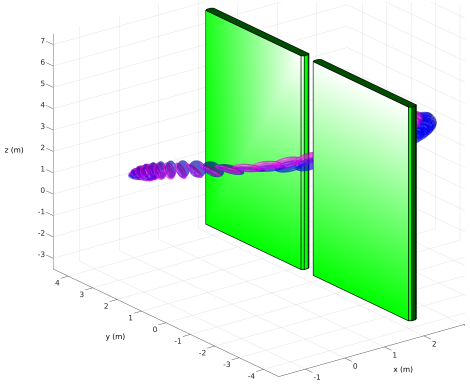
(a) UAV Position, ξ.

(b) UAV Velocity, $\dot{\xi}$.

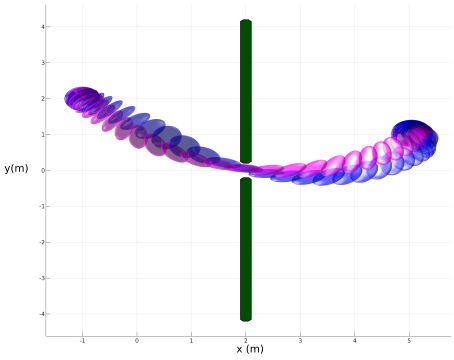
(c) UAV Euler angles.

(d) UAV propeller forces.

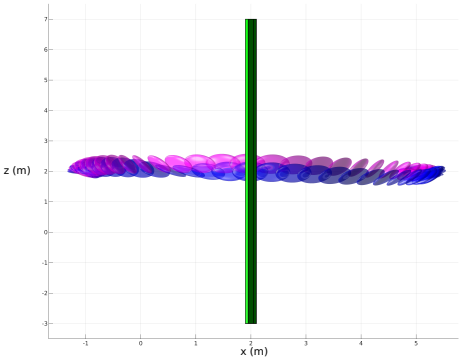
Figura 6.9: Comparison between the proposed schemes performing the same maneuver shown in Figure 6.8.



(a) Isometric View.



(b) X-Y plane view.



(c) X-Z plane view.

Figura 6.10: Ellipsoidal set $\mathcal{V}(t)$ during the numerical experiments. The blue ellipsoids represent the UAV controlled by the NMPC scheme given by (6.12) and the magenta ones represent the UAV controlled by fast motion scheme.

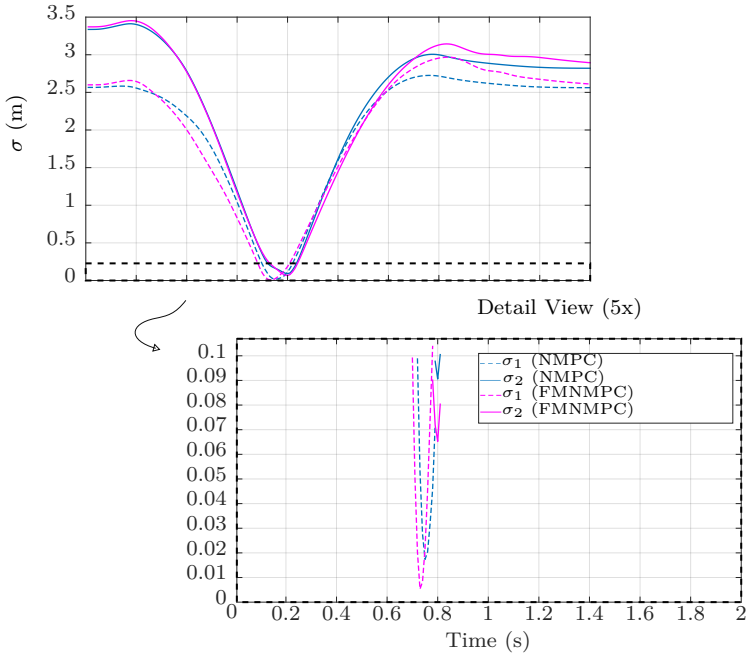


Figura 6.11: Minimum distance between the UAV and obstacles along all the numerical experiments. The term σ_ℓ is always greater than 0 for all cases, which shows that the obstacle avoidance capability is maintained by fast motion formulation.

6.4 Final Remarks

The proposed NMPC based on the ellipsoidal-polytopic formulation is a potential solution to the presented problem of fast motion control of underactuated vehicles with obstacle-avoidance capability due to its better obstacle representation and its smaller computational cost when compared to the previous formulation presented in Chapter 5. In the quadrotor UAV application, it could be noted that the proposed controller allowed the aircraft to fly through narrow spaces, i.e. when the UAV attitude influences the success of the deviation maneuver. On the second front of the research, the proposed fast motion scheme, based on the exponential weighting strategy, has presented the desirable fast behavior.

7 Conclusions

This chapter summarizes the main contributions obtained by this doctoral thesis, and concludes the text. Future work proposals are also detailed at the end of this chapter.

7.1 Overview and contributions

This doctoral thesis developed NMPC schemes formulated on $\mathsf{SE}(3)$ for aggressive motion control problems involving a class of underactuated vehicles. Several control challenges were investigated gradually throughout the text, the majority of which stemmed from the system's underactuation, non-Euclidean state space, aggressive behavior, and ability to avoid obstacles. In Chapter 4, the stabilization control problem was addressed. Two practically asymptotically stable NMPC strategies were presented, one of which was designed to regard the mission time as an economic criterion. Closed-loop stability and recursive feasibility of the proposed formulations were provided from dissipativity-based analyses. In Chapter 5, the trajectory tracking problem with obstacle avoidance capability was addressed. In addition to formulating the controller on $\mathsf{SE}(3)$, the proposed problem was intensified by allowing aggressive maneuvers to improve obstacle avoidance efficiency. To take the vehicle's attitude into account during the obstacle deviation, an algebraic condition ensuring that two ellipsoidal sets are disjoints was implemented as a penalty function in the cost functional. In Chapter 6, two major improvements were pursued. Firstly, the controllers proposed in Chapter 4 were extended to the obstacle-avoidance problem. Furthermore, in order to better represent the obstacles and reduce computational

costs, an ellipsoidal-polytopic algebraic condition was developed and incorporated into the proposed NMPC schemes. Therefore, although some theoretical questions remain, this thesis attempted to solve the majority of the problems involving aggressive maneuvers of underactuated motion systems modeled on $\mathsf{SE}(3)$. As demonstrated throughout the experiments in Chapters 4, 5, and 6, the proposed NMPC schemes allow autonomous underactuated vehicles to recover from an upside down situation, move through narrow spaces, avoid obstacles with fast movements, and reach the destination point as soon as possible, without any additional controller or optimization layer.

In summary, the following main contributions were obtained from this doctoral thesis:

- Design of NMPC schemes that fully explore the dynamic equations of a class of underactuated vehicles globally represented by $\mathsf{SE}(3)$ manifold, without concerning about representational singularities and without decoupling the problem into attitude and position control.
- Incorporation of an algebraic condition ensuring that two ellipsoids are disjoint as a penalty function in the cost functional.
- Derivation of an algebraic condition ensuring that a polytope and an ellipsoid are disjoint, incorporating it as a penalty function in the cost functional.
- Design of NMPC schemes on $\mathsf{SE}(3)$ that consider the vehicle's attitude in the collision avoidance, allowing aggressive maneuvers to improve the performance during obstacle deviation.
- Design of NMPC schemes on $\mathsf{SE}(3)$ that consider the mission time reduction as an economic criterion.
- Demonstration of the closed-loop stability and recursive feasibility of the proposed NMPC schemes on $\mathsf{SE}(3)$ for the stabilization problem of underactuated vehicles from dissipativity-based analysis.
- Design of ellipsoidal based NMPC scheme on $\mathsf{SE}(3)$ without terminal conditions able to perform trajectory tracking, with constant disturbance rejection, while avoiding obstacles with aggressive maneuver capability.
- Design of ellipsoidal-polytopic based NMPC schemes on $\mathsf{SE}(3)$ without terminal conditions able to perform point-to-point motion while avoiding obstacles with aggressive maneuver capability.

7.2 List of Publications

The following articles were published, accepted for publication, or submitted during the elaboration of this doctoral thesis:

Journal papers:

1. Pereira, J. C., Leite, V. J. S., & Raffo, G. V. (2022). A Stabilizing Nonlinear Model Predictive Control without Terminal Conditions for Underactuated Vehicles on $\mathsf{SE}(3)$. To be submitted.

2. (Pereira et al., 2021a) Pereira, J. C., Leite, V. J. S., & Raffo, G. V. (2020). Nonlinear Model Predictive Control on $\mathsf{SE}(3)$ for Quadrotor Aggressive Maneuvers. *Journal of Intelligent & Robotic Systems*.

Conference papers:

1. (Pereira et al., 2021b) Pereira, J. C., Leite, V. J. S., & Raffo, G. V. (2021). An ellipsoidal-polytopic based approach for aggressive navigation using nonlinear model predictive control. In *2021 International Conference on Unmanned Aircraft Systems ICUAS* (pp. 827-835).

2. (Pereira et al., 2019a) Pereira, J. C., Leite, V. J. S., & Raffo, G. V. (2019a). Manobra Agressiva de VANT Quadrotor via Abordagem Baseada em Backstepping. In *XIV Conferência Brasileira de Dinâmica, Controle e Aplicações* (pp. 1-7).

3. (Pereira et al., 2019b) Pereira, J. C., Leite, V. J. S., & Raffo, G. V. (2019b). Nonlinear Model Predictive Control on $\mathsf{SE}(3)$ for Quadrotor Trajectory Tracking and Obstacle Avoidance. In *2019 19th International Conference on Advanced Robotics (ICAR)* (pp. 155-160).

7.3 Future Works

As future works, the proposed NMPC schemes can be extended to a robust formulation based on tubes to ensure robustness against uncertainties and improve the collision avoidance capability. Also, some questions still have to be answered, such as how to ensure the stability, optimality and recursive feasibility when soft constraints are considered as non-convex penalty functions in the cost functional. Regarding the computational cost issue, frameworks that allow to design and embed optimization-based control are in development, which generate self-contained C++/C code to solve the proposed NMPC schemes and to implement them in real experiments using fast optimization algorithms.

Bibliography

Afonso, R. J., Maximo, M. R., & Galvão, R. K. (2020). Task allocation and trajectory planning for multiple agents in the presence of obstacle and connectivity constraints with mixed-integer linear programming. *International Journal of Robust and Nonlinear Control*, 30(14), 5464–5491.

Aguiar, A. P. & Hespanha, J. P. (2007). Trajectory-tracking and path-following of underactuated autonomous vehicles with parametric modeling uncertainty. *IEEE Transactions on Automatic Control*, 52(8), 1362–1379.

Alessandretti, A., Aguiar, A. P., & Jones, C. N. (2013). Trajectory-tracking and path-following controllers for constrained underactuated vehicles using model predictive control. In *2013 European Control Conference (ECC)* (pp. 1371–1376).

Alexis, K., Nikolakopoulos, G., & Tzes, A. (2011). Switching model predictive attitude control for a quadrotor helicopter subject to atmospheric disturbances. *Control Engineering Practice*, 19, 1195–1207.

Alexis, K., Nikolakopoulos, G., & Tzes, A. (2014). On trajectory tracking model predictive control of an unmanned quadrotor helicopter subject to aerodynamic disturbances. *Asian Journal of Control*, 16(1), 209–224.

Alexis, K., Papachristos, C., R.Siegwart, & Tzes, A. (2016). Robust model predictive flight control of unmanned rotorcrafts. *J Intell Robot Syst*, 81, 443–469.

Andersson, J. A. E., G., J., Horn, G., Rawlings, J. B., & Diehl, M. (2018). CasADi – A software framework for nonlinear optimization and optimal control. *Mathematical Programming Computation*, 11, 1–36.

Andersson, O., Wzorek, M., Rudol, P., & Doherty, P. (2016). Model-predictive control with stochastic collision avoidance using bayesian policy optimization. In *2016 IEEE International Conference on Robotics and Automation (ICRA)* (pp. 4597–4604).

Andrade, R., Raffo, G. V., & Normey-Rico, J. E. (2016). Model predictive control of a tilt-rotor uav for load transportation. In *2016 European Control Conference (ECC)* (pp. 2165–2170).

Athans, M. & Falb, P. L. (1966). *Optimal Control - An Introduction to the Theory and Its Applications*. Dover.

Bai, G., Meng, Y., Liu, L., Luo, W., Gu, Q., & Liu, L. (2019). Review and comparison of path tracking based on model predictive control. *Electronics*, 8(10), 1077–1119.

Barry, A. J., Jenks, T., Majumdar, A., Lin, H., Ros, I. G., Biewener, A. A., & Tedrake, R. (2014). Flying between obstacles with an autonomous knife-edge maneuver. In *2014 IEEE International Conference on Robotics and Automation (ICRA)* (pp. 2559–2559).

Berntorp, K., Quirynen, R., Uno, T., & Cairano, S. D. (2020). Trajectory tracking for autonomous vehicles on varying road surfaces by friction-adaptive nonlinear model predictive control. *Vehicle System Dynamics*, 58(5), 705–725.

Bhat, S. P. & Bernstein, D. S. (2000). A topological obstruction to continuous global stabilization of rotational motion and the unwinding phenomenon. *Systems & Control Letters*, 39(1), 63–70.

Bock, H. & Plitt, K. (1984). A multiple shooting algorithm for direct solution of optimal control problems. *IFAC Proceedings Volumes*, 17(2), 1603–1608. 9th IFAC World Congress: A Bridge Between Control Science and Technology, Budapest, Hungary, 2-6 July 1984.

Borenstein, J. & Koren, Y. (1989). Real-time obstacle avoidance for fast mobile robots. *IEEE Transactions on Systems, Man, and Cybernetics*, 19(5), 1179–1187.

Borenstein, J. & Koren, Y. (1991). The vector field histogram-fast obstacle avoidance for mobile robots. *IEEE Transactions on Robotics and Automation*, 7(3), 278–288.

Brockett, R. W. (1983). Asymptotic stability and feedback stabilization. In *Differential Geometric Control Theory* (pp. 181–191).: Birkhauser.

Bulka, E. & Nahon, M. (2019a). Automatic control for aerobatic maneuvering of agile fixed-wing UAVs. *J Intell Robot Syst*, 80, 85–100.

Bulka, E. & Nahon, M. (2019b). High-speed obstacle-avoidance with agile fixed-wing aircraft. In *2019 International Conference on Unmanned Aircraft Systems (ICUAS)* (pp. 971–980).

Camacho, E. F. & Bordons, C. (2007). *Nonlinear Model Predictive Control: An Introductory Review*, (pp. 1–16). Springer Berlin Heidelberg: Berlin, Heidelberg.

Caravantes, J. & Gonzalez-Vega, L. (2018). On the interference problem for ellipsoids: Experiments and applications. In *Mathematical Software – ICMS 2018* (pp. 89–97).: Springer International Publishing.

Casau, P., Sanfelice, R. G., Cunha, R., Cabecinhas, D., & Silvestre, C. (2013). Global trajectory tracking for a class of underactuated vehicles. In *2013 American Control Conference* (pp. 419–424).

Casau, P., Sanfelice, R. G., Cunha, R., Cabecinhas, D., & Silvestre, C. (2015). Robust global trajectory tracking for a class of underactuated vehicles. *Automatica*, 58, 90–98.

Castillo, A., Sanz, R., Garcia, P., Qiu, W., Wang, H., & Xu, C. (2019). Disturbance observer-based quadrotor attitude tracking control for aggressive maneuvers. *Control Engineering Practice*, 82, 14–23.

Castillo-Lopez, M., Olivares-Mendez, M. A., & Voos, H. (2018a). Evasive maneuvering for uavs: An mpc approach. In *ROBOT 2017: Third Iberian Robotics Conference* (pp. 829–840). Cham: Springer International Publishing.

Castillo-Lopez, M., Sajadi-Alamdari, S. A., Sanchez-Lopez, J. L., Olivares-Mendez, M. A., & Voos, H. (2018b). Model predictive control for aerial collision avoidance in dynamic environments. In *2018 26th Mediterranean Conference on Control and Automation (MED)* (pp. 1–6).

Chana, W. F. & Coleman, J. F. (1996). World's first VTOL airplane convair/navy XFY-1 pogo. In *SAE International Powered Lift Conference and Exposition* (pp. 1–6).

Chaturvedi, N. A., Sanyal, A. K., & McClamroch, N. H. (2011). Rigid-body attitude control. *IEEE Control Systems Magazine*, 31(3), 30–51.

Chen, H. & Allgöwer, F. (1998). A quasi-infinite horizon nonlinear model predictive control scheme with guaranteed stability. *Automatica*, 34(10), 1205–1217.

Chuong La, H., Potschka, A., & Bock, H. G. (2017). Partial stability for nonlinear model predictive control. *Automatica*, 78, 14–19.

Cory, R. & Tedrake, R. (2008). Experiments in fixed-wing uav perching. In *AIAA Guidance, Navigation and Control Conference and Exhibit* (pp. 1–12).

Crowther, W. (2000). Perched landing and takeoff for fixed wing uavś. In *Symposium on Unmanned Vehicles for Aerial, Ground and Naval Military Operations, Conference Location: Ankara, Turkey* (pp. 1–11).

Cutler, M. & How, J. P. (2015). Analysis and control of a variable-pitch quadrotor for agile flight. *Journal of Dynamic Systems, Measurement, and Control*, 137(10), 1–15.

Dentler, J., Kannan, S., Mendez, M. A. O., & Voos, H. (2016). A real-time model predictive position control with collision avoidance for commercial low-cost quadrotors. In *2016 IEEE Conference on Control Applications (CCA)* (pp. 519–525).

Dongbing Gu & Huosheng Hu (2005). A stabilizing receding horizon regulator for nonholonomic mobile robots. *IEEE Transactions on Robotics*, 21(5), 1022–1028.

Dongbing Gu & Huosheng Hu (2006). Receding horizon tracking control of wheeled mobile robots. *IEEE Transactions on Control Systems Technology*, 14(4), 743–749.

Douthwaite, J. A. (2020). *Multi-agent Collision Avoidance Using Interval Analysis and Symbolic Modelling with its Application to the Novel Polycopter*. University of Sheffield: Ph.D Thesis.

Douthwaite, J. A., Zhao, S., & Mihaylova, L. S. (2018). A comparative study of velocity obstacle approaches for multi-agent systems. In *2018 UKACC 12th International Conference on Control (CONTROL)* (pp. 289–294).

Egeland, O., Dalsmo, M., & Sørdalen, O. (1996a). Feedback control of a nonholonomic underwater vehicle with a constant desired configuration. *The International Journal of Robotics Research*, 15(1), 24–35.

Egeland, O., Dalsmo, M., & Sørdalen, O. (1996b). Feedback control of a nonholonomic underwater vehicle with a constant desired configuration. *The International Journal of Robotics Research*, 15(1), 24–35.

Ellis, M. & Christofides, P. D. (2014). Integrating dynamic economic optimization and model predictive control for optimal operation of nonlinear process systems. *Control Engineering Practice*, 22, 242–251.

Eskandarpour, A. & Sharf, I. (2020). A constrained error-based MPC for path following of quadrotor with stability analysis. *Nonlinear Dynamics*, 99, 899–918.

Faessler, M., Franchi, A., & Scaramuzza, D. (2018). Differential flatness of quadrotor dynamics subject to rotor drag for accurate tracking of high-speed trajectories. *IEEE Robotics and Automation Letters*, 3(2), 620–626.

Falanga, D., Mueggler, E., Faessler, M., & Scaramuzza, D. (2017). Aggressive quadrotor flight through narrow gaps with onboard sensing and computing using active vision. In *2017 IEEE International Conference on Robotics and Automation (ICRA)* (pp. 5774–5781).

Falcone, P., Borrelli, F., Asgari, J., Tseng, H. E., & Hrovat, D. (2007). Predictive active steering control for autonomous vehicle systems. *IEEE Transactions on Control Systems Technology*, 15(3), 566–580.

Faulwasser, T. & Findeisen, R. (2016). Nonlinear model predictive control for constrained output path following. *IEEE Transactions on Automatic Control*, 61(4), 1026–1039.

Faulwasser, T., Kern, B., & Findeisen, R. (2009). Model predictive path-following for constrained nonlinear systems. In *Proceedings of the 48h IEEE Conference on Decision and Control (CDC) held jointly with 2009 28th Chinese Control Conference* (pp. 8642–8647).

Ferreau, H. J., Kirches, C., Potschka, A., Bock, H. G., & Diehl, M. (2014). qpoases: a parametric active-set algorithm for quadratic programming. *Mathematical Programming Computation*, 6(4), 327–363.

Findeisen, R. & Allgöwer, F. (2004). Computational delay in nonlinear model predictive control. *IFAC Proceedings Volumes*, 37(1), 427–432. 7th International Symposium on Advanced Control of Chemical Processes (ADCHEM 2003), Hong-Kong, 11-14 January 2004.

Fiorini, P. & Shiller, Z. (1998). Motion planning in dynamic environments using velocity obstacles. *The International Journal of Robotics Research*, 17(7), 760–772.

Fjellstad & Fossen (1994). Quaternion feedback regulation of underwater vehicles. In *1994 Proceedings of IEEE International Conference on Control and Applications* (pp. 857–862).

Foehn, P. & Scaramuzza, D. (2018). Onboard state dependent LQR for agile quadrotors. In *IEEE International Conference on Robotics and Automation (ICRA)* (pp. 6566–6572).

Fontes, F. A. (2001). A general framework to design stabilizing nonlinear model predictive controllers. *Systems & Control Letters*, 42(2), 127–143.

Fontes, F. A. C. C. & Magni, L. (2003). Special section technical notes and correspondence. min-max model predictive control of nonlinear systems using discontinuous feedbacks. *IEEE Transactions on Automatic Control*, 48(10), 1750–1755.

Fox, D., Burgard, W., & Thrun, S. (1997). The dynamic window approach to collision avoidance. *IEEE Robotics Automation Magazine*, 4(1), 23–33.

Frank, A., McGrew, J., Valenti, M., Levine, D., & How, J. (2007). Hover, transition, and level flight control design for a single-propeller indoor airplane. In *AIAA Guidance, Navigation and Control Conference and Exhibit* (pp. 1–18).

Frasch, J. V., Gray, A., Zanon, M., Ferreau, H. J., Sager, S., Borrelli, F., & Diehl, M. (2013). An auto-generated nonlinear mpc algorithm for real-time obstacle avoidance of ground vehicles. In *2013 European Control Conference (ECC)* (pp. 4136–4141).

Frazzoli, E., Dahleh, M., & Feron, E. (2000). Trajectory tracking control design for autonomous helicopters using a backstepping algorithm. In *American Control Conference (ACC)*, volume 6 (pp. 4102–4107).

Garimella, G., Sheckells, M., & Kobilarov, M. (2017). Robust obstacle avoidance for aerial platforms using adaptive model predictive control. In *2017 IEEE International Conference on Robotics and Automation (ICRA)* (pp. 5876–5882).

Goncalves, V. M., Pimenta, L. C. A., Maia, C. A., Dutra, B. C. O., & Pereira, G. A. S. (2010). Vector fields for robot navigation along time-varying curves in n -dimensions. *IEEE Transactions on Robotics*, 26(4), 647–659.

Gong, X. (2019). Model predictive control for an unmanned helicopter. In *2019 IEEE International Conference on Unmanned Systems (ICUS)* (pp. 361–366).

Goodarzi, F., Lee, D., & Lee, T. (2013). Geometric nonlinear PID control of a quadrotor UAV on SE(3). In *Proceeding of European control conference* (pp. 3845–3850).

Goodarzi, F., Lee, D., & Lee, T. (2015). Geometric adaptive tracking control of a quadrotor unmanned aerial vehicle on SE(3) for agile maneuvers. *Journal of Dynamic Systems, Measurement, and Control*, 137(9), 1–12.

Gopalakrishnan, B., Singh, A. K., Kaushik, M., Krishna, K. M., & Manocha, D. (2017). PRVO: Probabilistic reciprocal velocity obstacle for multi robot navigation under uncertainty. In *2017 IEEE/RSJ International Conference on Intelligent Robots and Systems (IROS)* (pp. 1089–1096).

Green, W. E. & Oh, P. Y. (2005). A mav that flies like an airplane and hovers like a helicopter. In *Proceedings, 2005 IEEE/ASME International Conference on Advanced Intelligent Mechatronics.* (pp. 693–698).

Green, W. E. & Oh, P. Y. (2006). Autonomous hovering of a fixed-wing micro air vehicle. In *Proceedings 2006 IEEE International Conference on Robotics and Automation, 2006. ICRA 2006.* (pp. 2164–2169).

Green, W. E. & Oh, P. Y. (2009). A hybrid mav for ingress and egress of urban environments. *IEEE Transactions on Robotics*, 25(2), 253–263.

Grimm, G., Messina, M. J., Tuna, S. E., & Teel, A. R. (2005). Model predictive control: for want of a local control lyapunov function, all is not lost. *IEEE Transactions on Automatic Control*, 50(5), 546–558.

Grüne, L. (2013). Economic receding horizon control without terminal constraints. *Automatica*, 49(3), 725–734.

Grüne, L. & Pannek, J. (2017). *Nonlinear Model Predictive Control: Theory and Algorithms*. Springer International Publishing.

Grüne, L., Pannek, J., Seehafer, M., & Worthmann, K. (2010). Analysis of unconstrained nonlinear mpc schemes with time varying control horizon. *SIAM Journal on Control and Optimization*, 48(8), 4938–4962.

Grüne, L. & Pirkelmann, S. (2020). Economic model predictive control for time-varying system: Performance and stability results. *Optimal Control Applications and Methods*, 41(1), 42–64.

Grüne, L. & Stieler, M. (2014). Asymptotic stability and transient optimality of economic mpc without terminal conditions. *Journal of Process Control*, 24(8), 1187–1196.

Hall, J. & McLain, T. (2008). Aerobatic maneuvering of miniature air vehicles using attitude trajectories. In *AIAA Guidance, Navigation and Control Conference and Exhibit* (pp. 1–17).

Hamrah, R., Warier, R. R., & Sanyal, A. K. (2018). Discrete-time stable tracking control of underactuated rigid body systems on SE(3). In *2018 IEEE Conference on Decision and Control (CDC)* (pp. 2932–2937).

He, X., Sun, Z., Geng, Z., & Robertsson, A. (2022). Exponential set-point stabilization of underactuated vehicles moving in three-dimensional space. *IEEE/CAA Journal of Automatica Sinica*, 9(2), 270–282.

Heirung, T. A. N., Santos, T. L., & Mesbah, A. (2019). Model predictive control with active learning for stochastic systems with structural model uncertainty: Online model discrimination. *Computers & Chemical Engineering*, 128, 128–140.

Hermans, B., Patrinos, P., & Pipeleers, G. (2018). A penalty method based approach for autonomous navigation using nonlinear model predictive control. *IFAC-PapersOnLine*, 51(20), 234–240. 6th IFAC Conference on Nonlinear Model Predictive Control NMPC 2018.

Heshmati-Alamdari, S., Nikou, A., & Dimarogonas, D. V. (2021). Robust trajectory tracking control for underactuated autonomous underwater vehicles in uncertain environments. *IEEE Transactions on Automation Science and Engineering*, 18(3), 1288–1301.

Hess, R. A. & Jung, Y. C. (1989). An application of generalized predictive control to rotorcraft terrain-following flight. *IEEE Transactions on Systems, Man, and Cybernetics*, 19(5), 955–962.

Hoy, M., Matveev, A. S., & Savkin, A. V. (2015). Algorithms for collision-free navigation of mobile robots in complex cluttered environments: a survey. *Robotica*, 33(3), 463–497.

Hua, M.-D., Hamel, T., Morin, P., & Samson, C. (2013). Introduction to feedback control of underactuated VTOL vehicles: A review of basic control design ideas and principles. *Control Systems, IEEE*, 33, 61–75.

Ioan, D., Olaru, S., Niculescu, S., Prodan, I., & Stoican, F. (2019). Navigation in a multi-obstacle environment. from partition of the space to a zonotopic-based mpc. In *2019 18th European Control Conference (ECC)* (pp. 1772–1777).

Jadbabaie, A., Primbs, J., & Hauser, J. (2001). Unconstrained receding horizon control with no terminal cost. In *Proceedings of the 2001 American Control Conference*, volume 4 (pp. 3055–3060).

Jardine, P. T. & Givigi, S. N. (2019). A robust model-predictive guidance system for autonomous vehicles in cluttered environments. *IEEE Systems Journal*, 13(2), 2034–2045.

Johansen, T. A. (2017). Toward dependable embedded model predictive control. *IEEE Systems Journal*, 11(2), 1208–1219.

Johnson, E. N., Wu, A., Neidhoefer, J. C., Kannan, S. K., & Turbe, M. A. (2008). Flight-test results of autonomous airplane transitions between steady-level and hovering flight. *Journal of Guidance, Control, and Dynamics*, 31(2), 358–370.

Kalman, R. (1960). On the general theory of control systems. *IFAC Proceedings Volumes*, 1(1), 491–502. 1st International IFAC Congress on Automatic and Remote Control, Moscow, USSR, 1960.

Kalman, R. E., Ho, Y.-C., & Narendra, K. S. (1963). Controllability of linear dynamical systems. *Contributions to Differential Equations*, 1, 189–213.

Kamel, M., Alexis, K., Achtelik, M., & Siegwart, R. (2015). Fast nonlinear model predictive control for multicopter attitude tracking on SO(3). In *2015 IEEE Conference on Control Applications (CCA)* (pp. 1160–1166).: IEEE.

Kamel, M., Alonso-Mora, J., Siegwart, R., & Nieto, J. (2017). Robust collision avoidance for multiple micro aerial vehicles using nonlinear model predictive control. In *2017 IEEE/RSJ International Conference on Intelligent Robots and Systems (IROS)* (pp. 236–243).

Kamel, M., Burri, M., & Siegwart, R. (2017). Linear vs nonlinear MPC for trajectory tracking applied to rotary wing micro aerial vehicles. *IFAC-PapersOnLine*, 50(1), 3463–3469. 20th IFAC World Congress.

Kang, Y. & Hedrick, J. K. (2009). Linear tracking for a fixed-wing uav using nonlinear model predictive control. *IEEE Transactions on Control Systems Technology*, 17(5), 1202–1210.

Kanjanawanishkul, K. (2010). *Coordinated path following control and formation control of mobile robots*. University of Tübingen: Ph.D Thesis.

Kehrle, F., J.V, F., Kirches, C., & Sager, S. (2011). Optimal control of formula 1 race cars in a VDrift based virtual environment. In *18th IFAC World Congress* (pp. 11907–11912).

Khatib, O. (1985). Real-time obstacle avoidance for manipulators and mobile robots. In *Proceedings. 1985 IEEE International Conference on Robotics and Automation*, volume 2 (pp. 500–505).

Kim, J.-O. & Khosla, P. (1992). Real-time obstacle avoidance using harmonic potential functions. *IEEE Transactions on Robotics and Automation*, 8(3), 338–349.

Kim, M. & Oh, J. (2016). Study on optimal velocity selection using velocity obstacle (OVVO) in dynamic and crowded environment. *Autonomous Robots*, 40, 1459–1470.

Kobilarov, M. (2013). Trajectory tracking of a class of underactuated systems with external disturbances. In *2013 American Control Conference* (pp. 1044–1049).

Koenig, N. & Howard, A. (2004). Design and use paradigms for gazebo, an open-source multi-robot simulator. In *2004 IEEE/RSJ International Conference on Intelligent Robots and Systems (IROS) (IEEE Cat. No.04CH37566)*, volume 3 (pp. 2149–2154).

Kritayakirana, K. & Gerdes, C. J. (2012). Autonomous vehicle control at the limits of handling. *International Journal of Vehicle Autonomous Systems*, 10(4), 271–296.

Kuhne, F., Lages, W. F., & da Silva, J. M. G. (2005). Point stabilization of mobile robots with nonlinear model predictive control. In *IEEE International Conference Mechatronics and Automation, 2005*, volume 3 (pp. 1163–1168).

Kunz, K., Huck, S., & Summers, T. (2013). Fast model predictive control of miniature helicopters. In *2013 European Control Conference, ECC 2013* (pp. 1377–1382).

Kurzhanskiy, A. A. & Varaiya, P. (2006). Ellipsoidal toolbox (et). In *Proceedings of the 45th IEEE Conference on Decision and Control* (pp. 1498–1503).

Köhler, J., Müller, M. A., & Allgöwer, F. (2019). Nonlinear reference tracking: An economic model predictive control perspective. *IEEE Transactions on Automatic Control*, 64(1), 254–269.

Lages, W. F. & Alves, J. A. V. (2006). Real-time control of a mobile robot using linearized model predictive control. *IFAC Proceedings Volumes*, 39(16), 968–973. 4th IFAC Symposium on Mechatronic Systems.

Lee, T. (2015). Global exponential attitude tracking controls on SO(3). *IEEE Transactions on Automatic Control*, 60(10), 2837–2842.

Lee, T., Leok, M., & McClamroch, N. H. (2010). Geometric tracking control of a quadrotor uav on SE(3). In *49th IEEE Conference on Decision and Control (CDC)* (pp. 5420–5425).

Lee, T., Leok, M., & McClamroch, N. H. (2018). *Global Formulations of Lagrangian and Hamiltonian Dynamics on Manifolds*. Springer.

Leonard, N. (1995). Control synthesis and adaptation for an underactuated autonomous underwater vehicle. *IEEE Journal of Oceanic Engineering*, 20(3), 211–220.

Levin, J., Nahon, M., & Paranjape, A. (2019). Real-time motion planning with a fixed-wing uav using an agile maneuver space. *Autonomous Robots*, 43, 2111–2130.

Li, H., Xie, P., & Yan, W. (2017a). Receding horizon formation tracking control of constrained underactuated autonomous underwater vehicles. *IEEE Transactions on Industrial Electronics*, 64(6), 5004–5013.

Li, H. & Yan, W. (2017). Model predictive stabilization of constrained underactuated autonomous underwater vehicles with guaranteed feasibility and stability. *IEEE/ASME Transactions on Mechatronics*, 22(3), 1185–1194.

Li, S., Wang, Y., & Tan, J. (2017b). Adaptive and robust control of quadrotor aircrafts with input saturation. *Nonlinear Dynamics*, 89(1), 255–265.

Liang, H., Li, H., & Xu, D. (2021). Nonlinear model predictive trajectory tracking control of underactuated marine vehicles: Theory and experiment. *IEEE Transactions on Industrial Electronics*, 68(5), 4238–4248.

Lim, H., Kang, Y., Kim, C., Kim, J., & You, B. (2008). Nonlinear model predictive controller design with obstacle avoidance for a mobile robot. In *2008 IEEE/ASME International Conference on Mechtronic and Embedded Systems and Applications* (pp. 494–499).

Liniger, A., Domahidi, A., & Morari, M. (2015). Optimization-based autonomous racing of 1:43 scale rc cars. *Optimal Control Applications and Methods*, 36(5), 628–647.

Lipp, T. & Boyd, S. (2014). Minimum-time speed optimisation over a fixed path. *International Journal of Control*, 87(6), 1297–1311.

Liu, C., Chen, W.-H., & Andrews, J. (2012). Explicit non-linear model predictive control for autonomous helicopters. *Proceedings of the Institution of Mechanical Engineers, Part G: Journal of Aerospace Engineering*, 226(9), 1171–1182.

Liu, J., Jayakumar, P., Stein, J. L., & Ersal, T. (2017). Combined speed and steering control in high-speed autonomous ground vehicles for obstacle avoidance using model predictive control. *IEEE Transactions on Vehicular Technology*, 66(10), 8746–8763.

Liu, S., Mohta, K., Atanasov, N., & Kumar, V. (2018). Search-based motion planning for aggressive flight in SE(3). *IEEE Robotics and Automation Letters*, 3(3), 2439–2446.

Liu, Y., Yu, S., Guo, Y., Gao, B., & Chen, H. (2017). Receding horizon control for path following problems of wheeled mobile robots. *Control Theory and Applications*, 34, 424–432.

Loianno, G., Brunner, C., McGrath, G., & Kumar, V. (2017). Estimation, control, and planning for aggressive flight with a small quadrotor with a single camera and IMU. *IEEE Robotics and Automation Letters*, 2(2), 404–411.

Lu, G. (2015). Aggressive attitude control of unmanned rotor helicopters using a robust controller. *Journal of Intelligent & Robotic Systems*, 80(1), 165–180.

M. Ellis, M. & Christofides, P. D. (2015). Real-time economic model predictive control of nonlinear process systems. *AIChE Journal*, 61(2), 555–571.

Ma, A., Cheng, Q., Liu, K., & Xia, Y. (2019). Time optimal model predictive control for linear systems based on ellipsoidal and polytopic sets. *International Journal of Control*, 0(0), 1–9.

Marzat, J., Bertrand, S., Eudes, A., Sanfourche, M., & Moras, J. (2017). Reactive mpc for autonomous mav navigation in indoor cluttered environments: Flight experiments. *IFAC-PapersOnLine*, 50(1), 15996–16002. 20th IFAC World Congress.

Matsumoto, T., Konno, A., Suzuki, R., Oosedo, A., Go, K., & Uchiyama, M. (2010). Agile turnaround using post-stall maneuvers for tail-sitter VTOL UAVs. In *2010 IEEE/RSJ International Conference on Intelligent Robots and Systems* (pp. 1612–1617).

Mayhew, C. G., Sanfelice, R. G., Sheng, J., Arcak, M., & Teel, A. R. (2012). Quaternion-based hybrid feedback for robust global attitude synchronization. *IEEE Transactions on Automatic Control*, 57(8), 2122–2127.

Mayne, D. & Schroeder, W. (1997). Robust time-optimal control of constrained linear systems. *Automatica*, 33(12), 2103–2118.

Mayne, D. Q. & Michalska, H. (1990). Receding horizon control of nonlinear systems. *IEEE Transactions on Automatic Control*, 35(7), 814–824.

Mayne, D. Q., Rawlings, J. B., Rao, C. V., & Scokaert, P. O. M. (2000). Constrained model predictive control: Stability and optimality. *Automatica*, 36, 789–814.

Mehrez, M. W., Worthmann, K., Cenerini, J. P., Osman, M., Melek, W. W., & Jeon, S. (2020). Model predictive control without terminal constraints or costs for holonomic mobile robots. *Robotics and Autonomous Systems*, 127, 1–12.

Mellinger, D. & Kumar, V. (2011). Minimum snap trajectory generation and control for quadrotors. In *2011 IEEE International Conference on Robotics and Automation* (pp. 2520–2525).

Mellinger, D., Michael, N., & Kumar, V. (2012a). Trajectory generation and control for precise aggressive maneuvers with quadrotors. *The International Journal of Robotics Research*, 31(5), 664–674.

Mellinger, D., Michael, N., & Kumar, V. (2012b). Trajectory generation and control for precise aggressive maneuvers with quadrotors. *The International Journal of Robotics Research*, 31(5), 664–674.

Michalska, H. & Mayne, D. Q. (1993). Robust receding horizon control of constrained nonlinear systems. *IEEE Transactions on Automatic Control*, 38(11), 1623–1633.

Minguez, J., Lamiraux, F., & Laumond, J. (2008). *Motion Planning and Obstacle Avoidance*, (pp. 827–852). Springer Berlin Heidelberg: Berlin, Heidelberg.

Molenkamp, D., Kampeny, E. V., Visserz, C. C., & Chux, Q. P. (2017). Intelligent controller selection for aggressive quadrotor manoeuvring. In *AIAA Information Systems-AIAA Infotech* (pp. 1–15).: American Institute of Aeronautics and Astronautics.

Moore, J., Cory, R., & Tedrake, R. (2014). Robust post-stall perching with a simple fixed-wing glider using LQR-trees. *Bioinspiration & Biomimetics*, 9(2), 1–16.

Morin, P. & Samson, C. (2008). *Motion Control of Wheeled Mobile Robots*, (pp. 799–826). Springer Berlin Heidelberg: Berlin, Heidelberg.

Morrell, B., Rigter, M., Merewether, G., Reid, R., Thakker, R., Tzanetos, T., Rajur, V., & Chamitoff, G. (2018). Differential flatness transformations for aggressive quadrotor flight. In *IEEE International Conference on Robotics and Automation (ICRA)* (pp. 1–7).

Murilo, A. & Lopes, R. V. (2019). Unified NMPC framework for attitude and position control for a VTOL UAV. *Proceedings of the Institution of Mechanical Engineers, Part I: Journal of Systems and Control Engineering*, 233(7), 889–903.

Murray, R. M., Li, Z., & Sastry, S. S. (1994). *A Mathematical Introduction to Robotic Manipulation*. CRC Press.

Müller, M. A. & Worthmann, K. (2017). Quadratic costs do not always work in mpc. *Automatica*, 82, 269–277.

Nascimento, I. B. P. (2019). *Nonlinear Model Predictive Control Strategies for Autonomous Vehicles in Unknown Environments*. UFMG: Master Thesis.

Nascimento, I. B. P., Ferramosca, A., Pimenta, L. C. A., & Raffo, G. V. (2019). Nmpc strategy for a quadrotor uav in a 3d unknown environment. In *2019 19th International Conference on Advanced Robotics (ICAR)* (pp. 179–184).

Nascimento, T. P., Conceicao, A. G., & Moreira, A. P. (2014). Multi-robot systems formation control with obstacle avoidance. *IFAC Proceedings Volumes*, 47(3), 5703–5708. 19th IFAC World Congress.

Nesic, D., Mareels, I. M. Y., Bastin, G., & Mahony, R. (1998). Output dead beat control for a class of planar polynomial systems. *SIAM J. Control Optim.*, 36(1), 253–272.

Neunert, M., de Crousaz, C., Furrer, F., Kamel, M., Farshidian, F., Siegwart, R., & Buchli, J. (2016). Fast nonlinear model predictive control for unified trajectory optimization and tracking. In *2016 IEEE International Conference on Robotics and Automation (ICRA)* (pp. 1398–1404).

Nikhilraj, A., Simha, H., & Priyadarshan, H. (2019). Optimal energy trajectory generation for a quadrotor uav using geometrically exact computations on SE(3). *IEEE Control Systems Letters*, 3(1), 216–221.

Oliva-Palomo, F., Sanchez-Orta, A., Castillo, P., & Alazki, H. (2018). Nonlinear ellipsoid based attitude control for aggressive trajectories in a quadrotor: Closed-loop multi-flips implementation. *Control Engineering Practice*, 77, 150–161.

Ollero, A. & Amidi, O. (1991). Predictive path tracking of mobile robots. application to the CMU NavLab. In *Fifth International Conference on Advanced Robotics Robots in Unstructured Environments*, volume 2 (pp. 1081–1086).

Oroko, J. A. & Nyakoe, G. N. (2012). Obstacle avoidance and path planning schemes for autonomous navigation of a mobile robot: A review. In *Proceedings of the 2012 Mechanical Engineering Conference on Sustainable Research and Innovation*, volume 4 (pp. 314–318).

Ortolan, G. (2011). *Topics on geometric integration*. Università Degli Studi di Padova: PhD Thesis.

Pacheco, G. V., Pimenta, L. C., & Raffo, G. V. (2020). Distributed parameterized predictive control for multi-robot curve tracking. *IFAC-PapersOnLine*, 53(2), 3144–3149. 21st IFAC World Congress.

Papachristos, C., Alexis, K., & Tzes, A. (2013). Model predictive hovering-translation control of an unmanned tri-tiltrotor. In *2013 IEEE International Conference on Robotics and Automation* (pp. 5425–5432).

Paranjape, A. A., Meier, K. C., Shi, X., Chung, S., & Hutchinson, S. (2013). Motion primitives and 3-d path planning for fast flight through a forest. In *2013 IEEE/RSJ International Conference on Intelligent Robots and Systems* (pp. 2940–2947).

Park, S. (2012). Autonomous aerobatics on commanded path. *Aerospace Science and Technology*, 22(1), 64–74.

Patle, B., Babu L, G., Pandey, A., Parhi, D., & Jagadeesh, A. (2019). A review: On path planning strategies for navigation of mobile robot. *Defence Technology*, 15(4), 582–606.

Paul, R. P. (1981). *Robot Manipulators - Mathematics, Programming and Control*. Cambridge, MA: MIT Press.

Penicka, R. & Scaramuzza, D. (2022). Minimum-time quadrotor waypoint flight in cluttered environments. *IEEE Robotics and Automation Letters*, 7(2), 5719–5726.

Pereira, J., Leite, V., & Raffo, G. (2021a). Nonlinear model predictive control on SE(3) for quadrotor aggressive maneuvers. *J Intell Robot Syst*, 101(62), 1–15.

Pereira, J. C., Leite, V. J. S., & Raffo, G. V. (2019a). Manobra agressiva de vant quadrotor via abordagem baseada em backstepping. In *XIV Conferência Brasileira de Dinâmica, Controle e Aplicações* (pp. 1–7).

Pereira, J. C., Leite, V. J. S., & Raffo, G. V. (2019b). Nonlinear model predictive control on SE(3) for quadrotor trajectory tracking and obstacle avoidance. In *2019 19th International Conference on Advanced Robotics (ICAR)* (pp. 155–160).

Pereira, J. C., Leite, V. J. S., & Raffo, G. V. (2021b). An ellipsoidal-polytopic based approach for aggressive navigation using nonlinear model predictive control. In *2021 International Conference on Unmanned Aircraft Systems (ICUAS)* (pp. 827–835).

Pereira, L. A. A., Nunes, A. H. D., Rezende, A. M. C., Gonçalves, V. M., Raffo, G. V., & Pimenta, L. C. A. (2021c). Collision-free vector field guidance and mpc for a fixed-wing

uav. In *2021 IEEE International Conference on Robotics and Automation (ICRA)* (pp. 176–182).

Pettersen, K. & Egeland, O. (1999). Time-varying exponential stabilization of the position and attitude of an underactuated autonomous underwater vehicle. *IEEE Transactions on Automatic Control*, 44(1), 112–115.

Pflimlin, J. M., Soueres, P., & Hamel, T. (2007). Position control of a ducted fan VTOL UAV in crosswind. *International Journal of Control*, 80(5), 666–683.

Quigley, M., Conley, K., Gerkey, B., Faust, J., Foote, T., Leibs, J., Wheeler, R., & Ng, A. (2009). ROS: an open-source robot operating system. In *ICRA Workshop on Open Source Software*, volume 3 (pp. 1–6).

Raffo, G. V. (2011). *Robust control strategies for a Quadrotor helicopter: an underactuated mechanical system*. Universid de Sevilha: PhD Thesis.

Raffo, G. V., Ortega, M. G., & Rubio, F. (2010). An integral predictive/nonlinear $\mathcal{H}_\infty$ control structure for a quadrotor helicopter. *Automatica*, 46, 29–39.

Ramp, M. & Papadopoulos, E. (2018). Geometric surface-based tracking control of a quadrotor uav for aggressive maneuvers. In *2018 26th Mediterranean Conference on Control and Automation (MED)* (pp. 1–6).

Rawlings, J. B., Mayne, D. Q., & Diehl, M. (2017). *Model Predictive Control: Theory, Computation and Design*. Nob Hill Publishing, LLC, 2nd edition.

Reinhardt, D. & Johansen, T. A. (2019). Nonlinear model predictive attitude control for fixed-wing unmanned aerial vehicle based on a wind frame formulation. In *2019 International Conference on Unmanned Aircraft Systems (ICUAS)* (pp. 503–512).

Rezende, A. M. C., Gonçalves, V. M., Nunes, A. H. D., & Pimenta, L. C. A. (2020). Robust quadcopter control with artificial vector fields. In *2020 IEEE International Conference on Robotics and Automation (ICRA)* (pp. 6381–6387).

Rosmann, C., Makarow, A., Hoffmann, F., & Bertram, T. (2017). Time-optimal nonlinear model predictive control with minimal control interventions. In *2017 IEEE Conference on Control Technology and Applications (CCTA)* (pp. 19–24).

Rucco, A., Aguiar, A. P., Pereira, F. L., & de Sousa, J. B. (2016). A predictive path-following approach for fixed-wing unmanned aerial vehicles in presence of wind disturbances. In *Robot 2015: Second Iberian Robotics Conference* (pp. 623–634).

Rucco, A., Notarstefano, G., & Hauser, J. (2015). An efficient minimum-time trajectory generation strategy for two-track car vehicles. *IEEE Transactions on Control Systems Technology*, 23(4), 1505–1519.

Rösmann, C., Hoffmann, F., & Bertram, T. (2015). Timed-elastic-bands for time-optimal point-to-point nonlinear model predictive control. In *2015 European Control Conference (ECC)* (pp. 3352–3357).

Sanchez, I., Ferramosca, A., Raffo, G. V., Gonzalez, A. H., & D'Jorge, A. (2019). Obstacle avoiding path following based on nonlinear model predictive control using artificial variables. In *2019 19th International Conference on Advanced Robotics (ICAR)* (pp. 254–259).

Sanchez, I., Ferramosca, A., Raffo, G. V., Gonzalez, A. H., & D'Jorge, A. (2021). Nonlinear model predictive path following controller with obstacle avoidance. *J Intell Robot Syst*, 102(16), 1–18.

Santos, M., Rego, B., Raffo, G. V., & Ferramosca, A. (2017). Suspended load path tracking control strategy using a tilt-rotor uav. *Journal of Advanced Transportation*, (pp. 1–22).

Santos, M. A. (2018). *Tube-based MPC with Economical Criteria for Load Transportation Tasks Using Tilt-rotor UAVs*. UFMG: Master Thesis.

Santos, M. A., Ferramosca, A., & Raffo, G. V. (2018). Tube-based mpc with nonlinear control for load transportation using a uav. *IFAC-PapersOnLine*, 51(25), 459–465. 9th IFAC Symposium on Robust Control Design ROCOND 2018.

Santos, M. A., Ferramosca, A., & Raffo, G. V. (2021a). Energy-aware model predictive control with obstacle avoidance. In *2021 International Conference on Unmanned Aircraft Systems (ICUAS)* (pp. 647–655).

Santos, M. A., Ferramosca, A., & Raffo, G. V. (2021b). Tracking nonlinear model predictive control for obstacle avoidance. In *2021 Latin American Robotics Symposium (LARS), 2021 Brazilian Symposium on Robotics (SBR), and 2021 Workshop on Robotics in Education (WRE)* (pp. 30–35).

Sathya, A., Sopasakis, P., Parys, R. V., Themelis, A., Pipeleers, G., & Patrinos, P. (2018). Embedded nonlinear model predictive control for obstacle avoidance using panoc. In *2018 European Control Conference (ECC)* (pp. 1523–1528).

Scattolini, R. (2009). Architectures for distributed and hierarchical model predictive control – a review. *Journal of Process Control*, 19(5), 723–731.

Scott, J. K., Raimondo, D. M., Marseglia, G. R., & Braatz, R. D. (2016). Constrained zonotopes: A new tool for set-based estimation and fault detection. *Automatica*, 69, 126–136.

Selig, M. S. (2014). Real-time flight simulation of highly maneuverable unmanned aerial vehicles. *Journal of Aircraft*, 51(6), 1705–1725.

Shim, D. H., Kim, H. J., & Sastry, S. (2003). Decentralized nonlinear model predictive control of multiple flying robots. In *42nd IEEE International Conference on Decision and Control*, volume 4 (pp. 3621–3626).

Simo, J. & Vu-Quoc, L. (1988). On the dynamics in space of rods undergoing large motions — a geometrically exact approach. *Computer Methods in Applied Mechanics and Engineering*, 66(2), 125–161.

Small, E., Sopasakis, P., Fresk, E., Patrinos, P., & Nikolakopoulos, G. (2019). Aerial navigation in obstructed environments with embedded nonlinear model predictive control. In *2019 18th European Control Conference (ECC)* (pp. 3556–3563).

Sobolic, F. M. (2009). *Agile flight control techniques for a fixed-wing aircraft.* Massachusetts Institute of Technology: Thesis.

Stastny, T. J., Dash, A., & Siegwart, R. (2017). Nonlinear mpc for fixed-wing uav trajectory tracking: Implementation and flight experiments. In *AIAA Guidance, Navigation, and Control Conference* (pp. 1–14).

Sun, S., Romero, A., Foehn, P., Kaufmann, E., & Scaramuzza, D. (2022). A comparative study of nonlinear mpc and differential-flatness-based control for quadrotor agile flight.

Tang, S., Wüest, V., & Kumar, V. (2018). Aggressive flight with suspended payloads using vision-based control. *IEEE Robotics and Automation Letters*, 3(2), 1152–1159.

Tuna, S., Messina, M., & Teel, A. (2006). Shorter horizons for model predictive control. In *2006 American Control Conference* (pp. 863–868).

Ure, N. K. & Inalhan, G. (2012). Autonomous control of unmanned combat air vehicles: Design of a multimodal control and flight planning framework for agile maneuvering. *IEEE Control Systems Magazine*, 32(5), 74–95.

Valavanis, K., Hebert, T., Kolluru, R., & Tsourveloudis, N. (2000). Mobile robot navigation in 2-d dynamic environments using an electrostatic potential field. *IEEE Transactions on Systems, Man, and Cybernetics - Part A: Systems and Humans*, 30(2), 187–196.

van den Berg, J., Guy, S. J., Lin, M., & Manocha, D. (2011a). Reciprocal n-body collision avoidance. In *Robotics Research* (pp. 3–19). Berlin, Heidelberg: Springer Berlin Heidelberg.

van den Berg, J., Lin, M., & Manocha, D. (2008). Reciprocal velocity obstacles for real-time multi-agent navigation. In *ICRA* (pp. 1928–1935).

van den Berg, J., Snape, J., Guy, S. J., & Manocha, D. (2011b). Reciprocal collision avoidance with acceleration-velocity obstacles. In *2011 IEEE International Conference on Robotics and Automation* (pp. 3475–3482).

Van den Broeck, L., Diehl, M., & Swevers, J. (2010). Embedded optimization for input shaping. *IEEE Transactions on Control Systems Technology*, 18(5), 1146–1154.

Van den Broeck, L., Diehl, M., & Swevers, J. (2011). A model predictive control approach for time optimal point-to-point motion control. *Mechatronics*, 21(7), 1203–1212.

Verginis, C. K. & Dimarogonas, D. V. (2021). Adaptive robot navigation with collision avoidance subject to 2nd-order uncertain dynamics. *Automatica*, 123, 1–8.

Verschueren, R., De Bruyne, S., Zanon, M., Frasch, J. V., & Diehl, M. (2014). Towards time-optimal race car driving using nonlinear mpc in real-time. In *53rd IEEE Conference on Decision and Control* (pp. 2505–2510).

Verschueren, R., Ferreau, H. J., Zanarini, A., Mercangöz, M., & Diehl, M. (2017). A stabilizing nonlinear model predictive control scheme for time-optimal point-to-point motions. In *2017 IEEE 56th Annual Conference on Decision and Control (CDC)* (pp. 2525–2530).

Verschueren, R., Zanon, M., Quirynen, R., & Diehl, M. (2016). Time-optimal race car driving using an online exact hessian based nonlinear mpc algorithm. In *2016 European Control Conference (ECC)* (pp. 141–147).

Viswanathan, S. P., Sanyal, A. K., & Samiei, E. (2018). Integrated guidance and feedback control of underactuated robotics system in SE(3). *Journal of Intelligent & Robotic Systems*, 89, 251–263.

Wang, W., Wang, J., & Kim, M. (2001). An algebraic condition for the separation of two ellipsoids. *Computer Aided Geometric Design*, 18, 531–539.

Wang, Y., Ramirez-Jaime, A., Xu, F., & Puig, V. (2017). Nonlinear model predictive control with constraint satisfactions for a quadcopter. In *Journal of Physics: Conference Series*, volume 783 (pp. 012–025).

Wehbeh, J. & Sharf, I. (2022). An MPC formulation on SO(3) for a quadrotor with bidirectional thrust and nonlinear thrust constraints. *IEEE Robotics and Automation Letters*, 7(2), 4945–4952.

Wohner, B., Sevilla, F., Grueter, B., Diepolder, J., Afonso, R., & Holzapfel, F. (2021). Hierarchical nonlinear model predictive control for an autonomous racecar. In *2021 20th International Conference on Advanced Robotics (ICAR)* (pp. 113–120).

Wolf, I. J. & Marquard, W. (2016). Fast NMPC schemes for regulatory and economic NMPC – a review. *Journal of Process Control*, 44, 162–183.

Wolf, I. J., Muñoz, D. A., & Marquardt, W. (2014). Consistent hierarchical economic nmpc for a class of hybrid systems using neighboring-extremal updates. *Journal of Process Control*, 24(2), 389–398. ADCHEM 2012 Special Issue.

Worthmann, K., Mehrez, M. W., Zanon, M., Mann, G. K. I., Gosine, R. G., & Diehl, M. (2015). Regulation of differential drive robots using continuous time mpc without stabilizing constraints or costs. *IFAC-PapersOnLine*, 48(23), 129–135. 5th IFAC Conference on Nonlinear Model Predictive Control NMPC 2015.

Worthmann, K., Mehrez, M. W., Zanon, M., Mann, G. K. I., Gosine, R. G., & Diehl, M. (2016). Model predictive control of nonholonomic mobile robots without stabilizing constraints and costs. *IEEE Transactions on Control Systems Technology*, 24(4), 1394–1406.

Wächter, A. (2002). *An Interior Point Algorithm for Large-Scale Non linear Optimization with Applications in Process Engineering.* Carnegie Mellon University: PhD Dissertation.

Wächter, A. & Biegler, L. (2006). On the implementation of an interior-point filter line-search algorithm for large-scale nonlinear programming. *Math. Program*, 106, 25–57.

Xie, F. & Fierro, R. (2008). First-state contractive model predictive control of nonholonomic mobile robots. In *2008 American Control Conference* (pp. 3494–3499).

Yoshimura, Y., Matsuno, T., & Hokamoto, S. (2016). Global trajectory design for position and attitude control of an underactuated satellite. *Transactions of the Japan Society for Aeronautical and Space Sciences*, 59(3), 107–114.

Yu, G., Cabecinhas, D., Cunha, R., & Silvestre, C. (2019). Quadrotor trajectory generation and tracking for aggressive maneuvers with attitude constraints. *IFAC-PapersOnLine*, 52(12), 55–60. 21st IFAC Symposium on Automatic Control in Aerospace ACA 2019.

Yu, S., Guo, Y., Meng, L., Qu, T., & Chen, H. (2018). Mpc for path following problems of wheeled mobile robot. *IFAC-PapersOnLine*, 51(20), 247 – 252. 6th IFAC Conference on Nonlinear Model Predictive Control NMPC 2018.

Yu, S., Li, X., Chen, H., & Allgöwer, F. (2015). Nonlinear model predictive control for path following problems. *International Journal of Robust and Nonlinear Control*, 25(8), 1168–1182.

Zhang, J., Liu, S., & Liu, J. (2014). Economic model predictive control with triggered evaluations: State and output feedback. *Journal of Process Control*, 24(8), 1197–1206. Economic nonlinear model predictive control.

Zhao, J., Diehl, M., Longman, R., Bock, H. G., & Schloeder, J. (2004). Nonlinear model predictive control of robots using real-time optimization. In *AIAA/AAS Astrodynamics Specialist Conference and Exhibit* (pp. 1–18).

Zhong, X., Zhong, X., & Peng, X. (2016). VCS-based motion planning for distributed mobile robots: collision avoidance and formation. *Soft Comput*, 20(5), 1897–1908.

Zhu, X., Yi, J., Ding, H., & He, L. (2020). Velocity obstacle based on vertical ellipse for multi-robot collision avoidance. *J Intell Robot Syst*, 99, 183–208.

A Rotation Matrices

This appendix defines and discusses some rotation matrix properties. The majority of them are based on Murray et al. (1994).

A.1 Properties of rotation matrices

Let $R \in \mathsf{SO}(3)$ be a rotation matrix and $r_1, r_2, r_3 \in \mathbb{R}^3$ be its columns. Since the columns of R are mutually orthonormal, it follows that

$$RR^\top = R^\top R = I. \tag{A.1}$$

From this, it follows that $\det R = \pm 1$. In addition, from linear algebra, $\det R = r_1^\top (r_2 \times r_3)$. Since the coordinate frame is right-handed, $r_2 \times r_3 = r_1$, so

$$\det R = r_1^\top r_1 = +1. \tag{A.2}$$

$\mathsf{SO}(3) \subset \mathbb{R}^{n \times n}$ is a Lie group under the operation of matrix multiplication, using the identity matrix I_3 as the identity element. That is why $\mathsf{SO}(3)$ is also referred as *rotation group* of $\mathbb{R}^3$. Another important property is that $R \in \mathsf{SO}(3)$ is unique for every configuration of a rigid body. Moreover, $R \in \mathsf{SO}(3)$ can also be used as a transformation, taking coordinates of a point from one frame to another. For example, each point $p^{\mathcal{B}}$ that belongs to the aircraft showed in Figure 3.2 can be written with respect to inertial frame $\mathcal{I}$ as $p^{\mathcal{I}} = R^{\mathcal{I}}_{\mathcal{B}} p^{\mathcal{B}}$. In other words, $R^{\mathcal{I}}_{\mathcal{B}}$, when considered as a map from $\mathbb{R}^3$ to $\mathbb{R}^3$, rotates the

coordinates of a point from frame $\mathcal{B}$ to frame $\mathcal{I}$.

Rotation matrices can be built from successive rotations using matrix multiplication

$$R_3^1 = R_2^1 R_3^2,$$

where a configuration 3 of a body is given by first rotating from configuration 1 to 2, and then 2 to 3 (*composition rule* for rotations). A rotation matrix represents a rigid body transformation in the sense of Definition 3.3.

Proposition A.1. (Murray et al., 1994). A rotation $R \in \mathsf{SO(3)}$ is a rigid body transformation, that is,

1. R preserves distance: $\|Rq - Rp\| = \|q - p\|$ for all $q, p \in \mathbb{R}^3$.
2. R preserves orientation: $R(v \times w) = Rv \times Rw$ for all $v, w \in \mathbb{R}^3$.

A.2 Exponential map for rotation

According to the Euler's Displacement Theorem, every rigid body rotational displacement is equivalent to a simple rotation about a fixed axis. In this context, let $\omega \in \mathbb{R}^3$ be a unit vector which specifies the rotation axis, and let $\theta \in \mathbb{R}$ be the angle of rotation in radians. Since every rotation of the object corresponds to a unique $R \in \mathsf{SO(3)}$, then it is possible to map R as a function of ω and θ.

Lemma A.1. (Murray et al., 1994). Given $R \in \mathsf{SO(3)}$ and $v, \omega \in \mathbb{R}^3$, the following properties hold:

$$R(v \times \omega) = (Rv) \times (R\omega), \tag{A.3}$$

$$R\mathcal{S}(\omega)R^T = \mathcal{S}(R\omega). \tag{A.4}$$

Considering the velocity of a point q attached to the rotating body, if the body is rotated at constant unit velocity about the axis ω, the velocity of the point, $\dot{q}$, may be written as

$$\dot{q}(t) = \omega \times q(t) = \mathcal{S}(\omega)q(t).$$

This is a time-invariant linear differential equation which may be integrated to give

$$q(t) = e^{\mathcal{S}(\omega)t}q(0).$$

Therefore, if the object is rotated about the axis ω at unit velocity for θ units of time, then

$$R(\omega, \theta) = e^{\mathcal{S}(\omega)\theta}. \tag{A.5}$$

Proposition A.2. (Murray et al., 1994). Given a skew-symmetric matrix $\mathcal{S}(\omega) \in \mathfrak{so}(3)$ and $\theta \in \mathbb{R}$,

$$e^{\mathcal{S}(\omega)\theta} \in \mathsf{SO(3)}.$$

Geometrically, the exponential map $\mathfrak{so}(3) \to \mathsf{SO(3)}$ generates the rotation corresponding to rotation by a specified amount θ about the axis represented by the skew-symmetric matrix $\mathcal{S}(\omega)$. This relationship between $\mathfrak{so}(3)$ and $\mathsf{SO(3)}$ is important to compute the derivative of rotation matrices from the angular velocity of the rigid body.

A.3 Derivative of rotation matrices

Any point q attached to the motion system in Figure 3.2 follows a path in inertial coordinates given by $q^{\mathcal{I}} = R^{\mathcal{I}}_{\mathcal{B}} q^{\mathcal{B}}$. Since $q^{\mathcal{B}}$ is fixed with respect to the body frame, the velocity of the point with respect to the inertial frame is given by

$$\dot{q}^{\mathcal{I}} = \frac{d}{dt} q^{\mathcal{I}} = \dot{R}^{\mathcal{I}}_{\mathcal{B}} q^{\mathcal{B}}. \tag{A.6}$$

This representation using $\dot{R}^{\mathcal{I}}_{\mathcal{B}}$ is somewhat inefficient, since it requires nine values to describe the velocity of a rotating body. In order to obtain a more compact structure, equation (A.6) is rewritten as

$$\dot{q}^{\mathcal{I}} = \dot{R}^{\mathcal{I}}_{\mathcal{B}} (R^{\mathcal{I}}_{\mathcal{B}})^{-1} R^{\mathcal{I}}_{\mathcal{B}} q^{\mathcal{B}}. \tag{A.7}$$

If the identity $RR^\top = I_3$ is differentiated, then

$$\dot{R}R^\top + R\dot{R}^\top = 0,$$

$$\dot{R}R^\top = -(R\dot{R}^\top).$$

Hence, $\dot{R}R^{-1} = \dot{R}R^\top$ is a skew-symmetric matrix, as well as $R^{-1}\dot{R}$ (if $R^\top R = I_3$ is differentiated). From this result, the instantaneous angular velocity of the rigid body viewed from the inertial coordinate frame $\mathcal{I}$, denoted by $\omega^{\mathcal{I}}_{\mathcal{IB}} \in \mathbb{R}^3$, is defined as

$$\mathcal{S}(\omega^{\mathcal{I}}_{\mathcal{IB}}) \triangleq \dot{R}^{\mathcal{I}}_{\mathcal{B}} (R^{\mathcal{I}}_{\mathcal{B}})^{-1}. \tag{A.8}$$

Similarly, the instantaneous angular velocity of the object viewed from the body coordinate frame $\mathcal{B}$, denoted by $\omega^{\mathcal{B}}_{\mathcal{IB}} \in \mathbb{R}^3$, is defined as

$$\mathcal{S}(\omega^{\mathcal{B}}_{\mathcal{IB}}) \triangleq (R^{\mathcal{I}}_{\mathcal{B}})^{-1} \dot{R}^{\mathcal{I}}_{\mathcal{B}}. \tag{A.9}$$

From these equations,

$$\mathcal{S}(\omega^{\mathcal{B}}_{\mathcal{IB}}) = (R^{\mathcal{I}}_{\mathcal{B}})^{-1} \mathcal{S}(\omega^{\mathcal{I}}_{\mathcal{IB}}) R^{\mathcal{I}}_{\mathcal{B}}, \tag{A.10}$$

which implies (see (A.4))

$$\omega_{\mathcal{IB}}^{\mathcal{B}} = (R_{\mathcal{B}}^{\mathcal{I}})^{-1}\omega_{\mathcal{IB}}^{\mathcal{I}}.$$

Returning to (A.7), yields

$$\dot{q}^{\mathcal{I}} = \mathcal{S}(\omega_{\mathcal{IB}}^{\mathcal{I}})R_{\mathcal{B}}^{\mathcal{I}}q^{\mathcal{B}} = \omega_{\mathcal{IB}}^{\mathcal{I}} \times q^{\mathcal{I}}. \tag{A.11}$$

Alternatively, using (A.10), the velocity of the point q in the body frame is given by

$$\dot{q}^{\mathcal{B}} \triangleq (R_{\mathcal{B}}^{\mathcal{I}})^{\top}\dot{q}^{\mathcal{I}} = \omega_{\mathcal{IB}}^{\mathcal{B}} \times q^{\mathcal{B}}. \tag{A.12}$$

Thus, both (A.11) and (A.12) demonstrate the physical meaning of the instantaneous angular velocity definitions (A.8) and (A.9).

Therefore, from (A.8) and (A.9), the derivative of the rotational matrix is given by

$$\dot{R}_{\mathcal{B}}^{\mathcal{I}} = R_{\mathcal{B}}^{\mathcal{I}}\mathcal{S}(\omega_{\mathcal{IB}}^{\mathcal{B}}), \tag{A.13}$$

or alternatively by

$$\dot{R}_{\mathcal{B}}^{\mathcal{I}} = \mathcal{S}(\omega_{\mathcal{IB}}^{\mathcal{I}})R_{\mathcal{B}}^{\mathcal{I}}. \tag{A.14}$$

B

Newton-Euler Dynamic Equations

This appendix derives the Newton-Euler dynamics equations for a single rigid body on $\mathsf{SE}(3)$. Let $g = (p, R) \in \mathsf{SE}(3)$ be the configuration of a coordinate frame attached to the center of mass of a rigid body relative to an inertial frame. From this assumption, i.e., the position of the rigid body equals to the position of its center of mass, the equations for both translational and angular motion can be derived independently.

Given an external force $f^{\mathcal{I}}$ applied at the center of mass, the translational equations of motion derived from Newton's Law are given by

$$f^{\mathcal{I}} = \frac{d}{dt}(m\dot{p}_{\mathcal{B}}^{\mathcal{I}}).$$

Since the mass of the rigid body is constant, yields

$$f^{\mathcal{I}} = m\ddot{p}_{\mathcal{B}}^{\mathcal{I}}. \tag{B.1}$$

For the rotational motion, given an external torque $\tau^{\mathcal{I}}$ applied at the rigid body, the angular equations of motion are described as

$$\tau^{\mathcal{I}} = \frac{d}{dt}(J^{\mathcal{I}}\omega^{\mathcal{I}}), \tag{B.2}$$

where $J^{\mathcal{I}}$ is the instantaneous inertia tensor relative to the inertial frame, and $\omega^{\mathcal{I}} = \omega_{\mathcal{I}\mathcal{B}}^{\mathcal{I}}$ is the instantaneous angular velocity (see Section A.3) of the object viewed from the inertial coordinate frame. However, in contrast to the mass which is assumed constant for most of

applications, the inertia tensor relative to the inertial frame varies according to the motion execution. One way to deal with that is to consider equation (B.2) viewed from the body coordinate frame. Besides, most of attitude sensors provide $\omega^{\mathcal{B}}_{\mathcal{IB}}$. Hence, for convenience, (B.2) is rewritten as

$$\tau^{\mathcal{B}} = f(J^{\mathcal{B}}, \omega^{\mathcal{B}}). \tag{B.3}$$

To find $f(\cdot)$ it is necessary to expand the right-hand side of equation (B.2) as follows

$$\begin{aligned}
\tau^{\mathcal{I}} &= \frac{d}{dt}(J^{\mathcal{I}}\omega^{\mathcal{I}}) = \frac{d}{dt}(R^{\mathcal{I}}_{\mathcal{B}}J^{\mathcal{B}}(R^{\mathcal{I}}_{\mathcal{B}})^{\top}\omega^{\mathcal{I}}) \\
&= R^{\mathcal{I}}_{\mathcal{B}}J^{\mathcal{B}}(R^{\mathcal{I}}_{\mathcal{B}})^{\top}\dot{\omega}^{\mathcal{I}} + \dot{R}^{\mathcal{I}}_{\mathcal{B}}J^{\mathcal{B}}(R^{\mathcal{I}}_{\mathcal{B}})^{\top}\omega^{\mathcal{I}} + R^{\mathcal{I}}_{\mathcal{B}}J^{\mathcal{B}}\dot{R}^{\mathcal{B}}_{\mathcal{I}}\omega^{\mathcal{I}} \\
&= R^{\mathcal{I}}_{\mathcal{B}}J^{\mathcal{B}}\dot{\omega}^{\mathcal{B}} + \dot{R}^{\mathcal{I}}_{\mathcal{B}}J^{\mathcal{B}}\omega^{\mathcal{B}} + R^{\mathcal{I}}_{\mathcal{B}}J^{\mathcal{B}}\dot{R}^{\mathcal{B}}_{\mathcal{I}}\omega^{\mathcal{I}} \\
(R^{\mathcal{I}}_{\mathcal{B}})^{\top}\tau^{\mathcal{I}} &= (R^{\mathcal{I}}_{\mathcal{B}})^{\top}(R^{\mathcal{I}}_{\mathcal{B}}J^{\mathcal{B}}\dot{\omega}^{\mathcal{B}} + \dot{R}^{\mathcal{I}}_{\mathcal{B}}J^{\mathcal{B}}\omega^{\mathcal{B}} + R^{\mathcal{I}}_{\mathcal{B}}J^{\mathcal{B}}\dot{R}^{\mathcal{B}}_{\mathcal{I}}\omega^{\mathcal{I}}) \\
\tau^{\mathcal{B}} &= J^{\mathcal{B}}\dot{\omega}^{\mathcal{B}} + (R^{\mathcal{I}}_{\mathcal{B}})^{\top}\dot{R}^{\mathcal{I}}_{\mathcal{B}}J^{\mathcal{B}}\omega^{\mathcal{B}} + J^{\mathcal{B}}\dot{R}^{\mathcal{B}}_{\mathcal{I}}\omega^{\mathcal{I}}.
\end{aligned}$$

By using (A.13) and (A.14) in the above equation, yields

$$\begin{aligned}
\tau^{\mathcal{B}} &= J^{\mathcal{B}}\dot{\omega}^{\mathcal{B}} + (R^{\mathcal{I}}_{\mathcal{B}})^{\top}R^{\mathcal{I}}_{\mathcal{B}}\hat{\omega}^{\mathcal{B}}J^{\mathcal{B}}\omega^{\mathcal{B}} + J^{\mathcal{B}}(\hat{\omega}^{\mathcal{I}}R^{\mathcal{I}}_{\mathcal{B}})^{\top}\omega^{\mathcal{I}} \\
&= J^{\mathcal{B}}\dot{\omega}^{\mathcal{B}} + \hat{\omega}^{\mathcal{B}}J^{\mathcal{B}}\omega^{\mathcal{B}} + J^{\mathcal{B}}(R^{\mathcal{I}}_{\mathcal{B}})^{\top}(\hat{\omega}^{\mathcal{I}})^{\top}\omega^{\mathcal{I}} \\
&= J^{\mathcal{B}}\dot{\omega}^{\mathcal{B}} + \omega^{\mathcal{B}} \times J^{\mathcal{B}}\omega^{\mathcal{B}} - J^{\mathcal{B}}(R^{\mathcal{I}}_{\mathcal{B}})^{\top}\omega^{\mathcal{I}} \times \omega^{\mathcal{I}}.
\end{aligned}$$

Since the cross product between two parallel vectors is zero, the last term of the last equation vanishes, and then

$$\tau^{\mathcal{B}} = J^{\mathcal{B}}\dot{\omega}^{\mathcal{B}} + \omega^{\mathcal{B}} \times J^{\mathcal{B}}\omega^{\mathcal{B}}. \tag{B.4}$$

Therefore, equations (B.1) (Newton's equation) and (B.4) (Euler's equation), derived on $\mathsf{SE}(3)$, describe the dynamics of a rigid body in terms of forces and torques applied at the center of mass of the motion system.